Fundamental Structural, Electronic, and Chemical Properties of Carbon Nanostructures: Graphene, Fullerenes, Carbon Nanotubes, and Their Derivatives

Tandabany C. Dinadayalane and Jerzy Leszczynski

Contents

T.C. Dinadayalane (✉)
Department of Chemistry, Clark Atlanta University, Atlanta, GA, USA
e-mail: dina@icnanotox.org

J. Leszczynski
Interdisciplinary Center for Nanotoxicity, Department of Chemistry and Biochemistry, Jackson State University, Jackson, MS, USA
e-mail: jerzy@icnanotox.org

J. Leszczynski et al. (eds.), *Handbook of Computational Chemistry*,
DOI 10.1007/978-94-007-6169-8_22-2

Abstract

This chapter provides information on various carbon allotropes and in-depth details of structural, electronic, and chemical properties of graphene, fullerenes, and single-walled carbon nanotubes (SWCNTs). We have written an overview of different computational methods that were employed to understand various properties of carbon nanostructures. Importance of application of computational methods in exploring different sizes of fullerenes and their isomers is given. The concept of isolated pentagon rule (IPR) in fullerene chemistry has been revealed. The computational and experimental studies involving Stone–Wales (SW) and vacancy defects in fullerene structures are discussed in this chapter. The relationship between the local curvature and the reactivity of the defect-free and defective fullerene and single-walled carbon nanotubes has been revealed. We reviewed the influence of different defects in graphene on hydrogen addition. The viability of hydrogen and fluorine atom additions on the external surface of the SWCNTs is revealed using computational techniques. We have briefly pointed out the current utilization of carbon nanostructures and their potential applications.

Introduction to Carbon Nanostructures

Carbon is one of the first few elements known in antiquity. The pure forms of this element include diamond and graphite, which have been known for few thousand years (http://www.nndc.bnl.gov/content/elements.html; Pierson 1993; Wikipedia – http://en.wikipedia.org/wiki/Carbon). Both of these materials are of immense importance in industry and in everyday life. Diamond and graphite are termed as giant structures since, by means of a powerful microscope, one could see millions and millions of atoms, all connected together in a regular array. Diamond would appear as a rigid and rather complex system like some enormous scaffolding construction. Carbon is also the major atomic building block for life. All life-forms on Earth have carbon central to their composition. More than 10 million carbon-containing compounds are known. Compounds containing only carbon atoms, particularly nano-sized materials, are intriguing and attract attention of scientists working in various disciplines. Before 1985, scientists deemed that there were only three allotropes of carbon, namely, diamond, graphite, and amorphous carbon such as soot and charcoal. Soccer ball-shaped molecule comprising of 60 carbon atoms, C_{60} buckyball named fullerene, was discovered in 1985, and it is another interesting carbon allotrope (Kroto et al. 1985). Carbon nanotubes (CNTs), a spin-off product of fullerene, were reported in 1991 by Iijima (1991). Important well-known carbon materials are depicted in Fig. 1. The publication of transmission

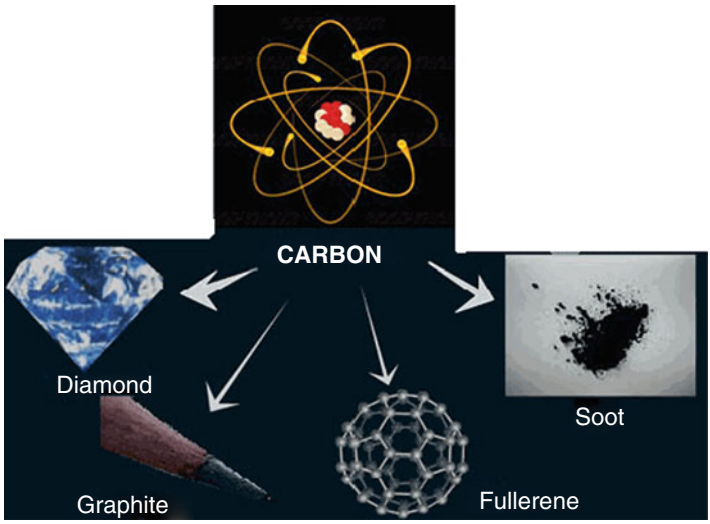

Fig. 1 Well-known carbon materials

electron microscope (TEM) images of CNTs by Iijima was a critical factor in convincing a broad community that "*there is plenty of room at the bottom*" and many new structures can exist at the nanoscale. Figure 2 shows eight allotropes of carbon. In addition to graphene, fullerenes, and carbon nanotubes, there are few other uncommon carbon nanostructures such as nanohorns (Iijima et al. 1999; Poonjarernsilp et al. 2009), nano-onions (Palkar et al. 2008; Zhou et al. 2009), nanobuds (He and Pan 2009; Nasibulin et al. 2007a, b; Wu and Zeng 2009), peapods (Launois et al. 2010; Li et al. 2009a; Smith et al. 1998), nanocups (Chun et al. 2009), and nanotori (Liu et al. 1997; Sano et al. 2001).

We performed a quick search in SciFinder on "fullerene," "carbon nanotubes," and "graphene" to reveal their importance and growth in current science, engineering, and technology. We received a total of nearly 60,000 references for the word "fullerene," ~145,000 references for "carbon nanotubes," and 110,000 for "graphene" when we searched these topics in November 2015. This is indicative that carbon nanomaterials have gained a momentum with the development of nanotechnology as the driving force of the modern science and engineering. Among various carbon nanostructures, CNTs play a special role in the nanotechnology era. The design and discovery of new materials is always exciting for the potential of new applications and properties (Cohen 1993; Serra et al. 1999). In this chapter, we aim to present an overview of carbon nanostructures, with a particular interest on structural, electronic, and chemical properties of graphene, fullerenes, and carbon nanotubes. Important topological defects in the graphene, fullerenes, and carbon nanotubes will be delineated. Thus, this chapter is intended to be an informative guide of carbon nanostructures and to provide description of current computational

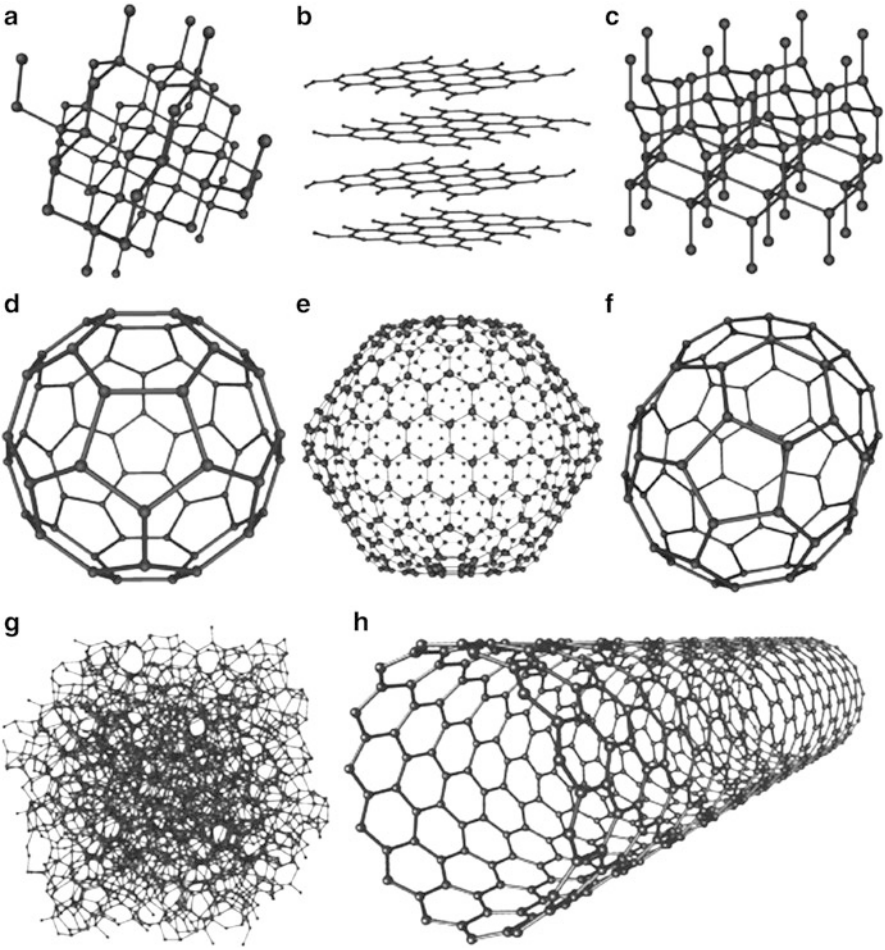

Fig. 2 Eight allotropes of carbon: (**a**) diamond, (**b**) graphite, (**c**) lonsdaleite, (**d**) C_{60} (buckminsterfullerene or buckyball), (**e**) C_{540}, (**f**) C_{70}, (**g**) amorphous carbon, and (**h**) single-walled carbon nanotube or buckytube (The picture adopted from Wikipedia – http://en.wikipedia.org/wiki/Allotropes_of_carbon)

chemistry applications involving these species to facilitate the pursuit of both newcomers to this field and experienced researchers in this rapidly emerging area.

Graphene

Carbon displays a unique feature of making a chemically stable two-dimensional (2D), one-atom-thick membrane called graphene in a three-dimensional (3D) world. Each carbon atom in graphene is covalently bonded to three other carbon atoms

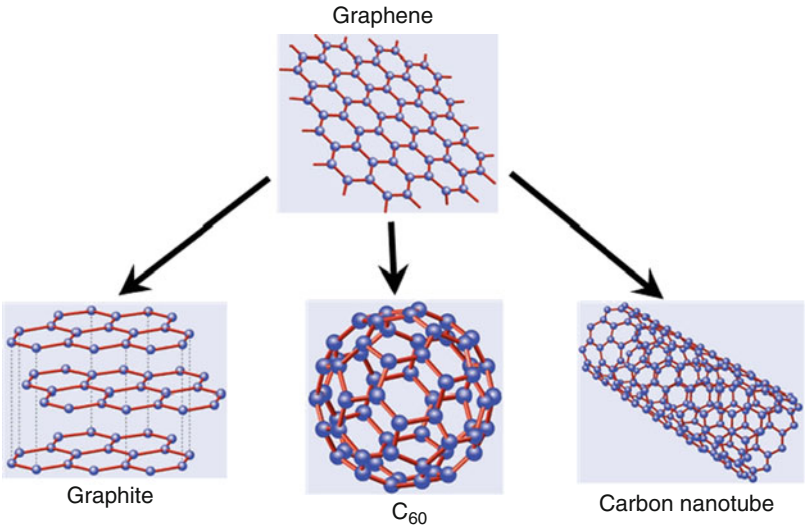

Fig. 3 Carbon-containing molecules (graphite, buckminsterfullerene (C_{60}), and carbon nanotube) derived from graphene

with sp^2 hybridization. Graphene is the thinnest known material and in the same time is the strongest material ever to be measured. It can sustain current densities six orders of magnitude higher than that of copper. It has extremely high strength and very high thermal conductivity and stiffness and is impermeable to gases (Geim 2009). There are many challenges and opportunities for graphene research because graphene is not a standard solid state material. It should be noted that electrons in graphene do not behave in the same way as in ordinary metals and semiconductors due to the unusual energy–momentum relation (Neto 2010). Well-known forms of carbon-containing molecules that derived from graphene are graphite, fullerene, and carbon nanotube, which are depicted in Fig. 3. Graphite consists of stacked layers of graphene sheets separated by 0.3 nm and is stabilized by weak van der Waals forces (He and Pan 2009). Buckminsterfullerene (C_{60}) is formed from graphene balled into a sphere by including some pentagons and hexagons into the lattice (Kroto et al. 1985). The combined experimental and computational study showed the direct transformation of graphene to fullerene (Chuvilin et al. 2010). Carbon nanotubes can be viewed as rolled-up cylinders of graphene. Therefore, graphene can be called "the mother" of all these three sp^2 carbon structures.

It was presumed that planar graphene cannot exist in free state since they are unstable compared to curved structures such as soot, nanotubes, and fullerenes. This presumption has changed since Novoselov et al. prepared graphitic sheets including single graphene layer and studied their electronic properties (Novoselov et al. 2004, 2005a). The detailed information of growth and isolation of graphene has been provided in the recent review by Geim (2009). Graphene is a prospective material

for nanoelectronics. The electron transport in graphene is described by Dirac-like equation (Geim and Novoselov 2007; Novoselov et al. 2005b; Ponomarenko et al. 2008). The experimental realization of graphene motivates several studies focusing on fundamental physics, materials science, and device applications (Abanin et al. 2006; Geim and Novoselov 2007; Novoselov et al. 2004; 2005a, b; Pereira et al. 2009; Ponomarenko et al. 2008). The studies pertinent to the chemistry of graphene sheets have also been reported (Abanin et al. 2006; Avouris et al. 2007; Geim and Novoselov 2007, Neto et al. 2009; Pereira et al. 2009). Graphene research is a hot topic in this decade, thanks to the recent advances in technology for growth, isolation, and characterization of graphene.

Graphene sheets need not always be as perfect as one thinks. Various defects such as Stone–Wales (SW) (Stone and Wales 1986), vacancies (Carlson and Scheffler 2006), pore defects (Jiang et al. 2009), and substitution atoms (Miwa et al. 2008; Zhu et al. 2005) can occur in the thin graphene sheet. Like the creation of vacancies by knocking atoms out of the graphene sheet, surplus atoms can be found as adatoms on the graphene surface. Ad-dimer defect can be introduced to graphene and is characterized by two adjacent five-membered rings instead of two adjacent seven-membered rings in Stone–Wales defect. Therefore, ad-dimer defect is called inverse Stone–Wales (ISW) defect. Figure 4 depicts some of the common defects in graphene sheet.

Experimental observations of defects in graphene have been reported recently (Meyer et al. 2008; Wang et al. 2008). Zettl and coworkers showed the direct image of Stone–Wales defects in graphene sheets using transmission electron microscopy (TEM) and explored their real-time dynamics. They found that the dynamics of defects in extended, two-dimensional graphene membranes are different than in closed-shell graphenes such as nanotubes or fullerenes (Meyer et al. 2008). High-resolution transmission electron microscopy (HRTEM) and atomic force microscopy (AFM) have been useful in identifying various defects in graphene. AFM and HRTEM images of graphene sheet with different defects are shown in Fig. 5. The effect of various defects on the physical and chemical properties of graphene was studied theoretically (Boukhvalov and Katsnelson 2008; Carpio et al. 2008; Duplock et al. 2004; Lherbier et al. 2008; Li et al. 2005). The characteristics of typical defects and their concentrations in graphene sheets are unclear.

Computational and experimental studies concerning defects in graphene sheet are critically important for basic understanding of this novel system, and such understanding will be helpful for scientists who actively work on applications of graphene-based materials. Although the surface physics of graphene sheets is currently at the center of attention, its chemistry has remained largely unexplored. Like any other molecule, graphene can involve in chemical reactions. The chemical functionalization is probably one of the best approaches to detect imperfections in a graphene sheet (Boukhvalov and Katsnelson 2008). The functionalized graphene can be suitable for specific applications. Research on bended, folded, and scrolled graphene is rapidly growing now.

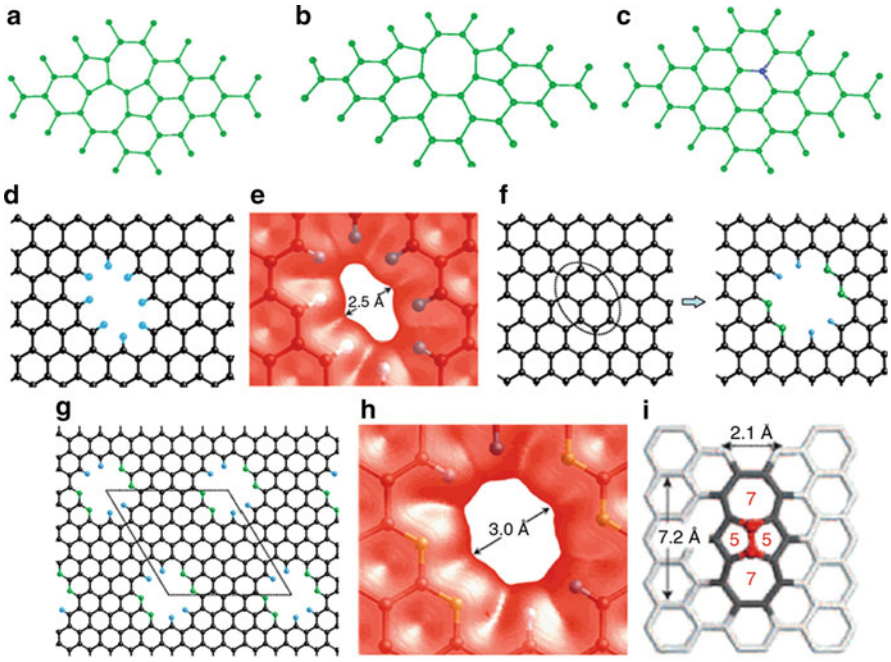

Fig. 4 Defects in graphene sheet; the segment of graphene containing (**a**) the Stone–Wales (SW) defect; (**b**) a bivacancy; (**c**) a nitrogen substitution impurity; (**d**) an all-hydrogen saturated pore in graphene; (**e**) the pore electron density isosurface of all-hydrogen passivated porous graphene; (**f**) creation of a nitrogen-functionalized pore within a graphene sheet: the carbon atoms in the dotted circle are removed, and four dangling bonds are saturated by hydrogen, while the other four dangling bonds together with their carbon atoms are replaced by nitrogen atoms; (**g**) the hexagonally ordered porous graphene. The *dotted lines* indicate the unit cell of the porous graphene; (**h**) the pore electron density isosurface of nitrogen-functionalized porous graphene; (**i**) an inverse Stone–Wales (ISW) defect. Color code for (**d**), (**f**), and (**g**): *C* black, *N* green, *H* cyan. Isosurface is at 0.02 e/Å^3 (The pictures were reprinted with permission from references Jiang et al. (2009) and Boukhvalov and Katsnelson (2008). Copyright 2008 and 2009 American Chemical Society)

Fullerenes

Discovery of fullerene C_{60} and other fullerene molecules is discussed below.

The fullerene era started in 1985; Kroto and his colleagues obtained cold carbon clusters when they carried out an experiment to simulate the condition of red giant star formation. With the use of the mass spectrometer, they found a large peak commensurate with 60 carbon atoms (Kroto et al. 1985). The molecule C_{60} was proposed to have a football structure, known to mathematicians as the truncated icosahedron. The shape is composed of 12 pentagons located around the vertices of an icosahedron and 20 hexagon rings placed at the centers of icosahedral faces. The C_{60} molecule was named "buckminsterfullerene" in honor of the renowned architect

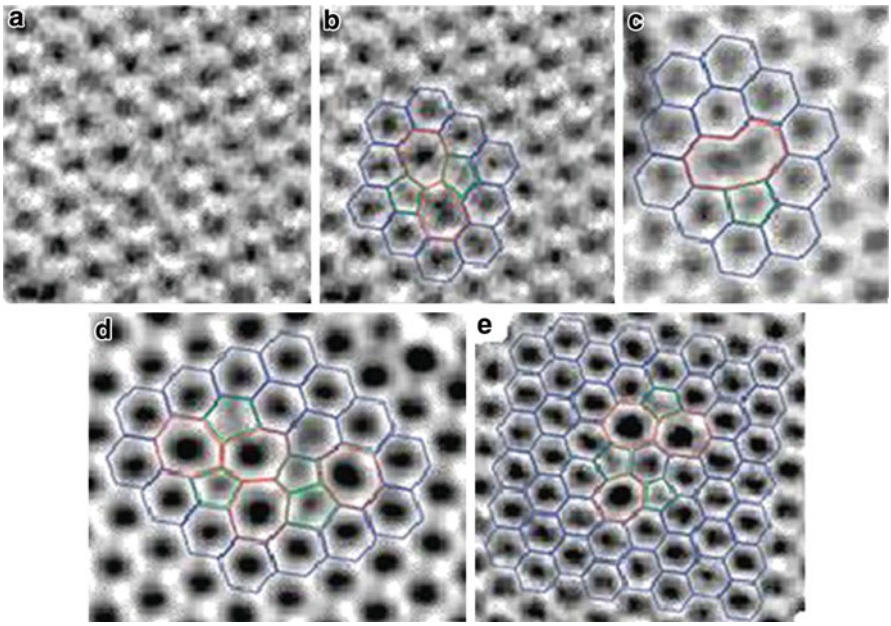

Fig. 5 (**a**) HRTEM image of a single graphene layer (atoms appear white). (**b**) Image of graphene with Stone–Wales defect (atomic configuration superimposed for easy recognition). (**c**) Image of vacancy defect with atomic configuration. (**d**) Defect image with atomic configuration consisting of four pentagons (*green*) and four heptagons (*red*). (**e**) Defect image with atomic configuration consisting of three pentagons (*green*) and three heptagons (*red*) (Pictures were reprinted with permission from reference Meyer et al. (2008). Copyright 2008 American Chemical Society)

Buckminster Fuller, who designed geodesic domes based on similar pentagonal and hexagonal structures. The carbon atoms in C_{60} fullerene are arranged in exactly the same way, albeit much smaller, as the patches of leather found on the common football (Fig. 6a).

Since the remarkable discovery of fullerenes in 1985 (Kroto et al. 1985), these new carbon allotropes have received significant attention from the scientific community and still exhibit vast interest (Lu and Chen 2005; Thilgen and Diederich 2006). The 1996 Nobel Prize in Chemistry was awarded to Sir Harold W. Kroto, Robert F. Curl, and the late Richard E. Smalley for their discovery of fullerenes. Essentially, the most prominent representative of the fullerene family is C_{60}. In early 1990, a method was discovered for producing macroscopic amounts of this fascinating molecule (Krätschmer et al. 1990). This breakthrough allowed scientists to explore the properties of C_{60} and understand its chemistry. Krätschmer et al. characterized the fullerene C_{60} using mass spectroscopy, infrared spectroscopy, electron diffraction, and X-ray diffraction (Krätschmer et al. 1990). Both Kroto et al. (1985) and Krätschmer et al. (1990), by means of mass spectroscopy, also characterized the fullerene C_{70}. Pure C_{60} and C_{70} fullerenes were isolated and

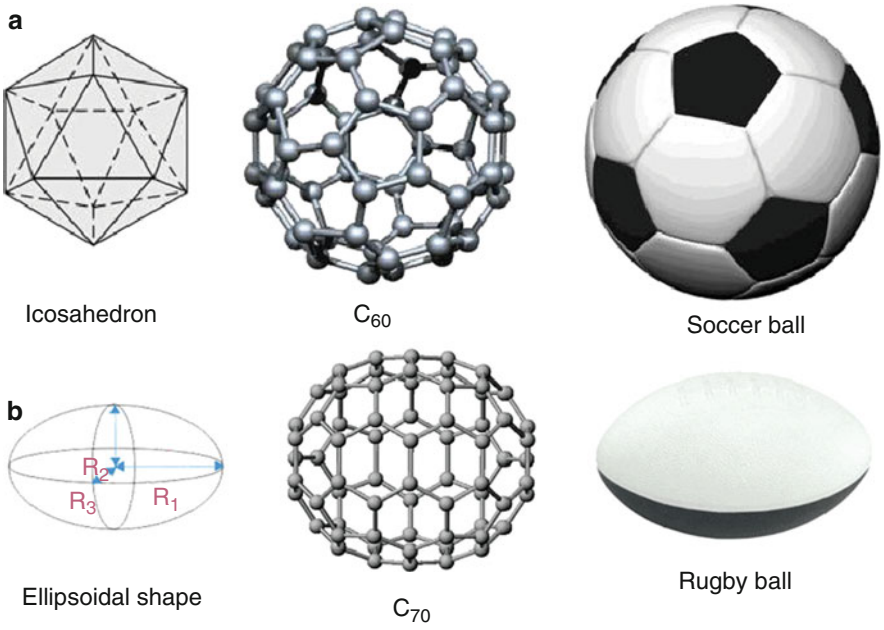

Fig. 6 The structures of fullerenes C_{60} and C_{70} and their familiar shapes. C_{60} and C_{70} are in icosahedron (I_h) and D_{5h} point groups

separated by Kroto and coworkers (Taylor et al. 1990). The stable fullerenes of C_{60} and C_{70} were reported in the ratio of approximately 5:1. ^{13}C nuclear magnetic resonance (NMR) spectroscopy was used to characterize the fullerenes (Taylor et al. 1990). These two molecules are members of a homologous series of hollow closed-cage molecules. The fullerene C_{70} belongs to a class of nonspherical fullerenes. It adopts an ellipsoidal shape (point group D_{5h}) and it looks like a "rugby ball" as shown in Fig. 6b. Existence of C_{60} was predicted by Eiji Osawa (1970). However, his prediction did not reach Europe or America since it was published in Japanese magazine.

In the eighteenth century, the Swiss mathematician Leonhard Euler demonstrated that a geodesic structure must contain 12 pentagons to close into a spheroid, although the number of hexagons may vary. Later research by Smalley and his colleagues showed that there should exist an entire family of these geodesic-dome-shaped carbon clusters (Kroto et al. 1985). Fullerenes form with an even number $n \geq 20$ of three connected vertices, $3n/2$ edges, 12 pentagonal faces, and $(n-20)/2$ hexagonal faces (Fowler and Manolopoulos 1995; Kroto et al. 1985). Thus, C_{60} has 20 hexagons, whereas its "rugby ball"-shaped cousin C_{70} has 25 hexagons. As hexagons are added or removed, the molecule begins to lose its roundness. Giant fullerenes take on a pentagonal shape. Smaller fullerenes look like asteroids. One should note that all of the fullerenes have the same Gaussian curvature sign; therefore all of them have a convex surface. The buckminsterfullerene C_{60}, shown in

Fig. 6, has a spherical-like shape and the full group of symmetry of the icosahedron (I_h), which means that it could be rotated by the angle of $2\pi/5$ around the center of each pentagon and reflected in the mirror located on each plane of its symmetry. Another class of spherical fullerenes like C_{140} and C_{260} lacks the mirror symmetry *h*; hence, their maximum symmetry group is icosahedral (*I*) (Terrones et al. 2002).

The fullerenes C_{60} and C_{70} were identified in carbon flames, and their ratios depend on the temperature, pressure, carbon/oxygen ratio, and residence time in the flame (Howard et al. 1991). The molecular structure of C_{70} was deduced from electron diffraction using a simulated-annealing method (McKenzie et al. 1992). Scientists tried to understand the crystal structures of C_{60} and C_{70} using X-ray diffraction technique (David et al. 1991, 1992; Fischer et al. 1991; Valsakumar et al. 1993). At ambient temperature and pressure, C_{60} crystals have face-centered cubic (fcc) structure with a lattice constant of 14.17 Å (David et al. 1991), while the C_{70} crystals adopt to a hexagonal close-packed (hcp) structure with $a = 10.1$ Å and $c = 17.0$ Å (David et al. 1992). The average diameters of C_{60} and C_{70} fullerenes are about 7 and 9 Å, respectively. Since the discovery of C_{60} followed by C_{70} (Kroto et al. 1985; Taylor et al. 1990), different sizes of carbon cage fullerenes were revealed. In early 1990, the carbon cages of C_{76}, C_{84}, C_{90}, and C_{94} were characterized by mass spectrometry, ^{13}C NMR, electronic absorption (ultraviolet–visible), and vibrational (infrared) spectroscopy techniques (Diederich et al. 1991a). As compared with C_{60} and C_{70}, the isolation of higher fullerenes is really challenging, and their characterization is complicated by the presence of a varying number of isomers.

Fullerenes are generally represented by a formula C_n, where n is an even number and denotes the number of carbon atoms present in the cage. Theoretical calculations predicted that fullerenes larger than C_{76} should have at least two isomeric forms (Manolopoulos and Fowler 1991). For fullerenes C_{84} and C_{96}, 24 and 187 distinct isomers were predicted, respectively (Manolopoulos and Fowler 1991, 1992). Three isomers for C_{78} and two isomers for C_{84} were isolated and characterized by ^{13}C NMR spectroscopy (Kikuchi et al. 1992a). Some of the isomers of C_{78} and C_{82} proposed by experimental ^{13}C NMR spectroscopy are depicted in Fig. 7. Many of the unique properties of fullerenes originate from their unusual cage structures. Therefore, determining the ground-state geometries of the fullerenes was considered to be an important step in understanding their unusual properties.

Experimental works are very limited for higher fullerenes beyond C_{84} because such species are difficult to isolate in pure form in quantities suitable for comprehensive study. Synthesis of C_{60}, in isolable quantities, was achieved using flash vacuum pyrolysis (FVP) technique by Scott and coworkers by 12 steps in 2002, and no other fullerenes were formed as by-products (Scott et al. 2002). Larger fullerene C_{78} was synthesized using the same FVP technique used for C_{60} synthesis (Amsharov and Jensen 2008). This shows a promise for the synthesis of higher fullerenes. It is noteworthy to mention that there has been a lot of experimental and theoretical studies involving fragments of fullerenes, called "buckybowls" (Barth and Lawton 1966; Dinadayalane and Sastry 2001, 2002a, b; Dinadayalane et al. 2001, 2002, 2003, 2004; Mehta and Rao 1998; Mehta et al. 1997; Priyakumar and Sastry 2001a,

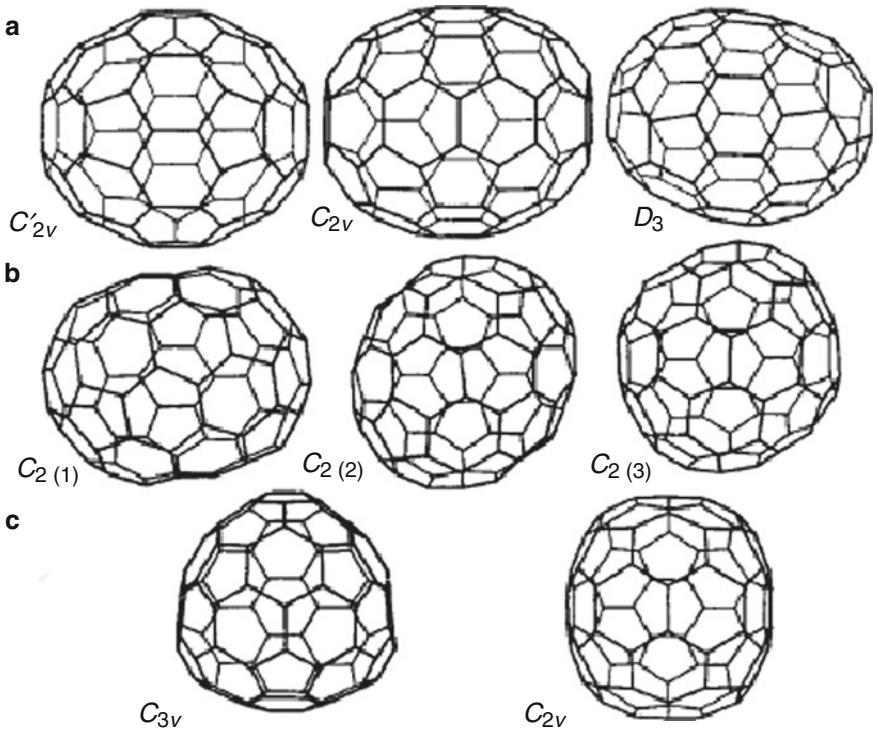

Fig. 7 The structures of fullerene isomers suggested by the ^{13}C NMR measurements. (**a**) Three isomers of C_{78} fullerene with $C_{2v}^{'}$, C_{2v}, and D_3 point group. (**b**) Three structural candidates for C_{82} fullerene with C_2 symmetry. (**c**) Structures of C_{3v}- and C_{2v}-C_{82} isomers. (The picture was reprinted with permission from Macmillan Publishers Ltd.: Nature, reference Kikuchi et al. (1992a)), Copyright 1992)

b, c; Sakurai et al. 2003; Sastry and Priyakumar 2001; Sastry et al. 1993, 2000; Seiders et al. 1999; Sygula and Rabideau 1999; Wu and Siegel 2006). The smallest buckybowl "corannulene" was synthesized nearly 20 years prior to the discovery of fullerene C_{60} (Barth and Lawton 1966). Another small fragment of C_{60} called "sumanene" was successfully synthesized in 2003 after so many futile attempts by different groups (Sakurai et al. 2003).

Fullerene can be classified into (a) classical fullerene and (b) nonclassical fullerene. The former one is a closed carbon cage containing 12 pentagons and any number of hexagons, while a nonclassical fullerene can have heptagons, octagons, and an additional number of pentagons or squares. Growing classical fullerenes from nonclassical fullerenes, for example, from C_{50} to C_{60} by the dimer addition, was proposed (Hernández et al. 2001). However, there is no clear experimental evidence for fullerene formation through this route. The experimental evidence was reported for the formation of fullerenes by collisional heating of carbon rings in the gas phase (Helden et al. 1993). Various mechanisms have been proposed so far

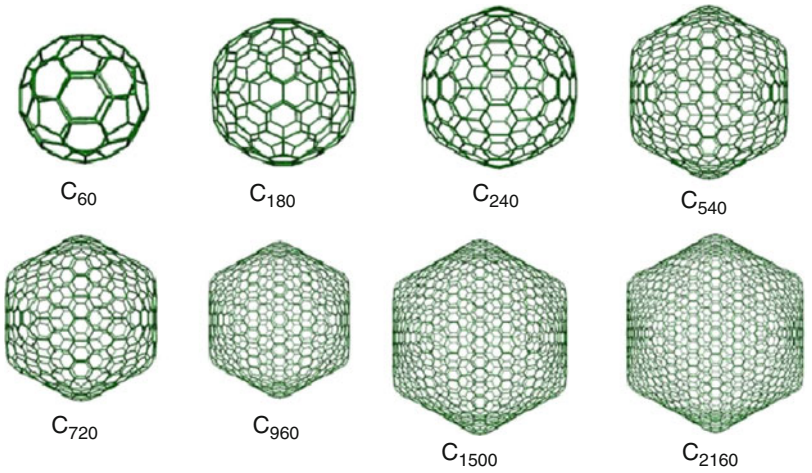

Fig. 8 The structures of giant fullerenes (Reprinted with permission from Zope et al. (2008). Copyright 2008 by the American Physical Society)

for the formation of fullerenes. They can be divided into two major models: the pentagon road (PR) model (Klein and Schmalz 1990; Maruyama and Yamaguch 1998; Smalley 1992) and the fullerene road (FR) model (Heath 1991).

Since the discovery of C_{60}, scientists showed vast interest in larger fullerenes. Therefore, the family of fullerenes increased, and now it also includes C_{70}, C_{76}, C_{78}, C_{82}, C_{84}, C_{86}, C_{88}, C_{90}, C_{92}, C_{94}, and C_{96} (Diederich et al. 1991a, b; Kikuchi et al. 1992b; Kimura et al. 1995; Miyake et al. 2000; Mizorogi and Aihara 2003; Taylor et al. 1992, 1993). The fundamental understanding of the size dependence of the closed carbon cage structures is important for tailoring these systems for possible nanotechnology applications. Larger fullerenes that have an icosahedral symmetry can also be constructed. This procedure generates 12 pentagons positioned around vertices of an icosahedron, while all other carbon rings are hexagonal. In general, there are two kinds of fullerenes with I_h symmetry, one being $n = 60\ k^2$ and the other $n = 20\ k^2$, where n is the number of carbon atoms and k is any positive integer (Miyake et al. 2000). Figure 8 depicts some of the giant fullerene structures, where C_{180} and C_{720} belong to $180\ k^2$ family of icosahedral fullerenes, but all other structures belong to $60\ k^2$ family of icosahedral fullerenes. For more than a decade, these giant fullerenes have been fascinating molecules for theoreticians (Calaminici et al. 2009; Dulap and Zope 2006; Dunlap et al. 1991; Gueorguiev et al. 2004; Lopez-Urias et al. 2003; Tang and Huang 1995; Tang et al. 1993; Zope et al. 2008).

The closed carbon cages smaller than C_{60} consist of adjacent pentagons. Such smaller fullerenes are predicted to have unusual electronic, magnetic, and mechanical properties that arise mainly from the high curvature of their molecular surface (Kadish and Ruoff 2002). A dodecahedron consisting of 20 carbon atoms with only pentagon rings is topologically the smallest possible fullerene. The

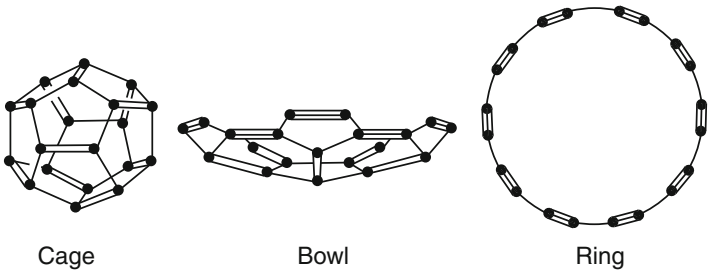

Fig. 9 Isomers of C_{20}: cage-, bowl-, and ring-shaped structures (Reprinted with permission from Macmillan Publishers Ltd.: Nature, reference Prinzbach et al. (2000), Copyright 2000)

well-known isomers of C_{20} are cage, bowl, and ring as shown in Fig. 9. The bowl-shaped isomer is reminiscent of corannulene. The realization of the smallest carbon closed-cage C_{20}, which exclusively contains 12 pentagons, was doubtful until 2000. The C_{20} closed cage has extreme curvature and high reactivity, which led to doubts about its existence and stability (Wahl et al. 1993). Prinzbach et al. produced the smallest fullerene C_{20} from its perhydrogenated form in the gas phase and also obtained the bowl- and ring-shaped isomers for comparison purposes (Prinzbach et al. 2000). All these structures were characterized by photoelectron spectroscopy (PES) and their electron affinities vary significantly (Prinzbach et al. 2000). Theoretical calculations at different levels predicted dissimilar energetic ordering for these three isomers. However, all revealed very small relative energies of isomers. MP2 method predicted the fullerene to be the most stable followed by the bowl and then the ring, and this prediction is very similar to the calculations of density functional theory (DFT) using the local density approximation (LDA). Complete reversal of the stability ordering was obtained in the calculations with Becke–Lee–Yang–Parr (BLYP) functional. Some other DFT functionals predicted the bowl to be the most stable structure, closely followed by the fullerene isomer (Scuseria 1996). Hybrid density functional theory and time-dependent DFT formalism validated the synthesis of the smallest cage fullerene C_{20} by comparing the computed photoelectron spectra with the experimental results (Saito and Miyamoto 2001).

Closed-cage structure of C_{36} was detected by mass spectroscopy in very early days of fullerene science (Kroto 1987; Rohlfing et al. 1994). Zettl's group claimed the first preparation of C_{36} in the solid form (Piskoti et al. 1998). However, the existence of C_{36} has not been fully confirmed to date. C_{36} has 15 conventional fullerene isomers, out of which the D_{6h} and D_{2d} have a minimal number of pentagons (Fowler and Manolopoulos 1995). Therefore, these two are potential candidates for the most stable structure. In general, the number of isomers increases as the carbon cage size increases for these small fullerenes as shown in Fig. 10.

Fullerenes from C_{20} to C_{58} have been extensively studied by theoreticians (Fowler and Manolopoulos 1995; Scuseria 1996; Shao et al. 2007). They have been predicted to have narrow HOMO–LUMO gaps and high reactivity. The structures,

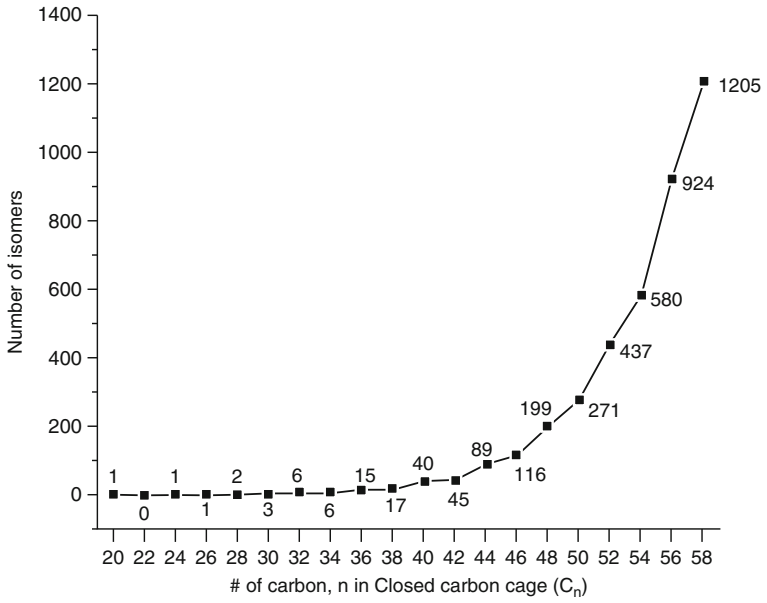

Fig. 10 Number of isomers for the closed carbon cages from C_{20} to C_{58} (Data was taken from reference Fowler and Manolopoulos 1995))

aromaticity, reactivity, and other properties of fullerenes smaller than 60 carbon atoms were reviewed (Lu and Chen 2005). Readers may refer to the review by Lu and Chen and the references therein for detailed understanding and further knowledge if required (Lu and Chen 2005). Selected structures of smaller fullerenes and their isomers are depicted in Fig. 11. Schlegel diagram is commonly used by scientists to sketch the fullerenes in planar view, which is very helpful in identifying atoms and the C−C bonding networks (Fowler and Heine 2001; Thilgen and Diederich 2006; Troyanov and Tamm 2009). Figure 12 depicts the Schlegel diagram for fullerenes C_{20}, C_{36}, C_{60}, and C_{70}.

Natural Abundance of Fullerenes

Scientists discovered the presence of natural fullerenes on Earth. Interestingly, occurrence of fullerenes such as C_{60} and C_{70} was reported in shungite, a meta-anthracite coal from a deposit near Shunga, Russia (Buseck et al. 1992). The presence of C_{60} at very low concentrations in Cretaceous–Tertiary boundary sites in New Zealand was published (Heymann et al. 1994). Fullerenes (C_{60} and C_{70}) were found in a unit of shock-produced impact breccias (Onaping Formation) from the Sudbury impact structure in Ontario, Canada (Becker et al. 1994). The abundance of naturally occurring fullerenes was found in carbon materials, for example, coal, rocks, interstellar media, and even dinosaur eggs (Heymann et al. 2003).

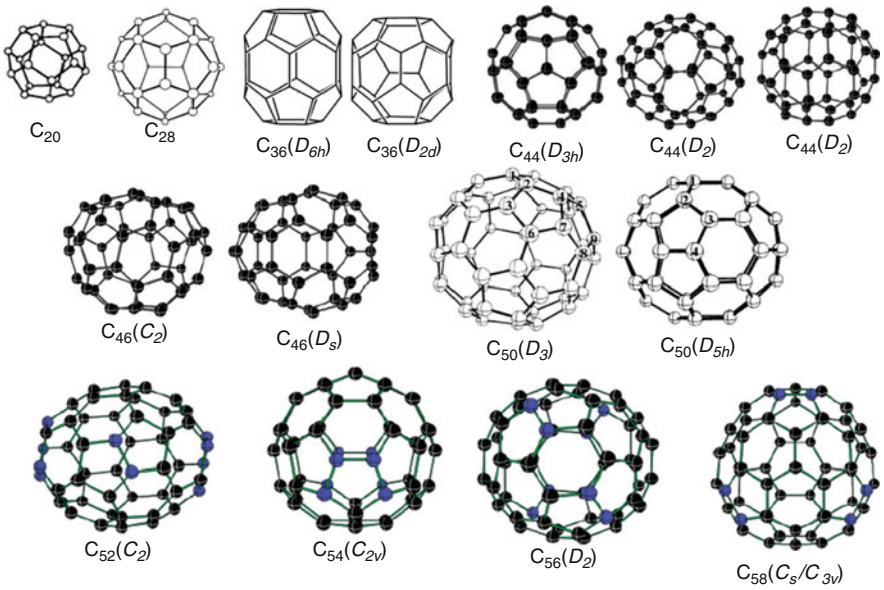

Fig. 11 Representative structures of smaller fullerenes and low-energy isomers are given for some of them. The pentagon–pentagon fusions are highlighted in blue color only for C_{52}, C_{54}, C_{56}, and C_{58}. The point groups are given in parentheses (Reprinted with permission from reference Lu and Chen (2005). Copyright 2005 American Chemical Society)

Fullerene Nano-capsules

In the area of fullerene science, one should not forget to mention an interesting property of holding the atoms or ions or molecules inside the fullerene cage (Thilgen and Diederich 2006). Fullerenes are potential nano-capsules. Experimental detection of the nano-capsules of fullerenes such as La@C_{60}, La@C_{70}, La@C_{74}, La@C_{76}, La@C_{78}, La@C_{82}, and Ce_2@C_{80} was reported (Kessler et al. 1997; Kubozono et al. 1996; Moro et al. 1993; Saunders et al. 1993; Thilgen and Diederich 2006; Yamada et al. 2005, 2010). Fullerenes are known in the field of radioactive chemistry/physics. Radioactive nuclear materials can be stored by encapsulating inside the fullerenes. U@C_{28}, Gd@C_{60}, and Gd@C_{82} are few examples of encapsulated radioactive materials (Guo et al. 1992; Kubozono et al. 1996). The stability of these metallic fullerenes could bring the new effective solution of the radioactive waste elimination. For the substance enclosed in the fullerene nano-capsule, carbon atoms act like a defense shield, and the fullerene containers are good for protecting their contents from water and acid. The structures, stabilities, and reactivities of encapsulated fullerenes (nano-capsules) and doped fullerenes have been the subject of theoretical interest (Guo et al. 1992; Lu et al. 2000; Park et al. 2005; Simeon et al. 2005; Wang et al. 2003; Wu and Hagelberg 2008; Zhao and Pitzer 1996). The closed-cage "fullerenes" or "heterofullerenes" can be placed inside the

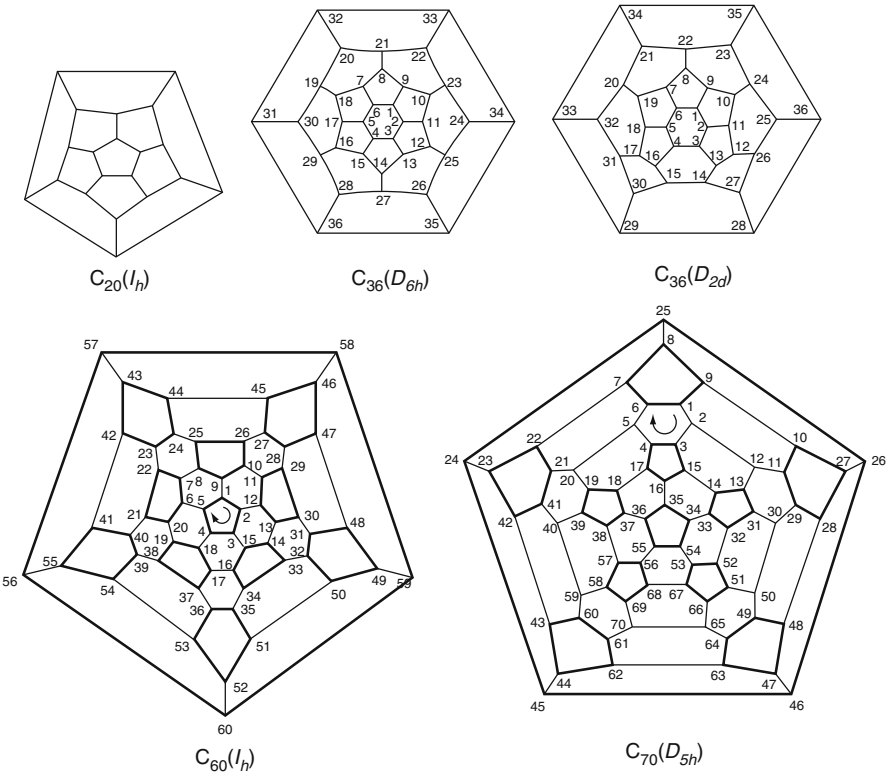

Fig. 12 Schlegel diagrams of C_{20}, C_{36}, C_{60}, and C_{70} fullerenes. The point groups are given in parentheses, systematic numbering recommended by IUPAC (Pictures were reprinted with permission from reference Thilgen and Diederich (2006). Copyright 2006 American Chemical Society. Reference Fowler and Heine (2001). Copyright 2001 Royal Society of Chemistry)

single-walled carbon nanotubes, for example, C_{60}@SWCNT (Hirahara et al. 2000; Okada 2007; Smith et al. 1999). Leszczynski and coworkers have explored the mechanism of the catalytic activity of fullerene derivatives using reliable computational methods (Sulman et al. 1999; Yanov et al. 2004). Fullerenes are certainly worthy of scientific study because of their unique shape and intriguing properties.

Isolated Pentagon Rule (IPR) in Fullerenes

A wide range of methods available for producing fullerenes concluded that C_{60} is the most abundant and is followed by C_{70} (Kadish and Ruoff 2002). The pristine C_{60} (I_h) contains two different C–C bonds: the one at the junction of two six-membered rings and the other one at the junction of a five- and a six-membered rings. These two bonds are usually labeled as a [6,6] and [5,6] C–C bonds, respectively. The pristine

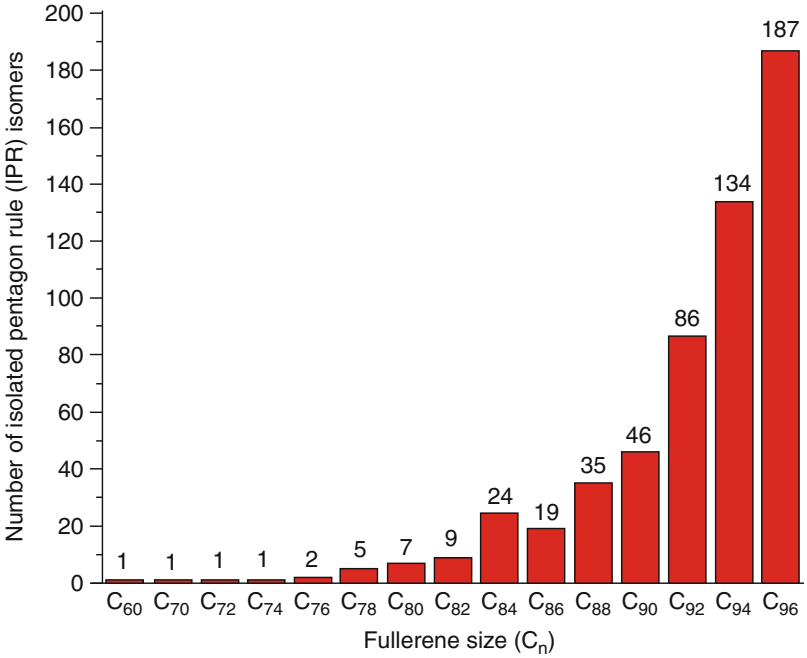

Fig. 13 Fullerene size versus number of isolated pentagon rule (*IPR*) isomers (The data was taken from reference Manolopoulos and Fowler (1992))

C_{70} (D_{5h}) has eight distinguishable C–C bonds. It has been known to chemists that energetically it is not favorable to have two pentagons sharing the same C−C bond. There are 1812 mathematical ways of forming a closed cage with 60 carbon atoms (isomers), but the buckminsterfullerene C_{60} (I_h) is the most special and stable because all of its pentagons are isolated by hexagons. This condition is called the "isolated pentagon rule" (IPR), which tends to make fullerenes more stable (Fowler and Manolopoulos 1995).

In fact, C_{60} is the smallest fullerene cage that obeys the isolated pentagon rule. Fullerenes C_{62}, C_{64}, C_{66}, and C_{68} do not satisfy the IPR. The next fullerene, which follows the IPR, is C_{70} (it has 8149 possible isomers). Also, C_{72} has an IPR structure. Most of the higher fullerenes have proven to follow IPR (Kroto 1987). Only one IPR-obeying isomer exists for C_{60} and for C_{70} (Fowler and Manolopoulos 1995), while the number of possible IPR isomers increases rapidly with increase in the size of the fullerenesas shown in Fig. 13. Fullerene C_{78} has five isomers that satisfy the IPR. Three isomers (two with C_{2v} and one with D_3 symmetry) out of these five were identified and characterized using ^{13}C NMR spectra (Kikuchi et al. 1992a). The fourth isomer (D_{3h}-C_{78}) has been recently separated and characterized in the form of $C_{78}(CF_3)_{12}$ (Shustova et al. 2006, 2007), and the last one has been synthesized using FVP technique (Amsharov and Jensen 2008). Theoretical study predicted that

C_{82} has nine IPR-satisfying isomers (Manolopoulos and Fowler 1991), out of which three isomers with C_2 symmetry were experimentally characterized using ^{13}C NMR spectroscopy, which gave 41 NMR lines with nearly equal intensity (Kikuchi et al. 1992a).

There are 24 geometric isomers satisfying IPR and 51,568 non-IPR isomers are possible for fullerene C_{84} (Fu et al. 2009). Earlier experimental ^{13}C NMR spectroscopy studies characterized two IPR isomers with D_2 and D_{2d} point groups (Kikuchi et al. 1992a; Taylor et al. 1993). Third isomer was also identified and reported (Achiba et al. 1995; Crassous et al. 1999). Pure D_2-C_{84} was synthesized (Dennis and Shinohara 1998). A theoretical study revealed that C_{84} cage is special in the family of fullerenes from C_{60} to C_{90} since the number of preferable isomers is larger than in the case of other fullerenes. The geometries of all of the 24 IPR isomers of fullerene C_{84} along with their point groups were reported (Okada and Saito 1996). Two IPR isomers of C_{86} out of possible 19 isomers were separated using multistage HPLC (high-performance liquid chromatography) (Miyake et al. 2000), and these two isomers were characterized to have C_2 and C_s point groups by ^{13}C NMR spectroscopy (Taylor et al. 1993). Burda et al. showed the experimental evidence for the photoisomerization of higher fullerenes. They confirmed thetheoretical prediction that C_{86} has less number of IPR-satisfying isomers (19 isomers) than C_{84} (24 isomers) (Fig. 14; Burda et al. 2002). Experimental studies based on ^{13}C NMR spectroscopy revealed that fullerenes C_{88} and C_{92} possess 35 and 86 IPR isomers, respectively, and HPLC was used to separate the isomers (Achiba et al. 1996; Miyake et al. 2000; Tagmatarchis et al. 2002). Computational methods

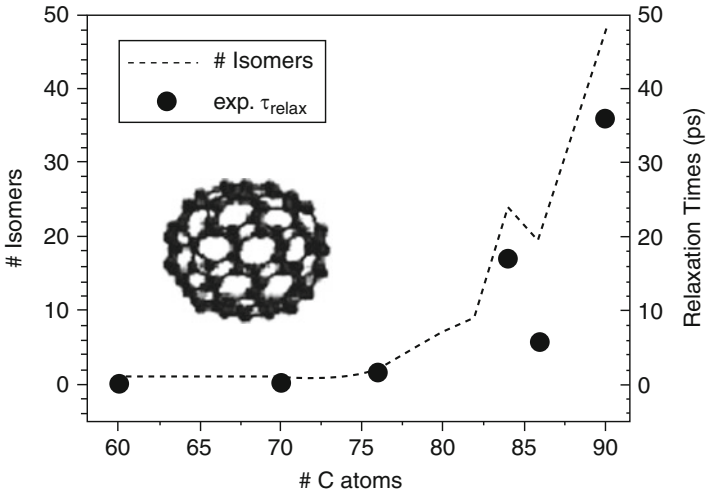

Fig. 14 Correlation between the number of isomers (*dotted line* as a visual guide) for each fullerene and the time constant for the formation of the lowest excited singlet state monitored at 550 nm (*dots*) (Reprinted with permission from reference Burda et al. (2002). Copyright 2002 American Chemical Society)

were used to calculate relative energies of the IPR isomers and the ^{13}C NMR spectra of fullerenes (Shao et al. 2006; Slanina et al. 2000a, b; Sun 2003). The computed ^{13}C NMR spectra were interpreted with the available experimental data (Beavers et al. 2006; Chaur et al. 2009a, b; Melin et al. 2007; Rojas et al. 2007; Scheina and Friedrich 2008; Shao et al. 2006; Slanina et al. 2000a, b; Sun 2003; Xie et al. 2004). Theoretical calculations predicted that C_{88} (**33**) is one of the most stable IPR isomers (Shao et al. 2006). The number provided in the parenthesis is the isomer number. In consistent to the theoretical prediction, Troyanov and Tamm reported the isolation and X-ray crystal structures of trifluoromethyl derivatives of C_{88} (**33**) and C_{92} (**82**) fullerene isomers complying with the isolated pentagon rule (Troyanov and Tamm 2009).

Rojas et al. showed the experimental evidence of the decreasing trend in the gas-phase enthalpy of formation and strain energy per carbon atom as the size of the cluster increases. Thus, the fullerenes become more stable as they become larger in size (Rojas et al. 2007). Interestingly, molecules encapsulated inside the carbon cages stabilize the fullerene isomers that violate IPR (Beavers et al. 2006; Fu et al. 2009; Thilgen and Diederich 2006). Several IPR and non-IPR endohedral fullerenes (single metal, di-metal, or tri-metal nitride encapsulated fullerenes) were isolated and characterized experimentally (Beavers et al. 2006; Chaur et al. 2009a, b; Fu et al. 2009; Melin et al. 2007; Thilgen and Diederich 2006), and their isolation motivated significant theoretical interest (Fu et al. 2009; Park et al. 2005; We and Hagelberg 2008). The structures and relative energies of the IPR isomers of buckybowls were examined using computational methods (Dinadayalane and Sastry 2003). Head-to-tail exclusion rule was proposed in explaining the stability of carbon cage structures that obey the IPR (Scheina and Friedrich 2008).

Fullerenes with less than 60 carbon atoms cannot have isolated pentagons and therefore they should be highly unstable and reactive. Xie et al. synthesized non-IPR D_{5h}-C_{50} fullerene, which is a little sister of C_{60}, by introduction of chlorine atoms at the most reactive pentagon–pentagon vertex fusions. They confirmed the D_{5h}-C_{50} structure by mass spectrometry, infrared, Raman, ultraviolet–visible, and fluorescence spectroscopic techniques (Xie et al. 2004). The report of novel small cage "Saturn-shaped" $C_{50}Cl_{10}$ structure encourages the possibility of obtaining other small non-IPR fullerenes and their derivatives. The investigations of the properties and applications of small fullerenes and their derivatives are now open.

Common Defects in Fullerenes

Stone and Wales examined rotation of C−C bonds in various fullerene structures using approximate Huckel calculations. The 90° rotation of C−C bond in fullerene is called Stone–Wales (SW) or "pyracylene" rearrangement (Fig. 15; Stone and Wales 1986). Austin et al. reported that 94 % of all fullerene C_{60} isomers can rearrange to buckminsterfullerene by SW transformation (Austin et al. 1995). The C_{78} cage represents the smallest fullerene in which SW rearrangement can give

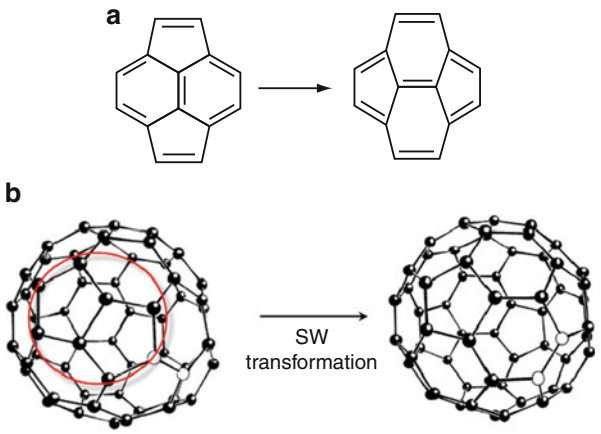

Fig. 15 (**a**) Stone–Wales or "pyracylene" transformation in fullerenes interchanges pentagons and hexagons; (**b**) Stone–Wales transformation of C_{2v} isomer of C_{60} with two adjacent pentagons gives the most stable I_h buckminsterfullerene; the C−C bond involved in 90° rotation is highlighted, and the two adjacent pentagons are marked in the fullerene structure in left-hand side

stable IPR isomers, C_{78}:5 (D_{3h}) ↔ C_{78}:3 (C_{2v}) ↔ C_{78}:2 (C_{2v}) ↔ C_{78}:4 (D_{3h}), where the numbers 5, 3, 2, and 4 indicate the isomer numbers (Austin et al. 1995). In case of higher fullerenes, the number of IPR isomers that can be transformed one into another by SW rearrangement considerably increases. For example, the SW transformation gives 9 and 21 stable IPR isomers for C_{82} and C_{84}, respectively (Fowler and Manolopoulos 1995). The SW transformation is usually thought to be the possible mechanism for achieving fullerene isomers (Austin et al. 1995; Fowler and Manolopoulos 1995; Stone and Wales 1986).

It was proposed that fullerenes can have seven-membered rings in addition to five- and six-membered rings (Taylor 1992). Troshin et al. isolated and characterized the C_{58} fullerene derivatives in which the cage structure contains the seven-membered ring. The structures were characterized using mass spectrometry, IR, and NMR spectroscopy (Troshin et al. 2005). Smalley and coworkers found that laser irradiation can fragment C_{60} into C_{58}, C_{56}, C_{54}, and other smaller cages with even number of carbon atoms via losing C_2 fragments (O'Brien et al. 1988). The formation of seven-membered rings was considered to play an important role in the fragmentation process of fullerenes (Murry et al. 1993). The laser desorption/ionization of products generated from the reactions of C_{60} with O_3 gives the odd-numbered clusters such as C_{59}, C_{57}, C_{55}, and C_{53} (Christian et al. 1992; Deng et al. 1993). Vacancy defects destroy the original topology of five- and six-membered rings in fullerenes (Christian et al. 1992; Deng et al. 1993; Hu and Ruckenstein 2003, 2004; Lee and Han 2004; Murry et al. 1993; O'Brien et al. 1988). They generate various sizes of rings such as four-, seven-, eight-, and nine-membered rings and also produce the new five- and six-membered rings depending on the number of carbon atom vacancies (Fig. 16; Christian et al. 1992; Deng et al.

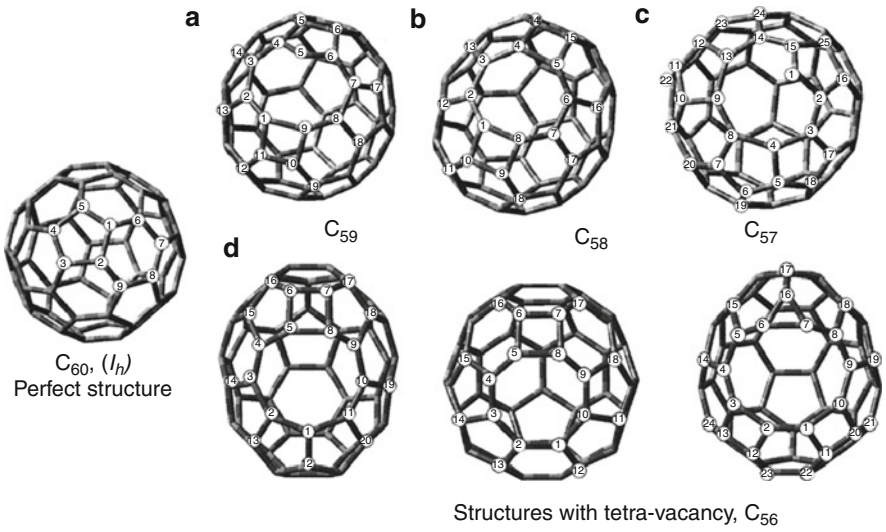

Fig. 16 Buckminsterfullerene (perfect structure); vacancy defect fullerenes generated from C_{60}: (**a**) mono-vacancy, (**b**) di-vacancy, (**c**) tri-vacancy, (**d**) three different structures of tetra-vacancy (Reprinted with permission from Hu and Ruckenstein (2004). Copyright 2004, American Institute of Physics)

1993; Hu and Ruckenstein 2003, 2004; Lee and Han 2004; Murry et al. 1993; O'Brien et al. 1988).

Carbon Nanotubes (CNTs)

Discovery and Classification of CNTs

Modern "nanotechnology revolution" was flourished by the discovery of fullerenes and has been escalating since the isolation of multi- and single-walled carbon nanotubes. The detection of carbon nanotubes by Iijima in 1991 is one of the landmarks in nanotechnology (Iijima 1991). In the interview to Nature Nanotechnology, Iijima told that the discovery of carbon nanotubes was unexpected but not entirely accidental because he had accumulated a lot of experience in looking at short-range order in carbon species such as amorphous carbon and very thin graphite sheets (Iijima 2007). The discovery of buckminsterfullerene by Kroto, Curl, Smalley, and coworkers motivated Iijima's interest in finding out new carbon allotropes (Kroto et al. 1985).

There are two structural forms of carbon nanotubes: multi-walled carbon nanotubes (MWCNTs) and single-walled carbon nanotubes (SWCNTs). The former one was reported by Iijima (1991). The SWCNTs were reported independently by Iijima as well as Bethune groups (Bethune et al. 1993; Iijima and Ichihashi 1993). The existence of carbon nanotubes was reported as early as 1952 and also in 1976

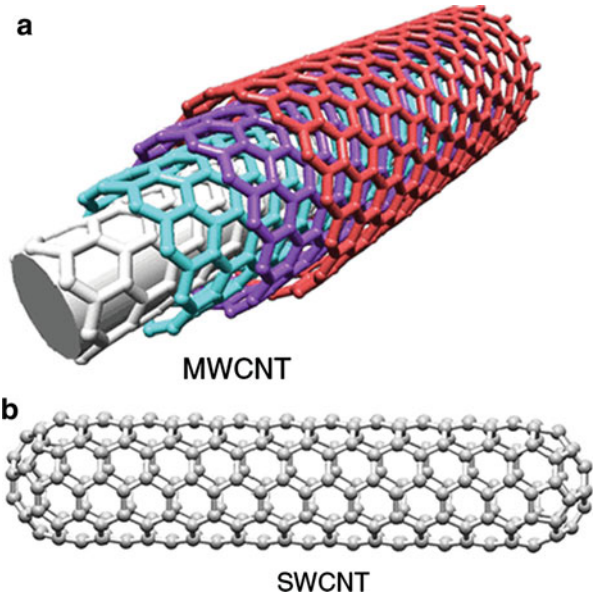

Fig. 17 Representative structures of (**a**) multi-walled and (**b**) single-walled carbon nanotubes

(Oberlin et al. 1976; Radushkevich and Lukyanovich 1952). However, those reports did not reach the wide range of scientific community because they were published in unpopular journals, and at that time, no fabrication process was known that would lead to the synthesis of macroscopic amounts of carbon nanotubes (Oberlin et al. 1976; Radushkevich and Lukyanovich 1952). Monthioux and Kuznetsov documented the history of carbon nanotube since 1952 (Monthioux and Kuznetsov 2006). Synthesis of carbon nanotube using coal pyrolysis was reported (Moothi et al. 2015).

High-resolution electron microscopy (HREM) images of the CNTs showed the resemblance of a "Russian doll" structural model that is based on hollow concentric cylinders capped at both ends. The model structures of multi-walled and single-walled carbon nanotubes are shown in Fig. 17. A wide range of methods, such as arc evaporation of graphite, laser ablation, chemical vapor deposition (CVD), vapor phase decomposition or disproportionation of carbon-containing molecules, etc., have been reported for the synthesis of multi-walled and single-walled carbon nanotubes (Dresselhaus et al. 2001). It remains unclear whether SWCNTs and MWCNTs are formed via the same mechanism. It is also unclear whether various methods used to produce carbon nanotubes are mechanistically consistent (Dresselhaus et al. 2001). For the transformation pathway, fullerenes are known to be a suitable carbon source for MWCNT growth under certain conditions (Suchanek et al. 2001). An ideal MWCNT consists of cylindrical tubes in which the neighboring tubes are weakly bonded through van der Waals forces. The MWCNT is incommensurate when each of its walls has its own chirality independent of other walls.

SWCNT, which is a one-dimensional (1D) system, can be considered as the conceptual rolling of a section of two-dimensional (2D) graphene sheet into a seamless cylinder forming the nanotube. The structure of SWCNT is uniquely described by two integers (n, m), which refer to the number of $\vec{a}_1$ and $\vec{a}_2$ unit vectors of the 2D graphene lattice that are contained in the chiral vector, $C_h = n\vec{a}_1 + m\vec{a}_2$. The chiral vector determines whether the nanotube is a semiconductor, metal, or semimetal. From the (n, m) indices, one can calculate the nanotube diameter (d_t), the chirality or chiral angle (θ), the electronic energy bands, and the density of electronic states. The nanotube diameter (d_t) determines the number of carbon atoms in the circular cross section of the nanotube shell, one atom in thickness (Saito et al. 1998). The tube diameter and chiral angle can be written in terms of (n, m) as

$$\text{Tube diameter, } d_t = \left(\sqrt{3}/\pi\right) \; a_{cc}\left(\sqrt{m^2 + mn + n^2}\right).$$

$$\text{Chiral angle, } \theta = \tan^{-1}\left\{\sqrt{3}\; m/\left(2n + m\right)\right\},$$

where a_{cc} is the nearest-neighbor carbon atom distance of 1.421 Å.

Among the large number of possible C_h vectors, there are two inequivalent high-symmetry directions. These are termed "zigzag" and "armchair" and are designated by (n,0) and (n,n), respectively. Either achiral (armchair and zigzag) or chiral SWCNTs can be constructed depending on the orientation of the six-membered rings with respect to the nanotube axis. Schematic representation of the structures of armchair, zigzag, and chiral SWCNTs is shown in Fig. 18. Theoretical studies in 1992 predicted that the electronic properties of "ideal" SWCNTs depend on the width and chirality of the tubes (Hamada et al. 1992; Mintmire et al. 1992; Saito et al. 1992). The electronic properties of an SWCNT vary in a periodic way between being metallic and semiconductor. SWCNTs are metals if (n−m)/3 represent an integer; otherwise, they are called semiconductors (Dresselhaus et al. 2002).

Several metallic (n, m) nanotubes have almost the same diameter d_t (from 1.31 to 1.43 nm), but have different chiral angles: $\theta = 0$, 8.9, 14.7, 20.2, 24.8, and 30.0° for nanotubes (18, 0), (15, 3), (14, 5), (13, 7), (11, 8), and (10, 10), respectively (Dresselhaus et al. 2002). Few people realize that CNTs constitute a large family with a wide variety of sizes and properties, which are determined by their structure and composition, including chirality, number of walls, ordering of the wall, defects, surface functionalization, and other features.

Strano sorted out chiral SWCNTs into left-handed and right-handed tubes (Strano 2007). Significant progress has been made in the area of carbon nanotubes. Scientists are able to disperse, identify, sort, and now also isolate various types of carbon nanotubes (Arnold et al. 2006; Peng et al. 2007; Strano 2003, 2007). Specific methods were found to grow long SWCNTs and control the nanotube diameters (Lu et al. 2008; Zhang et al. 2008). Controlled synthesis of nanotubes

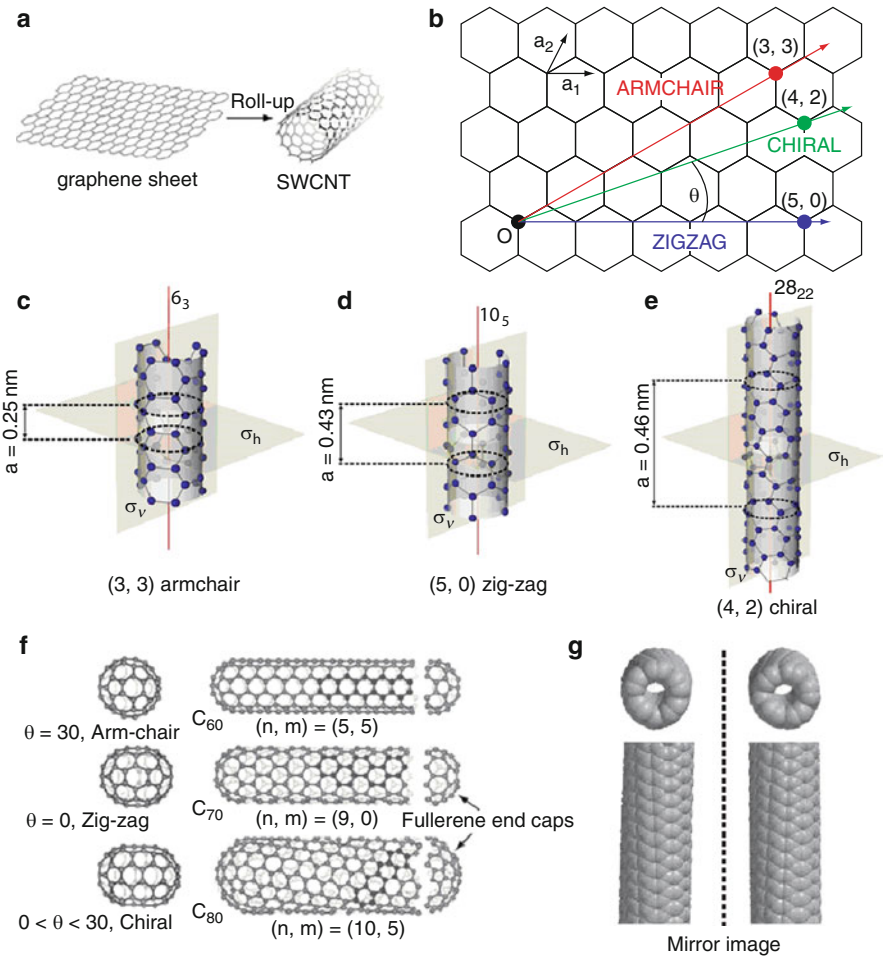

Fig. 18 (**a**) The roll-up of graphene sheet into SWCNT; (**b**) picture shows how to roll up graphene sheet to generate three different types of SWCNTs; (**c**) (3,3) armchair SWCNT; (**d**) (5,0) zigzag SWCNT; (**e**) (4,2) chiral SWCNT; (**f**) three types of SWCNTs (armchair, zigzag, and chiral) with fullerene end caps. These can be viewed as the growth of SWCNTs by adding several layers of hexagonal rings at the middle of different fullerenes; (**g**) mirror image of the chiral SWCNT; the structures (**c**), (**d**), and (**e**) are given exactly same types of SWCNTs that are mentioned in (**b**). In (**c**)–(**e**), σ_v and σ_h indicate the vertical plane of symmetry and horizontal plane of symmetry, respectively. Further, in these three structures, the *red line* is the axis of rotation; the distance of one unit cell for these three types of SWCNTs is provided; the number of carbon atoms (x) in each layer and the number of layers (y) required for one unit cell is given as x_y, for example, – 6_3 means six carbon atoms in each layer and three layers required for one unit cell of (3,3) armchair SWCNT (Pictures (**b**) and (**g**) were reprinted with permission from Macmillan Publishers Ltd.: Nature Nanotech., reference Strano (2007), Copyright 2007)

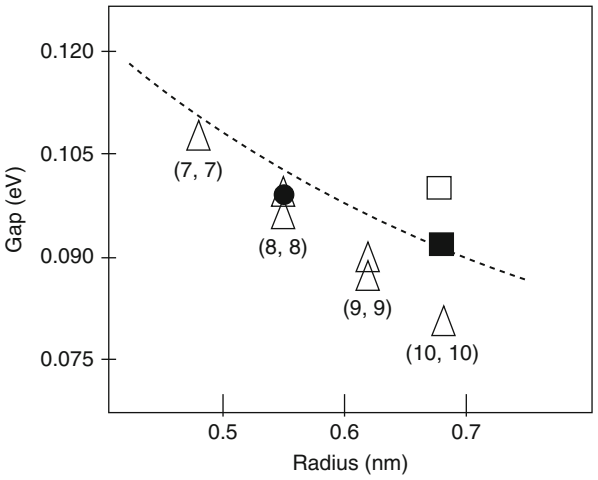

Fig. 19 Tube radius versus observed band gap. Each experimental data point (Δ) represents an average gap value measured on a distinct (*n*,*n*) tube. Theoretical results (*solid square*, *open square*, and *solid circle*) are also shown for comparison (Reprinted with permission from reference Ouyang et al. (2002). Copyright 2002 American Chemical Society)

opens up exciting opportunities in nanoscience and nanotechnology (Dai 2002). A range of methods was found for effective separation of metallic and semiconducting SWCNTs. Although some synthetic procedures have been known, they are not easy methods for synthesizing bulk quantities of metallic and semiconducting SWCNTs (Zhang et al. 2008). Scientists succeeded the preferential growth of SWCNTs with metallic conductivity (Rao et al. 2009a).

Raman and electronic spectroscopy techniques are useful in characterizing metallic and semiconducting SWCNTs. The radial breathing mode (RBM) in Raman spectra of SWCNTs is helpful in determining the diameter and chiral indices (*n*, *m*) of the nanotubes (Dresselhaus et al. 2002, 2005, 2007; Harutyunyan et al. 2009; Rao et al. 2009a). Experimental resultspointed out decreasing band gap with increasing radius of the armchair SWCNTs (Fig. 19; Ouyang et al. 2002). Another breakthrough in carbon nanotube chemistry was accounted by Zhang and Zuo, who have determined a quantitative atomic structure of MWCNT containing five walls with diameter ranging from 17 to 46 Å and the C−C bond lengths of individual SWCNTs using electron diffraction technique (Zhang and Zuo 2009). Their results indicate that there are three different bond lengths in chiral walls and two different bond lengths in achiral walls (Zhang and Zuo 2009). Electron diffraction technique was used in determination of atomic structure of SWCNTs and the chiral indices (*n*,*m*) of CNTs (Jiang et al. 2007; Qin 2007). Rao et al. have revealed the efficient growth of SWCNTs of diameter 1–3 nm from diamond nanoparticles and fullerenes (Rao et al. 2009b). Recently, experimental reports are available to create three-dimensional graphene-CNT hollow fibers with radially aligned CNTs seamlessly sheathed by a cylindrical graphene layer through a

one-step chemical vapor deposition using an anodized aluminum wire template for efficient energy conversion and storage (Xue et al. 2015; Yu et al. 2014; Zhu et al. 2012).

SWCNTs have stimulated vast interest due to their unique structural, mechanical, electronic, thermal, and chemical properties and their potential applications in diversified areas. There has been enormous growth in patents related to carbon nanotubes, fuelled by predictions that the market for nanotubes will be $9 billion by 2020. Between 1994 and 2006, it was estimated that 1865 nanotube-related patents were issued in the USA. Still, there is a cumulative backlog of more than 4500 patent applications relevant to CNT as reported in 2008 (MacKenzie et al. 2008).

Since there are reports of the natural abundance of fullerenes (Becker et al. 1994; Buseck et al. 1992; Heymann et al. 1994, 2003), the issue of the natural occurrence of carbon nanotubes has also attracted the attention of researchers. In 2004, TEM images that appear to be MWCNTs isolated from a Greenland ice core were reported (Esquivel and Murr 2004). The images of hollow carbon fibers from oil-well samples were reported (Velasco-Santos et al. 2003). However, we do not have any evidence for naturally occurring SWCNTs.

Various Defects in Carbon Nanotubes

Carbon nanotubes are not as perfect as they were thought to be earlier. Defects such as pentagons, heptagons, Stone–Wales defects, vacancies, adatoms, and dopants can occur in the nanotube during the growth or in processing and handling of the CNTs (Charlier 2002). Figure 20 depicts different types of defects in SWCNTs. Heptagon defects are found to play a crucial role in the topology of nanotube-based molecular junctions, for making X and Y type nanotube connections (Menon and Srivastava 1997). Long ago, theoretical studies proposed that pentagon–heptagon pair can be found in the intramolecular junctions of two SWCNT segments of different chiralities (Fig. 20d; Charlier et al. 1996; Chico et al. 1996). Experimental study revealed that ion irradiation-induced defects in the SWCNTs and the dangling bonds produced by irradiation are rapidly saturated (Chakraborty et al. 2007).

Low-energy electron and photon also induce damage in SWCNTs. The defect formation in SWCNTs is strongly dependent on the nanotube diameter, suggesting that the curvature-induced strain energy plays a crucial role in the damage (Suzuki and Kobayashi 2007). The defect formation and healing are reversible processes (Berthe et al. 2007; Suzuki and Kobayashi 2007). The defects in the SWCNTs affect their electronic, optical, and chemical properties. A competition between the defect formation and healing at room temperature or even below was reported. Raman spectroscopy, electrical measurements, and photoluminescence (PL) spectroscopy were used to examine the defect formation. However, the type of defects was not confirmed. Chemically stable topological defect, Stone–Wales defect, was ruled out because the activation energy for the defect healing was quite small (1 eV). Low-energy electron and photon can break C−C bonds in SWCNTs, as it was concluded

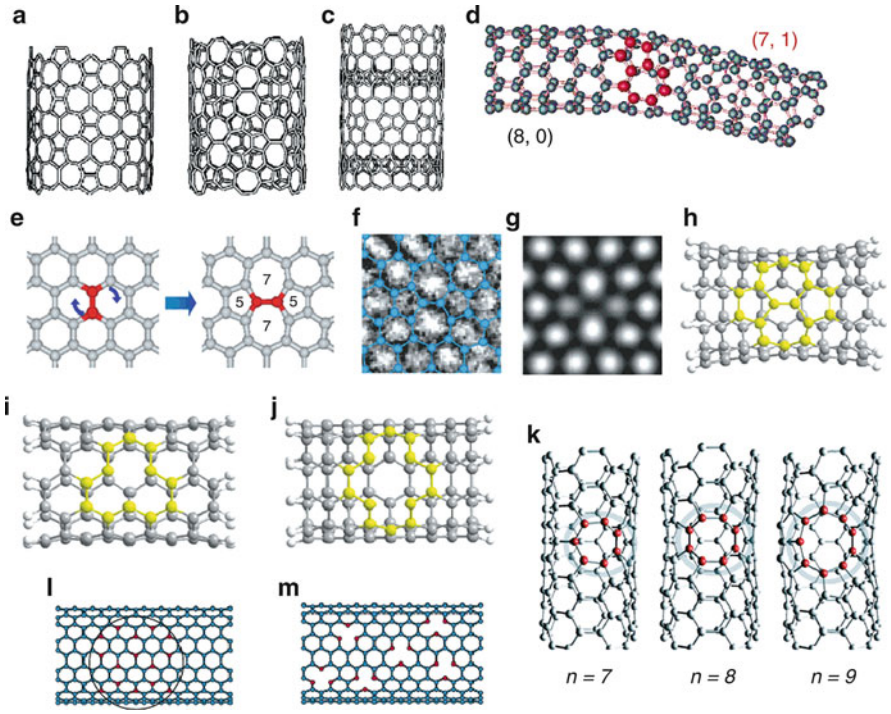

Fig. 20 (**a**) to (**c**) Nonchiral Haeckelite nanotubes of similar diameter; (**b**) nanotube segment containing only heptagons and pentagons paired symmetrically. (**b**) Nanotube segment exhibiting repetitive units of three agglomerated heptagons, surrounded by alternating pentagons and hexagons. (**c**) Nanotube segment containing pentalene and heptalene units bound together and surrounded by six-membered rings. (**d**) Atomic structure of an (8,0)-(7,1) intermolecular junction; the large red balls denote the atoms forming the pentagon–heptagon pair. (**e**) The SW transformation leading to the 5-7-7-5 defect, generated by rotation of a C−C bond in a hexagonal network. (**f**) HRTEM image obtained for the atomic arrangement of the SW defect. (b) Simulated HRTEM image for the model shown in (**f**). (**h**) (5,5) armchair SWCNT with a Stone–Wales defect. (**i**) Ideal single-vacancy defect in (5,5) armchair SWCNT. (**j**) Ideal double-vacancy defect in (5,5) armchair SWCNT. (**k**) Defect (5,5) SWCNT with seven ($n = 7$)-, eight ($n = 8$)-, and nine ($n = 9$)-membered rings. (**l**) SWCNT doped with boron [B atoms are bonded to three C atoms; B in *red spheres* and C in *blue spheres*]. (**m**) SWCNT doped with nitrogen [N atoms are bonded to two C atoms; N in *red spheres* and C in *blue spheres*] (Pictures (**a**)–(**d**), (**l**), and (**m**) were reprinted with permission from reference Charlier (2002). Copyright 2002 American Chemical Society. Pictures (**e**)–(**g**) were reprinted with permission from Macmillan Publishers Ltd.: Nature, reference Suenaga et al. (2007), copyright 2007. Pictures (**h**–**j**) were reprinted with permission from reference Yang et al. (2006a). Copyright 2006 American Chemical Society. Picture (**k**) was reprinted with permission from Nishidate and Hasegawa (2005). Copyright 2005 by the American Physical Society)

based on energetic criterion. Thus, the experimental study proposed that the defects may be a vacancy and an adatom (Suzuki and Kobayashi 2007).

The Stone–Wales defect is one of the important defects in carbon nanotubes. Stone and Wales showed that a dipole consisting of a pair of five- and seven-membered rings could be created by 90° rotation of a C−C bond in a hexagonal

network (Stone and Wales 1986). Such a dipole was later called Stone–Wales defect. SW transformation is thought to play an important role during the growth of carbon nanotubes. Miyamoto et al. reported an unambiguous identification of SW defect in carbon and boron nitride nanotubes using photoabsorption and vibrational spectroscopy (Miyamoto et al. 2004). Experimental vibrational frequency of 1962 cm^{-1} was reported to be a signature in identifying SW defect in carbon nanotube (Miyamoto et al. 2004). Identifying and characterizing topological defects in SWCNTs are highly challenging tasks. A powerful microscope with high resolution and high sensitivity is required for characterizing the topological defects in CNTs. Using HRTEM, the first direct image of the pentagon–heptagon pair defect (Stone–Wales defect) in the SWCNT was reported (Suenaga et al. 2007). Computational studies examined the structures and defect formation energies of the SWCNTs with defects containing different sizes of rings (seven-, eight-, and nine-membered rings) (Nishidate and Hasegawa 2005) and different types of defects (Amorim et al. 2007; Dinadayalane and Leszczynski 2007a, b; Ding 2005; Wang et al. 2006; Yang et al. 2006a, b).

Computational Approaches Used to Study Carbon Nanostructures: An Overview

Theory and computation play an important role in understanding structures and reactivity of carbon nanosystems such as graphene, fullerenes, and carbon nanotubes. Computational nanoscience often complements the experiments and is very useful for the design of novel carbon nanomaterials as well as predicting their properties. Theory is helpful in obtaining knowledge on the mechanism of reactions and fragmentations of carbon clusters. Thus, we provide an overview of the computational approaches employed to study various carbon nanostructures in this chapter. Carbon nanostructures are very large systems. Hence, performing very high-level quantum chemical calculations is not possible even when using modern supercomputers.

Many-body empirical potentials, empirical tight-binding molecular dynamics, and local density functional (LDF) methods were used to perform electronic structure calculations of carbon nanosystems including fullerenes and model CNTs in early of the last decade (Robertson et al. 1992; Zhang et al. 1993). In the mid-1990s, electronic structure calculations for large fullerenes with I_h point group were performed using Huckel approximation (Tang and Huang 1995). In the late 1990s, scientists performed geometry optimizations for large fullerenes using molecular mechanics (MM3), semiempirical methods (MNDO (Dewar and Thiel 1977), AM1 (Dewar et al. 1985) and PM3 (Stewart 1989)), and Semi-Ab Initio Model 1 (SAM1) (Dewar et al. 1993). The single-point energy calculations were affordable at that time using ab initio Hartree–Fock (HF) method in combination with small basis sets such as 3-21G and 4-31G (Slanina et al. 1997). The computing power has been tremendously increasing since 2000. Thus, currently theoreticians enjoy investigating medium-sized molecules using reliable quantum chemical methods

and exploring carbon nanoclusters beyond molecular mechanics and semiempirical methods.

The popular B3LYP functional, which is a combination of Becke's three-parameter (B3) (Becke 1993) hybrid functional incorporating exact exchange with Lee, Yang, and Parr's (LYP) (Lee et al. 1988) correlation functional, has been employed with small- and medium-sized basis sets like STO-3G, 3-21G, 4-31G, and 6-31G(d) for calculations on fullerenes and carbon nanotubes (Bettinger et al. 2003; Dinadayalane and Leszczynski 2007b; Feng et al. 2005; Matsuo et al. 2003; Yumura et al. 2005a, b; Zhou et al. 2004). Computational studies indicate that the B3LYP functional can yield reliable answers for the properties of carbon compounds and carbon nanostructures (Bettinger et al. 2003; Dinadayalane and Leszczynski 2007b; Feng et al. 2005; Matsuo et al. 2003; Yumura et al. 2005a, b; Zhou et al. 2004). PBE1PBE/6-311G(d) level has been used for calculating relative energies and ^{13}C NMR spectra of fullerene isomers (Shao et al. 2006, 2007). The PBE1PBE functional was concluded to be very reliable DFT functional since it yields the same relative energy ordering as the high-level coupled cluster calculations for the top three isomers of C_{20} (cage, bowl, and ring isomers) (An et al. 2005).

In comparison with ab initio MP2 or CCSD methods, DFT is less time-consuming and computationally feasible for large carbon nanosystems. For studying chemical reactivity in fullerenes and nanotubes, ONIOM approach is more cost-effective than treating the whole molecule with DFT. ONIOM is a hybrid methodology in which the molecule is partitioned into two or more fragments. The most important part (one fragment) of the molecule is treated with high-level method, and the other parts are treated with low-level methods (Maseras and Morokuma 1995; Morokuma et al. 2006; Osuna et al. 2009). The performance of ONIOM approach by taking different density functional theory levels was examined against the experimental results for the Diels–Alder reaction between cyclopentadiene and C_{60} (Osuna et al. 2009). Two-layer ONIOM approach ONIOM(B3LYP/6-31G(d):AM1), where B3LYP/6-31G(d) and AM1 are used for high and low layers, was utilized to study chemisorption of alkoxide ions with the perfect and Stone–Wales defective armchair (5,5) SWCNTs of cap-ended and H-terminated structures (Wanbayor and Ruangpornvisuti 2008).

Independent theoretical studies considered DFT methods in investigating the structures and properties of SWCNTs (Akdim et al. 2007; Amorim et al. 2007; Andzelm et al. 2006; Bettinger 2005; Dinadayalane and Leszczynski 2007a, b; Govind et al. 2008; Lu et al. 2005; Nishidate and Hasegawa 2005; Robertson et al. 1992; Wang et al. 2006; Yang et al. 2006a, b; Zhang et al. 1993). The B3LYP functional with double-ζ basis set was often employed to investigate the electronic structures of pristine and defective SWCNTs and also the influence of defects on functionalization of SWCNTs (Akdim et al. 2007; Andzelm et al. 2006; Dinadayalane and Leszczynski 2007b; Govind et al. 2008; Lu et al. 2005). Sometimes, more than one basis set was utilized for exploration of defective SWCNTs and the viability of metal adsorption in the defect tubes (Yang et al. 2006b). DFT with periodic boundary condition (PBC) as implemented in Gaussian 03 program package (Frisch et al. 2003) was used to examine the reactivity of

Stone–Wales defect in (5,5) and (10,0) SWCNTs (Bettinger 2005). The unit cell should be carefully chosen for the calculations involving PBC in order to simulate the tubes of infinite length. Popular DFT methods fail to provide reliable answers for π–π interactions involving fullerenes and other carbon clusters (Cuesta et al. 2006; Kar et al. 2008; Shukla and Leszczynski 2009). Although calculations at the MP2 and CCSD(T) levels are required to obtain very reliable results for π-stacking interactions (Dinadayalane et al. 2007a; Lee et al. 2007; Sinnokrot and Sherrill 2004), they are not possible for such large systems with current computational facilities. Recently developed meta-hybrid density functional (M06-2X) has been reported to be a promising functional to calculate the binding energies for π–π interactions involving large carbon nanostructures (Zhao and Truhlar 2007, 2008).

Using powerful supercomputers, performing static and dynamic calculations at high-level ab initio and DFT methodologies is affordable for graphene and carbon nanotubes. Very recently, density functional theory (PBE functional, Perdew et al. 1996) calculations with plane-wave basis sets and periodic boundary conditions (PBCs) were employed to understand small-molecule interactions with the defective graphene sheets (Jiang et al. 2009). Vienna ab initio simulation package (VASP) has been used in several studies to perform static and dynamic calculations (Kresse and Furthmuller 1996a, b). Theoretical calculations are helpful to understand the electronic structure of graphene sheets and SWCNTs and their viability as ion separation systems and gas sensors (Jiang et al. 2009; Li et al. 2009b; Nishidate and Hasegawa 2005). The Stone–Wales defect formation energy for graphene and CNTs was calculated using DFT, invoking the local density approximation to the exchange-correlation potential as implemented in VASP (Ertekin et al. 2009).

The mechanical properties of CNTs have been investigated by theoreticians for the last two decades (Avila and Lacerda 2008; Chandra et al. 2004; Dereli and Sungu 2007; Yakobson et al. 1996). An array of methods has been employed for computing the Young's modulus of MWCNTs and different types of SWCNTs (armchair, zigzag, chiral). A wide range of Young's modulus values has been reported in the literature (Avila and Lacerda 2008; Chandra et al. 2004; Dereli and Sungu 2007; Mielke et al. 2004; WenXing et al. 2004; Yakobson et al. 1996). Most of the molecular dynamics methods used so far are classical or tight binding (Avila and Lacerda 2008; Chandra et al. 2004; Dereli and Sungu 2007; WenXing et al. 2004; Yakobson et al. 1996). Quantum chemical calculations on mechanical properties of carbon nanotubes or graphene sheets are scarce since they are still highly time-consuming (Mielke et al. 2004). It is not of our interest to discuss mechanical properties in this chapter since there are many papers and some of classic reviews on this subject available (Avila and Lacerda 2008; Chandra et al. 2004; Dereli and Sungu 2007; Mielke et al. 2004; WenXing et al. 2004; Yakobson et al. 1996). DFT and DFT-D approaches were used to study single and multiple Na adsorption and diffusion on graphene (Malyi et al. 2015). By using DFT and time-dependent DFT methods, one can obtain IR, Raman, NMR, and UV spectra. Recent advances in computer hardware and ab initio electronic structure methods have brought a substantial improvement in the capabilities of quantum chemists to predict and study the properties of carbon nanostructures. However, the application of state-of-the-art

quantum chemical methods to study the structures and properties of large carbon nanoclusters (graphenes, fullerenes, and CNTs) is still a great challenge.

Structural, Electronic, and Chemical Properties of Graphene, Fullerenes, and SWCNTs

Graphene

An experimental investigation of mechanical properties of monolayer graphene reported a breaking strength of 40 N/m and the Young's modulus of 1.0 TPa (Lee et al. 2008). Graphene displays a thermal conductivity of 5000 $Wm^{-1}K^{-1}$ at room temperature (Balandin et al. 2008). Graphene chemistry is expected to play an important role in producing graphene-based materials. Computational study using the density functional theory with generalized gradient approximation revealed the cooperative effects of degenerate perturbation and uniaxial strain on band gap opening in graphene. Furthermore, the band gap width could be continuously tuned by controlling the strain (Jia et al. 2016). In this chapter, we outline the Stone–Wales defect in graphene, chemisorption process (covalent functionalization) on graphene, and the influence of defects on chemisorption; particular interest is given to hydrogen chemisorption. Chemical functionalization in graphene should produce new 2D systems with distinct electronic structures and different electrical, optical, and chemical properties. Chemical changes can probably be induced even locally. The first known example of hydrogenated graphene is graphane, which is a 2D hydrocarbon with one hydrogen atom attached to every site of the honeycomb lattice (Elias et al. 2009; Sofo et al. 2007).

Stone–Wales defect is expected to enhance the tendency of graphitic layers to roll up into other carbon nanostructures such as fullerenes and nanotubes. Therefore, in-depth understanding of Stone–Wales defect in graphene is required. It is known that pentagons and heptagons induce curvature in graphitic materials. In perfect graphene, the equilibrium C−C bond length is reported as 1.42 Å using PBE functional with the plane-wave code CPMD (Hutter et al.). Further details of the calculations can be obtained from the paper of Ma et al. (2009). The C−C bond shared by two heptagons of the SW defect in graphene is compressed to 1.32 Å using the same method. Density functional theory and quantum Monte Carlo simulations reveal that the structure of the SW defect in graphene is not simple. Ma et al. systematically studied the polycyclic hydrocarbon size dependence on the structural distortion caused by the Stone–Wales defect formation. They considered different systems ranging from the smallest analog of SW defect, azupyrene ($C_{16}H_{10}$), to 1D tape-like structure of $C_{50}H_{28}$ and, finally, to 2D planar cluster of $C_{228}H_{38}$. As known earlier, azupyrene is planar. The optimized bond length of the C−C bond at the center of azupyrene is 1.38 Å, which is longer than the corresponding C−C bond length of 1.32–1.33 Å observed for the SW defect in graphene (Ma et al. 2009).

Large carbon clusters exhibit a tendency to buckle upon the creation of SW defects. Vibrational frequency calculations of the flat graphene sheet with the Stone–

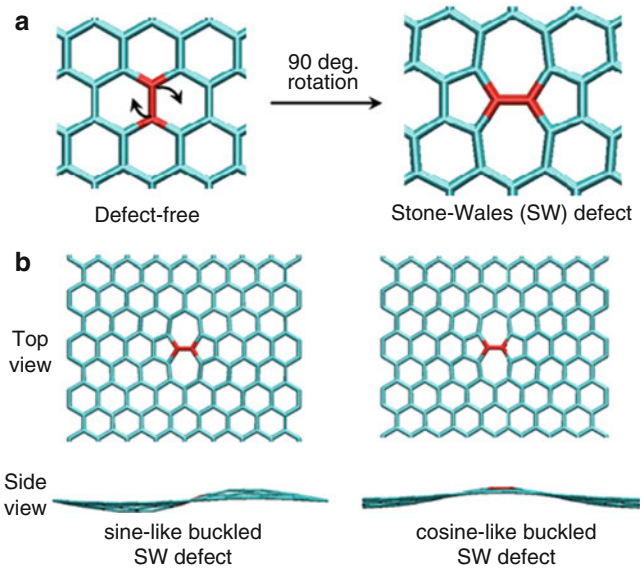

Fig. 21 (**a**) Stone–Wales transformation by 90° rotation of C–C bond in graphene sheet; (**b**) *top* and *side* views of sine-like and cosine-like buckled SW defect graphene sheets (The pictures were reprinted with permission from Ma et al. (2009)). Copyright 2009 by the American Physical Society)

Wales defect reveal that the structure is not a local minimum, but instead has two imaginary frequencies. The true minimum is a sine-like structure in which the C−C bond at the defect core is 0.01 Å longer than in the flat defect. Furthermore, many C−C bonds are slightly elongated in the buckled structure compared to the flat defect structure. The cosine-like SW defect structure was obtained as a transition state connecting to sine-like SW defect structure. The optimized structures of sine-like and cosine-like SW defect graphenes are depicted in Fig. 21. Vibrational frequencies also revealed that the maximum phonon frequencies corresponding to the stretch of the rotated C−C bond for the flat and buckled SW structure are 1880 and 1774 cm^{-1}, respectively. The corresponding frequency computed for perfect graphene is 1612 cm^{-1} (Ma et al. 2009). Theoretical study pointed out that for a graphene sheet of $C_{228}H_{38}$ containing a SW defect, the sine-like buckled structure becomes more stable (by ∼10 meV) than the flat SW defect (Ma et al. 2009).

Hydrogenation of Graphene With and Without Defects

Chemical modification of graphene has been less explored (Geim and Novoselov 2007). Attachment of atomic hydrogen to each site of the graphene lattice to create graphane is an elegant idea (Sofo et al. 2007). As a result, the hybridization of carbon atoms changes from sp^2 to sp^3, thus removing the conducting p-bands and

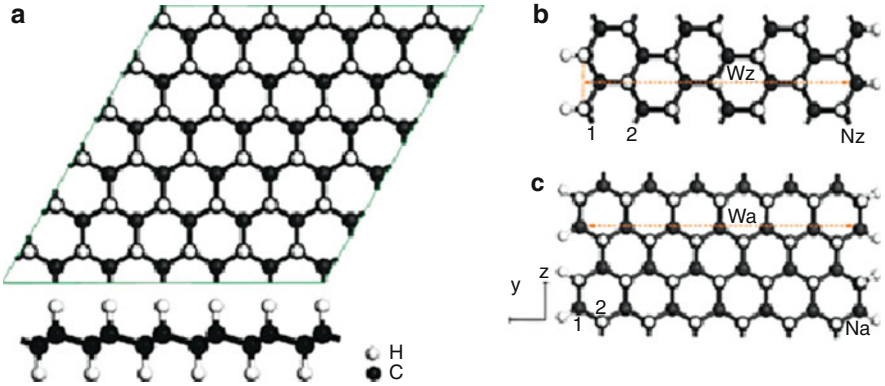

Fig. 22 (**a**) Top (*upper*) and side (*lower*) view of a 2D graphane layer. Geometric structures of the (**b**) 7 zigzag and (**c**) 13 armchair graphane nanoribbons. The ribbons are periodic along the z direction. The ribbon widths are denoted by W_z and W_a, respectively (Reprinted with permission from reference Li et al. (2009b)). Copyright 2009 American Chemical Society

opening energy gap (Boukhvalov et al. 2008; Sofo et al. 2007). In experiment, the fully hydrogenated graphene called "graphane" was produced by exposing graphene to hydrogen plasma discharge. Raman spectroscopy and transmission electron microscopy confirmed the reversible hydrogenation of single-layer graphene (Elias et al. 2009).

The structural and electronic properties of graphane were investigated using DFT PW91 functional with plane-wave basis set applying periodic boundary conditions as implemented in VASP (Li et al. 2009b). Computations revealed that hydrogenation of graphene nanoribbon is experimentally viable and the electronic properties of graphane are completely different from graphene nanoribbons. Figure 22 depicts the structures of graphane. Two types of graphane nanoribbons (zigzag and armchair edge) can be obtained by cutting the optimized graphane layer. The edge carbon atoms were all saturated with H atoms to avoid the effects of dangling bonds. The bond lengths of edge C−C and C−H bonds are almost as the inner C−C (1.52 Å) and C−H (1.11 Å) bonds. The calculated C−C bond length is similar to the bond length of 1.53 Å in diamond (sp^3 carbon atoms) and is longer than 1.42 Å characteristic of sp^2 carbon in graphene. Both spin-unpolarized and spin-polarized computations yielded same energy for ground-state graphane nanoribbons (Li et al. 2009b).

Figure 23a shows that computed band gap decreases monotonically with increasing ribbon width for both zigzag and armchair nanoribbons. Graphane nanoribbons are semiconductors. The formation energy increases with increasing ribbon width (Fig. 23b) irrespective of the type, indicating that narrow ribbons are more likely to form than the wider ribbons (Li et al. 2009b). Sofo et al. investigated the structures, formation energies, and vibrational frequencies of graphane using DFT with plane-wave basis set (Sofo et al. 2007). They found two favorable conformations of

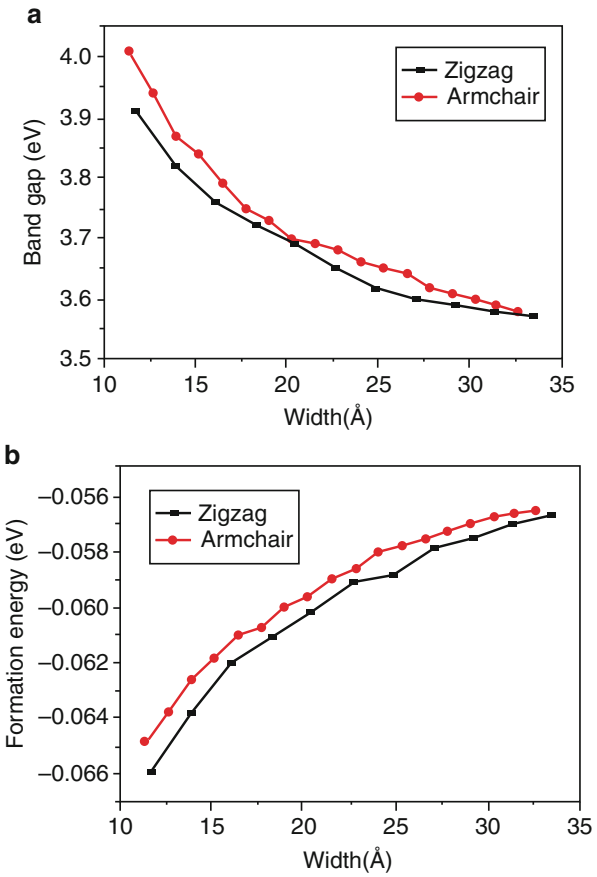

Fig. 23 Variation of the band gap (**a**) and the formation energy (**b**) of zigzag ($6 \leq Nz \leq 16$) and armchair ($10 \leq N_z \leq 27$) graphane nanoribbons as a function of ribbon width. N is the number of zigzag chains for a zigzag ribbon and the number of dimer lines along the ribbon direction for an armchair ribbon (Reprinted with permission from reference Li et al. (2009b). Copyright 2009 American Chemical Society)

graphane: chair-like conformer with the hydrogen atoms alternating on both sides of the plane and the boat-like conformer with the hydrogen atoms alternating in pairs. Chair conformer has one type of C−C bond (1.52 Å), while boat conformer possesses two different types of C−C bonds (bond lengths of 1.52 Å and 1.56 Å). The boat conformer is less stable than the chair conformer due to the repulsion of the two hydrogen atoms bonded to first-neighbor carbon atoms on the same side of the sheet. This repulsion results in slightly longer C−C bonds in boat conformer. Calculated C−H bond stretching frequencies are 3026 cm^{-1} and 2919 cm^{-1} for the boat and chair conformers, respectively. These C−H stretching modes are IR active, and they should be useful in characterizing these two types of conformers of graphane (Sofo et al. 2007). Molecular dynamics (MD) simulations using adaptive

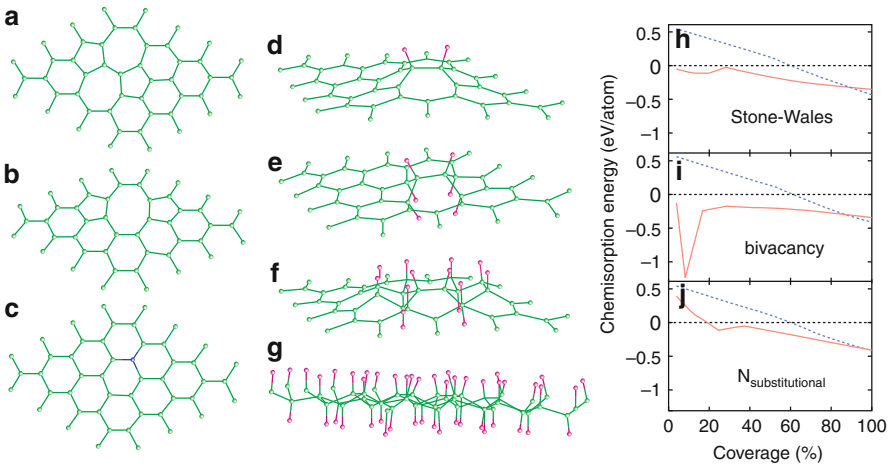

Fig. 24 Optimized geometric structures for graphene supercell containing (**a**) the Stone–Wales defect, (**b**) a bivacancy, and (**c**) a nitrogen substitution impurity. Optimized structures for the Stone–Wales (SW) defect functionalized by (**d**) 2, (**e**) 6, and (**f**) 14 hydrogen atoms and (**g**) completely covered by hydrogen. *Green circles* represent carbon atoms, *violet circles* represent hydrogen atoms, and *blue circle* represents nitrogen atom. Hydrogen atom chemisorption energy per atom as a function of coverage for a graphene sheet containing (**h**) a Stone–Wales (SW) defect, (**i**) a bivacancy, and (**i**) a nitrogen substitution impurity. The *blue dashed* line represents the results for the ideal infinite graphene sheet (Reprinted with permission from reference Boukhvalov and Katsnelson (2008). Copyright 2008 American Chemical Society)

intermolecular reactive empirical bond order (AIREBO) force field in LAMMPS package revealed the wrinkling characteristics in hydrogenated graphene annulus under circular shearing at the inner edge. Such hydrogenation-induced changes in topological and mechanical characteristics of graphene will be useful to develop novel graphene-based devices (Li et al. 2015).

Using density functional calculations, Boukhvalov and Katsnelson have studied hydrogenation of graphene sheets with defects such as Stone–Wales (SW), bivacancies, nitrogen substitution impurities, and zigzag edges. They performed calculations for chemisorptions of hydrogen atoms on the defects in the graphene from low to high coverage. The optimized geometries of the graphene supercells with varioustypes of defects as well as their hydrogenated structures are depicted in Fig. 24, which also displays the computed chemisorption energy as the function of coverage for the graphene containing different defects. The chemisorption energy of a single hydrogen atom to the defect-free graphene was given as 1.5 eV, while those of 0.30 eV for SW defects, 0.93 eV for bivacancies, and 0.36 eV for substitution impurities of nitrogen in graphene were reported. This indicates the significant influence of defects on single hydrogen atom chemisorption energy in graphene. The calculated chemisorption energy for different nonequivalent carbon atoms of the graphene containing SW defect reveals that the chemisorption energy for the entire area surrounding the SW defect is lower compared to the perfect graphene.

Further, the defects also decrease the chemisorption energy of two hydrogen atoms at adjacent positions compared to the defect-free graphene. It was reported that, for the complete coverage, the binding energy is smaller for the hydrogen chemisorption of graphene with defects than the perfect graphene. Thus, completely hydrogenated graphene is less stable with defects than without them (Boukhvalov and Katsnelson 2008).

Graphenes with various kinds of defects may have different types of properties and applications. Therefore, obtaining knowledge on graphenes with defects is important. DFT calculations showed only physisorption of water molecule with perfect graphene, while the vacancy defect greatly assists the dissociative chemisorption of water molecules in the graphene (Cabrera-Sanfelix and Darling 2007; Kostov et al. 2005). There can be many possible reaction pathways for the dissociation of water molecule over defective sites in the graphene (Kostov et al. 2005). Computational studies provide evidence that defects such as Stone–Wales and vacancy strongly influence the chemisorption of functional groups in the graphene (Boukhvalov and Katsnelson 2008; Boukhvalov et al. 2008; Cabrera-Sanfelix and Darling 2007; Kostov et al. 2005).

Fullerenes

Computational Studies of Fullerene Isomers

Computational methods were employed to systematically search and study the low-lying isomeric structures of fullerenes, and such thorough investigations have been useful to predict the best candidates for the lowest-energy structures of higher fullerenes because of the growing experimental interest (Shao et al. 2006, 2007; Slanina et al. 2000a, b; Sun 2003; Sun and Kertesz 2002; Zhao et al. 2004a, b). Fullerene C_{86} has 19 possible isomers obeying IPR, and all of these isomers were studied using B3LYP functional with different basis sets (Sun and Kertesz 2002). Among 19 isomers, the isomer **17** with C_2 symmetry is the most stable followed by isomer **16** with C_s symmetry, and these two isomers are shown in Fig. 25. It should be noted that these two isomers were experimentally observed. At the B3LYP/6-31G level, isomer **16** was predicted to be about 6 kcal/mol less stable than isomer **17**, albeit the former one has slightly larger HOMO–LUMO gap than the latter. The variation of relative stability at different theoretical levels for all 19 IPR-satisfying isomers of C_{86} is depicted in Fig. 26. The relative stabilities were calculated with respect to the lowest-energy isomer (**17**). The HF/3-21G level and the semiempirical AM1 Hamiltonian overestimate the relative energies compared to the density functional theory (DFT) levels (Sun and Kertesz 2002).

Experimental study identified two isomers of fullerene C_{86} and characterized them using ^{13}C NMR spectroscopy (Miyake et al. 2000). Based on the experimental NMR spectra, C_2 and C_s point groups were assigned for the two isomers, but there are more than single C_2 and C_s isomers. Theoretical calculations play a crucial role in identifying the correct structure by comparing theoretical and experimental ^{13}C NMR spectra. The ^{13}C NMR chemical shifts were calculated for all of the 19

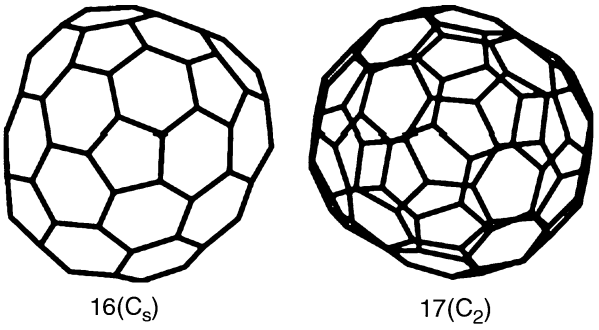

Fig. 25 Two experimentally observed IPR isomers of fullerene C_{86}. Their point groups are given in parentheses (Reprinted with permission from reference Sun and Kertesz (2002). Copyright 2002 Elsevier)

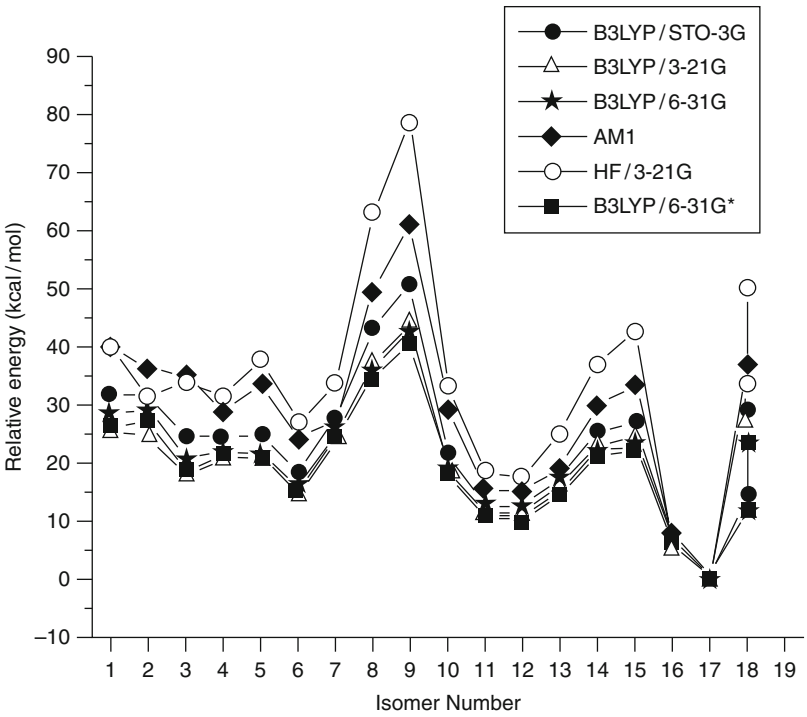

Fig. 26 The relative energy of IPR-satisfying isomers of C_{84} at various levels of theory. Isomers **1**, **5**, **7**, **11**, **12,** and **13** have C_1 symmetry. Isomers **2**, **3**, **4**, **6**, **14,** and **17** possess C_2 point group. Isomers **9** and **10** have C_{2v} point group. Isomers **8**, **15**, and **16** have C_s point group. Isomers **18** and **19** possess C_3 and D_3 point groups, respectively (The data was taken from reference Okada and Saito (1996))

IPR isomers of C_{86}, except isomer **8**. Theoretical ^{13}C NMR spectra complement the experimental spectra as evidenced from Fig. 27. Computational study revealed that isomer **17** has high thermodynamic and kinetic stability among the six IPR isomers of C_{84} possessing C_2 point group. The computed NMR spectrum of isomer

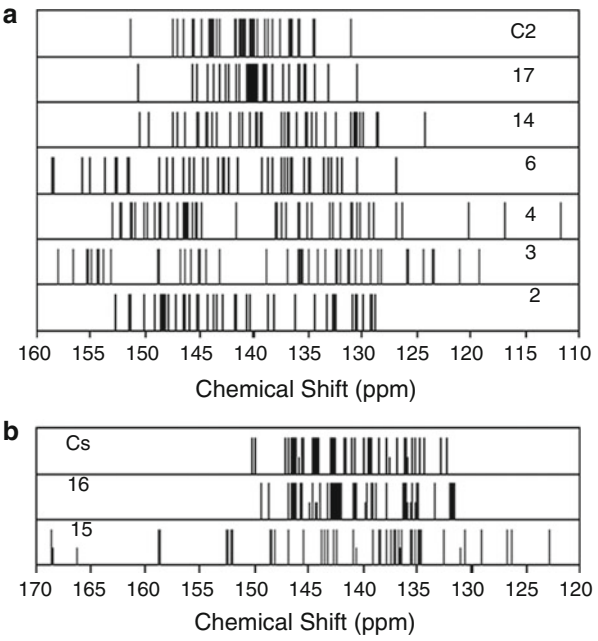

Fig. 27 Experimental and theoretical ^{13}C NMR spectra of (**a**) C_2 isomers of fullerene C_{86}. (**b**) C_s isomers of fullerene C_{86}. Theoretical spectra are labeled by isomer number and experimental spectrum labeled by symmetry (Reprinted with permission from reference Sun and Kertesz (2002). Copyright 2002 Elsevier)

17 supports the results of experimental spectrum. Among the C_s isomers, the second most stable isomer **16** has large HOMO–LUMO gap (Sun and Kertesz 2002). Isomers **6**, **10**, **11**, **12**, **13**, and **18** were predicted to have relative energies less than 20 kcal/mol and moderate HOMO–LUMO gap, thus indicating the possibility of experimental realization (Sun and Kertesz 2002).

Okada and Saito proposed the number of extractable fullerenes among the IPR-satisfying isomers of fullerenes from C_{60} to C_{90}. They found that C_{84} is unique since the number of preferable isomers is more than for other fullerenes and this was attributed to the abundant production of C_{84} after C_{60} and C_{70}. All 24 IPR-satisfying isomers of C_{84} were studied computationally (Okada and Saito 1996). A complete set of 187 isomers that obey IPR of fullerene C_{96} was systematically investigated using various theoretical methods including molecular mechanics (MM3), semiempirical (AM1, MNDO, and PM3), and quantum mechanical (HF/4-31G and B3LYP/6-31G) methods. All of the theoretical levels unequivocally predicted that isomer **183** with D_2 point group is the lowest-energy one. The relative energies for some of the isomers were reported to be quite method sensitive and varied dramatically with different methods. The computational study highlighted the importance of the entropy effect in examining the relative stability of IPR-obeying isomers of fullerene C_{96} (Zhao et al. 2004a). A large set of 450 IPR

isomers of C_{100} has been explored using the abovementioned semiempirical and molecular mechanics (MM3) methods. Systematic theoretical calculations predicted the isomer with D_2 point group (isomer **449**) as the lowest energy by all of the methods employed (Zhao et al. 2004a).

Shao et al. searched the lowest-energy isomer of the fullerenes C_{38} to C_{80} and C_{112} to C_{120}. For the first set (C_{38} to C_{80}), all IPR and all non-IPR isomers were considered, and only IPR-satisfying isomers were considered for the second set of fullerenes (C_{112} to C_{120}). Thus, a large set of molecules was taken for optimizations at the semiempirical density functional-based tight-binding (DFTB) method and the single-point energy calculations at the DFT (Shao et al. 2007). It is known that the fullerene with large HOMO–LUMO gap and high symmetry is not necessarily the lowest-energy structure. The decreasing trend of HOMO–LUMO gap was reported with increasing the fullerene size (Shao et al. 2006, 2007). An unexpected manner of pentagonal adjacency was observed in the low-lying isomers in the series of fullerenes C_{38} to C_{80} (Shao et al. 2007).

In a comprehensive computational study, Shao et al. identified 20 isomers as the best candidates for the lowest-energy structures. Among the 20 isomers, 10 isomers with relative energies less than 1 kcal/mol aredepicted in Fig. 28 (Shao et al. 2007). Thus, these 10 isomers can be observed experimentally. The ^{13}C NMR chemical shifts for these 10 isomers were calculated. Theoretical study predicted that C_{116}:**6061** can be more easily isolated and characterized in the laboratory than other higher fullerenes from C_{112} to C_{120} (Shao et al. 2007). In a different study, Shao et al. proposed the seven best candidates of the lowest-energy isomers for the fullerenes C_{98} to C_{110} based on the systematic study using DFTB and DFT

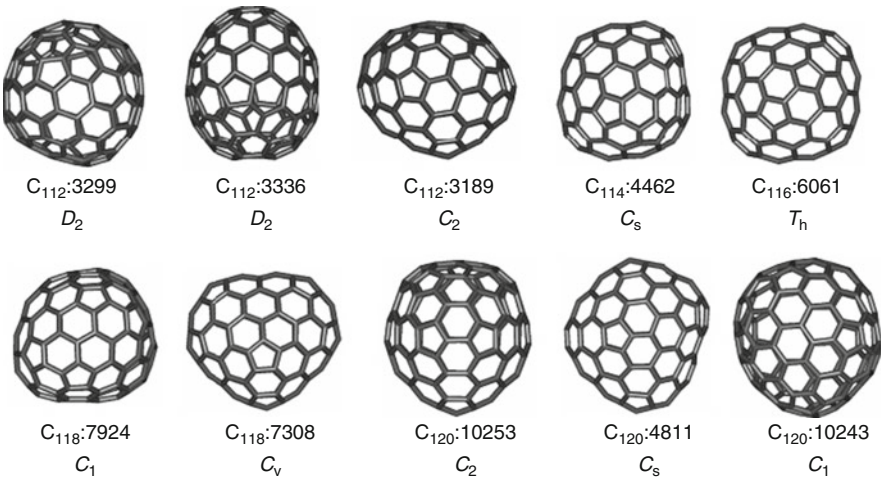

Fig. 28 Best candidates for the lowest-energy structure of higher fullerenes (C_{112} to C_{120}). The isomer number and point group are given (Reprinted with permission from reference Shao et al. (2007). Copyright 2007 American Chemical Society)

methods. They pointed out that C_{102} (C_1: **603**) and C_{108} (D_2: **1771**) isomers can be easily synthesized (Shao et al. 2006). The concepts of cage connectivity and frontier π-orbitals play important roles to understand the relative stability of charged fullerene isomers without performing extensive quantum chemical calculations. This theoretical study correctly predicted the structures observed experimentally and explained why the isolated pentagon rule is often violated for fullerene anions, but the opposite is found for fullerene cations (Wang et al. 2015b).

Fullerenes C_{50} and $C_{50}Cl_{10}$ were computationally studied using B3LYP/6-31G(d) level due to the experimental report of the latter compound (Lu et al. 2004). The computational study thoroughly explored the structures, relative energies, HOMO–LUMO energies, and HOMO–LUMO gap for low-lying isomers of C_{50} and its anions. The computed IR, Raman, ^{13}C NMR, and UV–Vis spectra of the $C_{50}Cl_{10}$ with D_{5h} symmetry showed very good agreement with the reported experimental data. The pentagon–pentagon fusions were found to be the active sites of addition reactions in both D_3 and D_{5h} symmetric isomers of fullerene C_{50}. It was observed that HOMO and LUMO coefficients of C_{50} (D_{5h}) are distributed around the equatorial pentagon–pentagon fusion sites. This was given as a reason for the binding of Cl atoms around the equatorial pentagon–pentagon fusion sites of C_{50} yielded $C_{50}Cl_{10}$ (Lu et al. 2004).

Giant Fullerenes

Giant fullerenes have been the subject of theoretical interests (Calaminici et al. 2009; Dulap and Zope 2006; Dunlap et al. 1991; Gueorguiev et al. 2004; Lopez-Urias et al. 2003; Zope et al. 2008). The structures and stabilities of the giant fullerenes C_{180}, C_{240}, C_{320}, and C_{540} were investigated using high-level density functional theory calculations (Calaminici et al. 2009). The results of the uncorrected binding energy (in eV) per carbon atom for the giant fullerenes obtained using the VWN functional are depicted in Fig. 29. The inclusion of the basis set superposition error (BSSE) decreases the calculated binding energies but does not alter the trend. The increasing trend of binding energy indicates that the large fullerenes become more and more stable with increasing size. Fullerene C_{540} has a similar binding energy to diamond, giving the hope that such giant fullerenes could be prepared. However, the binding energy per carbon atom of the fullerene, C_{540}, is considerably lower than that of graphene (Calaminici et al. 2009). Gueorguiev et al. performed the calculations for giant fullerenes using semiclassical approximation LR-LCAO (linear response model in the framework of the linear combination of atomic orbitals). They reported the decreasing trend of HOMO–LUMO gaps (except C_{20}) and the considerably large increase of the static polarizability as increasing the size of the fullerene cage (Fig. 30; Gueorguiev et al. 2004). The static dipole polarizability per atom in C_{2160} is three times larger than that in C_{60} (Dunlap et al. 1991).

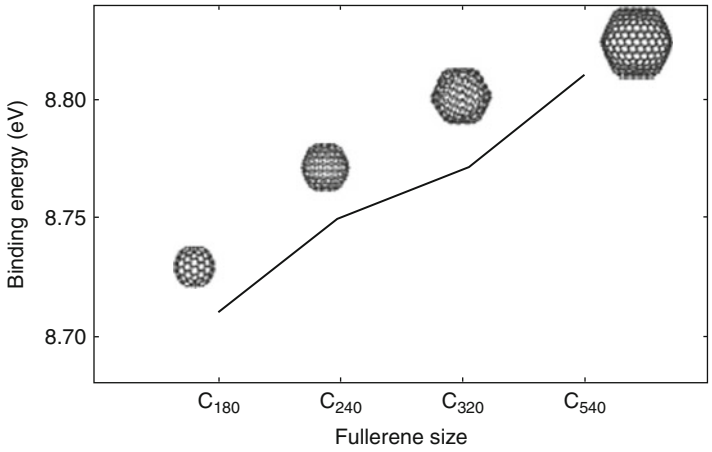

Fig. 29 Binding energy (in eV) for C_{180}, C_{240}, C_{320}, and C_{540} fullerenes. The calculations have been performed with the VWN functional in combination with DZVP basis sets (Reprinted with permission from reference Calaminici et al. (2009). Copyright 2009 American Chemical Society)

Local Strain in Curved Polycyclic Systems: POAV and Pyramidalization Angle

Fullerenes experience large strain energy because of their spherical shape. The curvature-induced pyramidalization of the carbon atoms of fullerenes weakens the π-conjugation. The curved π-conjugation in carbon networks of fullerenes has not only π-character but also substantial s-character. The π-orbital axis vector (POAV) analysis developed by Haddon is useful in measuring the local curvature of the nonplanar conjugated organic molecules, fullerenes, and SWCNTs (Haddon 1993; Haddon and Scott 1986). In general, the sp^2-hybridized carbon atom prefers to be in the planar arrangement, but it is pyramidalized in fullerenes. The local strain of carbon framework in fullerenes and SWCNTs is reflected in the pyramidalization angle θ_P at the carbon atoms (Niyogi et al. 2002). The pyramidalization angle (θ_P) equals to the difference between the π-orbital axis vector (POAV) and the normal right angle 90°: thus, $\theta_P = (\theta_{\sigma\pi} - 90°)$, where the $\theta_{\sigma\pi}$ is the angle between the π-orbital of the conjugated atom and the σ-orbital of the surrounding atoms. As shown in Fig. 31, the pyramidalization angle is 0° and 19.47° for a planar sp^2-hybridized carbon and a tetrahedral sp^3-hybridized carbon, respectively. All carbon atoms in the icosahedral C_{60} have the same $\theta_{\sigma\pi}$ of 11.6°.

Pyramidalization angle of a carbon atom in fullerenes and SWCNTs is helpful in predicting the chemical reactivity (Akdim et al. 2007; Bettinger 2005; Dinadayalane and Leszczynski 2007a, b; Lu and Chen 2005; Lu et al. 2005). The larger pyramidalization angle of carbon atom indicates the higher reactivity toward addition reactions in the curved systems of fullerenes and SWCNTs. Curvature-induced pyramidalization and the π-orbital misalignment cause local strain in SWCNTs (Fig. 32). Hence, carbon atoms of SWCNTs are more reactive than that of a perfect

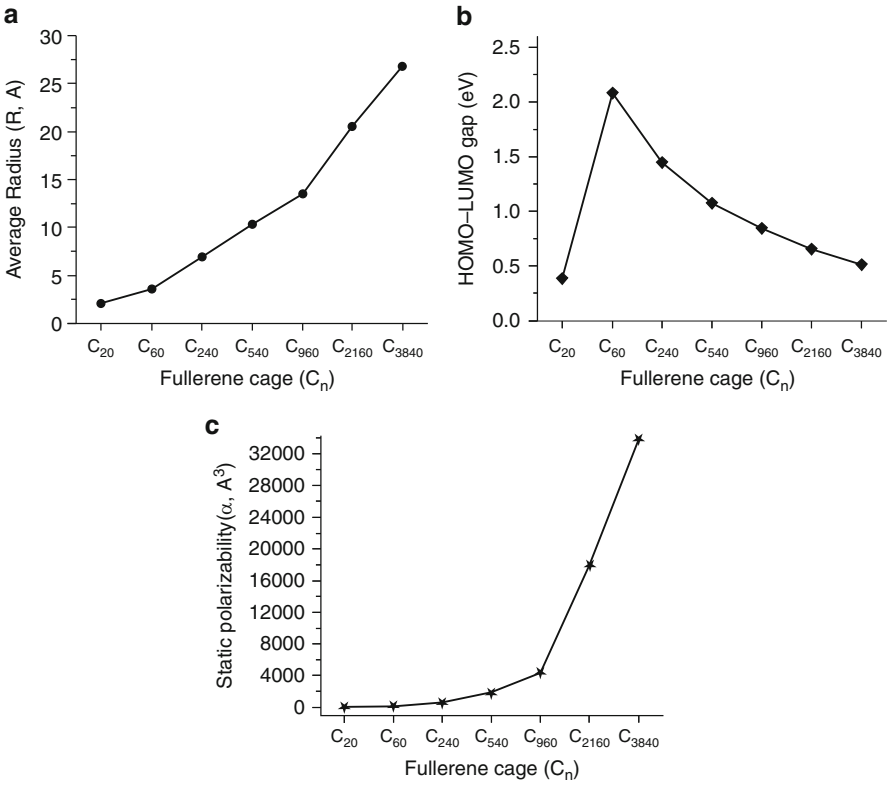

Fig. 30 The variation of (**a**) radius (R, Å), (**b**) HOMO–LUMO gap (ev), and (**c**) static polarizability as increasing the size of the fullerene cage (C_{20}, C_{60}, C_{240}, C_{540}, C_{960}, C_{2160}, and C_{3840}) (The data for the plots was taken from reference Gueorguiev et al. 2004))

graphene sheet (Niyogi et al. 2002; Park et al. 2003). Cyranski et al. studied the structures and energetics of the 12 lowest-energy isomers of neutral, closed-shell IPR fullerenes C_{60}-C_{96} using B3LYP/6-31G(d) level. They obtained the decreasing values of pyramidalization angles, while no regular trend was obtained for HOMO–LUMO gaps with increasing size of fullerenes (Fig. 32; Cyranski et al. 2004).

Decachloro-derivative of C_{50} fullerene has been synthesized and experimental characterization confirmed the existence of C_{50} cage. Two C_{20} caps and five C_2 units around the equator are present in the C_{50} core of $C_{50}Cl_{10}$ (Xie et al. 2004). The calculated pyramidalization angle for the carbon atoms of the C_{20} caps of fullerene C_{50} ranges from 10.7 to 12.88°, which are comparable to that of C_{60} (11.68°). However, a large pyramidalization angle (15.58°) is obtained for the equatorial C atoms (pentagon–pentagon fusion). Such large value was attributed to high reactivity of those carbon atoms in addition reactions to form exohedral adducts (Chen 2004; Lu et al. 2004). Such structural features were reasoned for the instability of a bare C_{50} cage and the stability of $C_{50}Cl_{10}$ (Chen 2004).

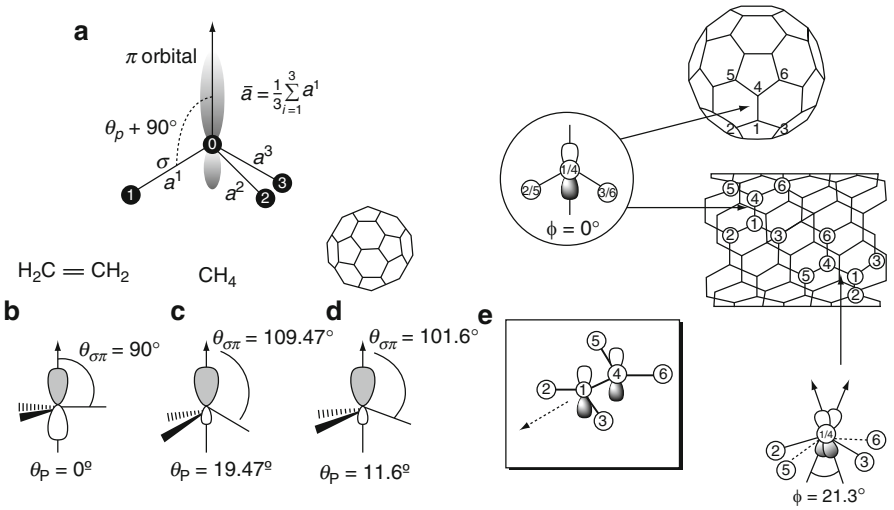

Fig. 31 (**a**) Pyramidalization angle (θ_P) is defined by the angle between the π-orbital and σ-bond minus 90° so that $\theta_P = 0°$ for a graphene sheet and $\theta_P = 19.47°$ for sp^3-hybridized carbon. For practical reasons, we take the average of three θ_P values: (**b**) θ_P for a perfect planar sp^2-hybridized carbon atom (e.g., in C_2H_4), (**c**) θ_P for a perfect tetrahedral sp^3-hybridized carbon atom (e.g., CH_4), (**d**) θ_P for a nonplanar sp^2-hybridized carbon atom (e.g., C atom in C_{60} or SWCNT). (**e**) The π-orbital misalignment angle (ϕ) along the C1–C4 bond in the (5,5) SWCNT and the fullerene C_{60} (Pictures were reprinted with permission from references Lu and Chen (2005), Niyogi et al. (2002), and Park et al. (2003). Copyright 2002, 2003 and 2005 American Chemical Society)

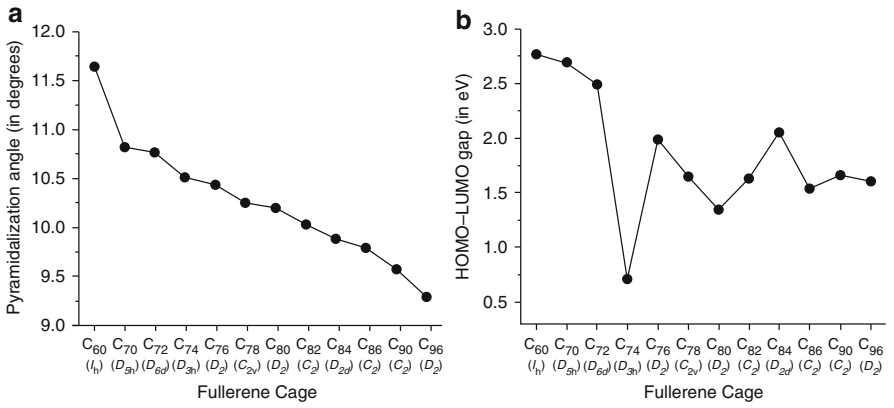

Fig. 32 (**a**) Variation of pyramidalization angle for the carbon atom of the most stable IPR fullerene as increasing the size of fullerene. (**b**) Variation of HOMO–LUMO gap for the most stable IPR fullerene as increasing the size of fullerene. The point groups are given in the parentheses. The values for these graphs were taken from reference Cyranski et al. (2004))

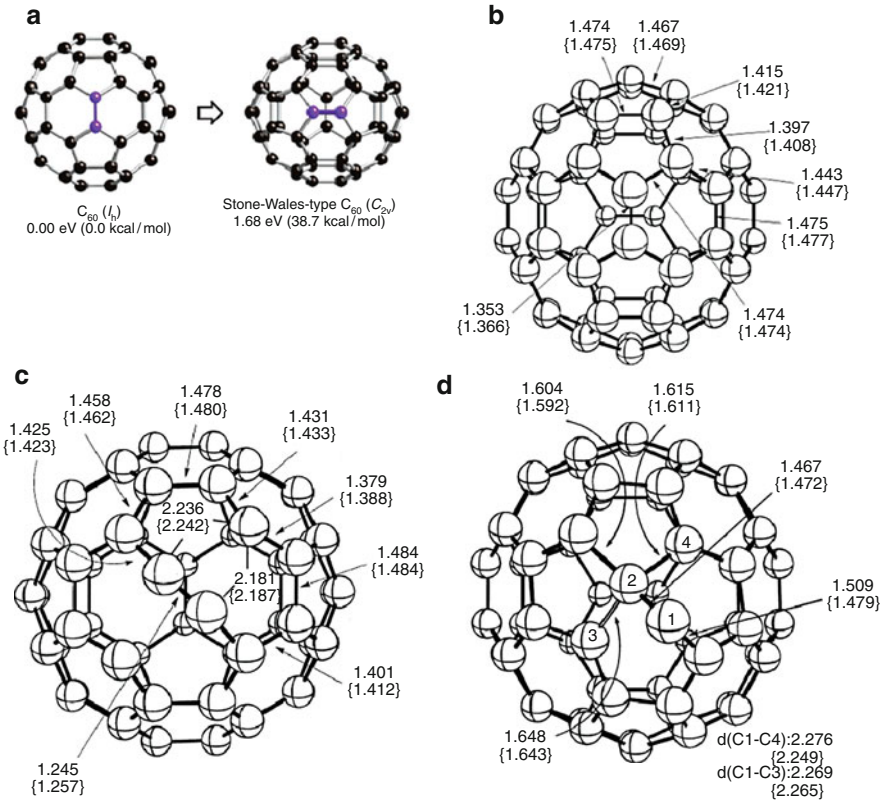

Fig. 33 (**a**) Buckminsterfullerene to C_{60}-C_{2v} with Stone–Wales defect generated by the 90° rotation of the C−C bond in *blue color* of C_{60} (I_h). (**b**) Optimized structure of the C_{2v} symmetry isomer. (**c**) Structure of the C_2 symmetry transition state for the concerted Stone–Wales transformation pathway. (**d**) Structure of the asymmetric transition state between carbene intermediate and C_{60}-C_{2v} isomer. Bond lengths were obtained at the B3LYP/6-31G* and PBE/6-31G* (in *curly brackets*) levels of theory and are given in Å (Pictures were reprinted with permission from reference Bettinger et al. (2003) and Yumura et al. (2007). Copyright 2003 and 2007 American Chemical Society)

Stone–Wales Defect in C_{60}

Fullereneisomers are likely to interconvert through Stone–Wales transformation (Stone and Wales 1986; Troyanov and Tamm 2009). Very recently, experimental study has reported that the chlorine-functionalized D_2-C_{76} IPR isomer transformed to non-IPR isomer, and this transformation was proposed to include seven single Stone–Wales rearrangements (Ioffe et al. 2009). Computational chemists strived to understand the energy barriers for the Stone–Wales transformation and the possible mechanisms involved in this rearrangement, particularly considering the C_{60} fullerene (Bettinger et al. 2003; Eggen et al. 1996; Yumura et al. 2007).

Stone–Wales transformation is a thermally forbidden rearrangement by following the orbital symmetry considerations of Woodward and Hoffmann (1969). The icosahedral C_{60} fullerene (buckminsterfullerene) gives an isomer of C_{60} with C_{2v} point group that violates the isolated pentagon rule. Two different pathways, namely, concerted and stepwise pathways, and two different (symmetric and asymmetric) transition states were identified theoretically for the Stone–Wales transformation in C_{60} fullerene. The C_{60}-C_{2v} isomer, which is a Stone–Wales-type defect structure with two adjacent pentagons, was reported to be less stable by 33.9–38.7 kcal/mol (1.47–1.68 eV) than the buckminsterfullerene using various density functional theory levels (Yumura et al. 2007).

Bettinger et al. listed the C−C bond lengths of C_{60} (I_h) and the activation barrier for the Stone–Wales defect transformation through different transition states at various levels of theory. Computed geometries of buckminsterfullerene at different levels showed shorter [6,6] C−C bond length than the [5,6] C−C bond length, in consistent with experimental results (Bettinger et al. 2003). Figure 33 depicts the concerted C_2 symmetric transition state and asymmetric transition state involved in SW transformation of C_{60}-I_h to C_{60}-C_{2v}. The intrinsic reaction coordinate calculations by Bettinger et al. support the concerted pathway rather than stepwise pathway for the SW transformation in the C_{60} fullerene. Based on the computed activation energies, both concerted and stepwise pathways are highly competitive. The rigorous computational study of SW transformation in buckminsterfullerene revealed that the empirical schemes such as Tersoff–Brenner potentials and density functional-based tight binding (DFTB) underestimate the barrier heights, and semiempirical AM1 appears to be promising for such investigations (Bettinger et al. 2003).

Computational Studies on Vacancy Defects in Fullerene C_{60}

Vacancy defects in fullerene C_{60} were studied using quantum chemical methods (Hu and Ruckenstein 2003, 2004; Lee and Han 2004). They were generated by removal of 1–4 carbon atoms in C_{60} as shown in Figs. 34 and 35. Different modes are possible to remove carbon atoms from C_{60} to generate vacancy defects; hence, different sizes of rings (four-, seven-, eight-, and nine-membered rings) were produced by removing carbon atoms in C_{60}. Removing one, two, three, and four adjacent carbon atoms from the C_{60} cluster generates two, three, three, and six different isomers for the C_{59}, C_{58}, C_{57}, and C_{56} clusters, respectively (Hu and Ruckenstein 2004; Lee and Han 2004). The odd-numbered clusters have unsaturated carbon, which favors being located in a six-membered ring rather than a five-membered ring. Two-atom vacancies give structure with seven- and eight-membered rings, whereas one-atom vacancy gives the structure with nine-membered ring. Four-atom vacancies provide the most stable structure with only five- and six-membered rings. Thus, increasing the number of vacancies need not increase the size of the hole (Hu and Ruckenstein 2003, 2004).

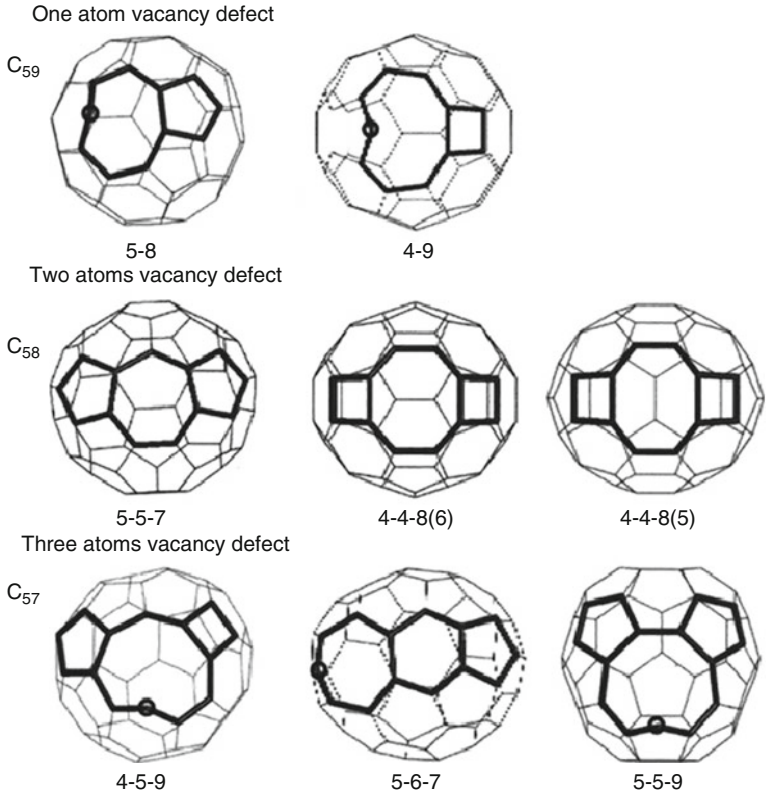

Fig. 34 B3LYP/6-31G(d) optimized structures of C_{59}, C_{58}, and C_{57} clusters. Description indicates *highlighted rings*. "A-B" denotes A- and B-membered ring. *Circle* denotes an unsaturated atom (Reprinted with permission from reference Lee and Han (2004). Copyright 2004, American Institute of Physics)

The singlet structures are more stable than the triplet ones for C_{58} cluster, while the reverse is true in the case of C_{57} clusters. The reported stabilization energy per atom at the B3LYP/6-311G(d)//B3LYP/6-31G(d) level is 2.18, 1.49, and 3.10 kcal/mol for the C_{59}, C_{58}, and C_{57}, respectively. Quantum chemical calculations provide relationship between structure and stability of the defect fullerene clusters (Hu and Ruckenstein 2003, 2004; Lee and Han 2004). In case of removal of four adjacent carbon atoms in C_{60}, additional five-membered rings are formed in geometry optimizations (e.g., isomer **1** in Fig. 35). The isomer **4** has only five- and six-membered rings (12 five-membered rings and 18 six-membered rings) and was predicted to be the most stable among the isomers depicted in Fig. 35. The stability energy for the isomers generated by removing four carbon atoms has the following sequence: isomer **4** > isomer **3** > isomer **2** > isomer **5** > isomer **6** > isomer **1**. All defect clusters have lower stability energy per atom than C_{60}. The removal of carbon atoms from C_{60} increases the HOMO and decreases the

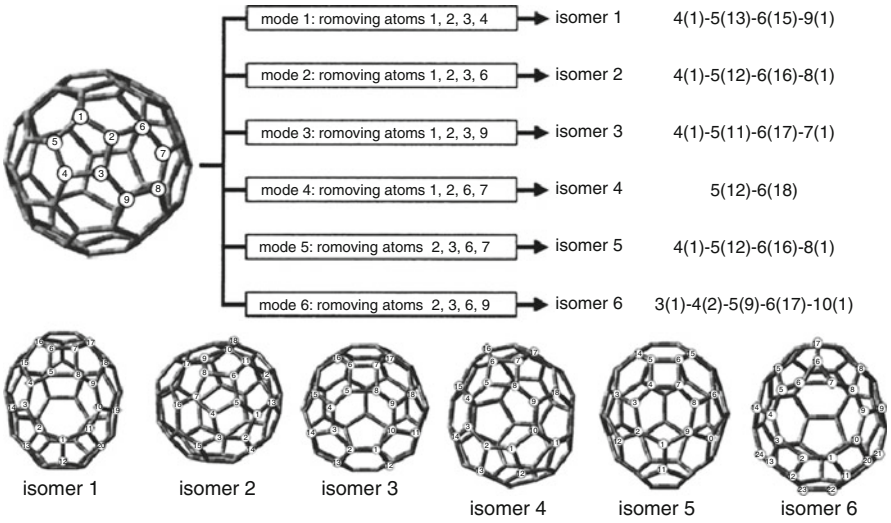

Fig. 35 Different modes to generate isomers of C_{60} with four vacancies by removing four adjacent atoms from the perfect C_{60} structure. Structures of isomers 1–6 of defect C_{60} with four vacancies. The ring size and the number of rings (in parentheses) for each isomer are given; for example, isomer 1-4(1)-5(13)-6(15)-9(1) means 1 four-membered, 13 five-membered, 15 six-membered, and 1 nine-membered rings (Reprinted with permission from reference Hu and Ruckenstein (2004). Copyright 2004, American Institute of Physics)

LUMO energy. Consequently, the defect structures exhibit lower HOMO–LUMO gap compared to C_{60}. No relationship was obtained between the stability energy per carbon atom and the HOMO–LUMO gap for the defective carbon clusters of C_{60} (Hu and Ruckenstein 2003).

Computational Studies of Single-Walled Carbon Nanotubes

Computational chemists explored the structures, electronic properties, and reactivities of SWCNTs of varying lengths and diameters (Bettinger 2004; Dinadayalane and Leszczynski 2009; Dinadayalane et al. 2007b; Galano 2006; Kaczmarek et al. 2007; Matsuo et al. 2003; Niyogi et al. 2002; Yang et al. 2006c). They also tried to understand the influence of different defects on these properties at reliable theoretical methods within the limitations of hardware and software (Akdim et al. 2007; Andzelm et al. 2006; Bettinger 2005; Dinadayalane and Leszczynski 2007a, b; Govind et al. 2008; Lu et al. 2005; Nishidate and Hasegawa 2005; Wanbayor and Ruangpornvisuti 2008; Wang et al. 2006; Yang et al. 2006a, b). A series of finite-length hydrogen-terminated armchair SWCNTs have been computationally studied to obtain knowledge on the influence of diameter and length on the structural and electronic properties (Galano 2006). The optimized armchair (n,n) SWCNTs possess D_{nh} and D_{nd} point groups for $\vartheta/2$ even and odd, respectively. The different

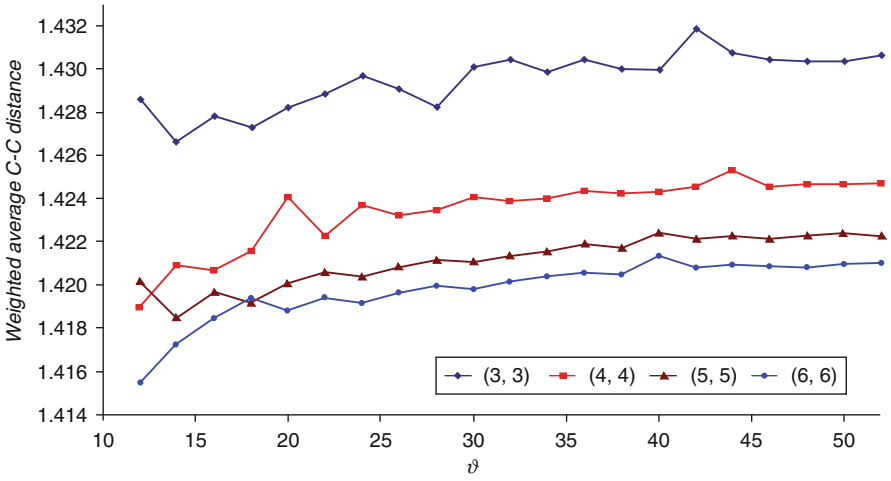

Fig. 36 Calculated weighted average values of the C–C distance as a function of the tube length for armchair (n,n) SWCNTs (Reprinted with permission from reference Galano (2006). Copyright 2006 Elsevier)

lengths of the armchair SWCNTs have the general formula $C_{(2n)k}H_{4n}$ with k= ϑ/2. Galano considered (3,3), (4,4), (5,5), and (6,6) armchair SWCNTs with k of 6 to 26 (i.e., from 6 to 26 carbon atom layers). There are two types of bonds in the perfect (*n*,*n*) armchair SWCNTs; one is perpendicular to the tube axis (r_I) and another one is nearly parallel to the tube axis (r_{II}). The maximum difference between r_I and r_{II} was obtained in the case of the narrow diameter (3,3) tube. The influence of diameter on the weighted average values of the C−C distances is larger than the influence of the tube length (Fig. 36; Galano 2006).

The frontier molecular orbitals (HOMO and LUMO) play an important role in SWCNTs since they are helpful in predicting a number of ground-state properties of molecules. According to Huckel theory, the (*n*,*n*) armchair SWCNTs should be metallic (Saito et al. 1998), but the finite-length armchair SWCNTs are semiconducting with a finite size of the HOMO–LUMO gap (Cioslowski et al. 2002). The computed HOMO–LUMO gaps for (3,3) to (6,6) SWCNTs were reported to be lower than the corresponding value for fullerene C_{60}. The HOMO–LUMO gap oscillates as the tube length increases for all of these armchair tubes (Fig. 37). The behavior of narrow diameter (3,3) tube is different from other armchair SWCNTs (Galano 2006).

Matsuo et al. classified the structures of finite-length armchair (5,5) and (6,6) SWCNTs as Kekule, incomplete Clar, and complete Clar networks depending on the exact length of the tubes. The (5,5) and (6,6) SWCNTs were elongated layer by layer of 10 and 12 carbon atoms, respectively (Matsuo et al. 2003). The local aromaticity of different lengths of the tubes was evaluated using the NICS (nucleus-independent chemical shift) calculations (GIAO-SCF/6-31G*//HF/6-31G* level).

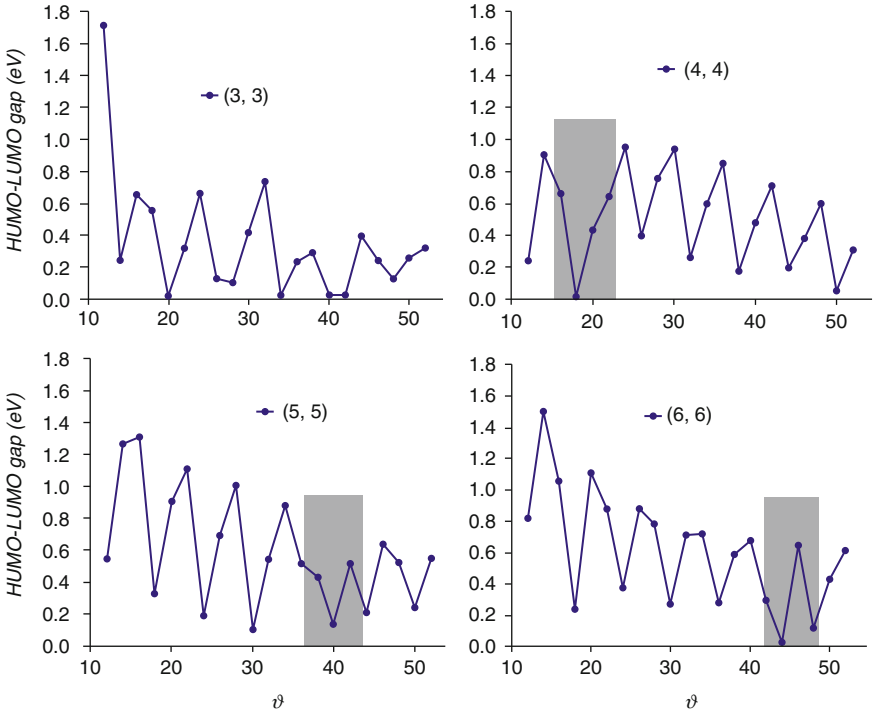

Fig. 37 Variations of HOMO–LUMO gaps as increasing the tube length for the armchair SWCNTs. There is no periodicity in (3,3) tube and the shaded region indicated the broken periodicity in other tubes (Reprinted with permission from reference Galano (2006). Copyright 2006 Elsevier)

Matsuo et al. pointed out that the geometry of $C_{50}H_{10}$ is similar to the equatorial belt of the fullerene C_{70}. Bond lengths of optimized structures exhibit oscillation with increase in tube length for both (5,5) and (6,6) armchair SWCNTs. The schematic structures of Kekule, incomplete Clar, and complete Clar networks for (5,5) and (6,6) SWCNTs are depicted in Fig. 38 along with the NICS values of dissimilar benzenoid rings. The energy of frontier molecular orbitals and HOMO–LUMO gap also oscillate as the length of the nanotube increases (Fig. 39). The Kekule structure shows larger HOMO–LUMO gap than the other two. It was reported that the band gap will eventually disappear at a certain tube length (Matsuo et al. 2003).

The pyramidalization angle (θ_P) and π-orbital misalignment angles are useful to gauge the reactivity of the carbon atom sites of SWCNTs. The end caps of SWCNTs resemble fullerene hemisphere; thus, the end caps are expected to be more reactive than sidewalls irrespective of the diameter of the SWCNTs. Carbon atoms in fullerene are more distorted than those in the corresponding SWCNTs. For example, the carbon atom of (10,10) armchair SWCNT has the pyramidalization angle (θ_P) of about 3.0°, while the carbon atom of the fullerene with corresponding

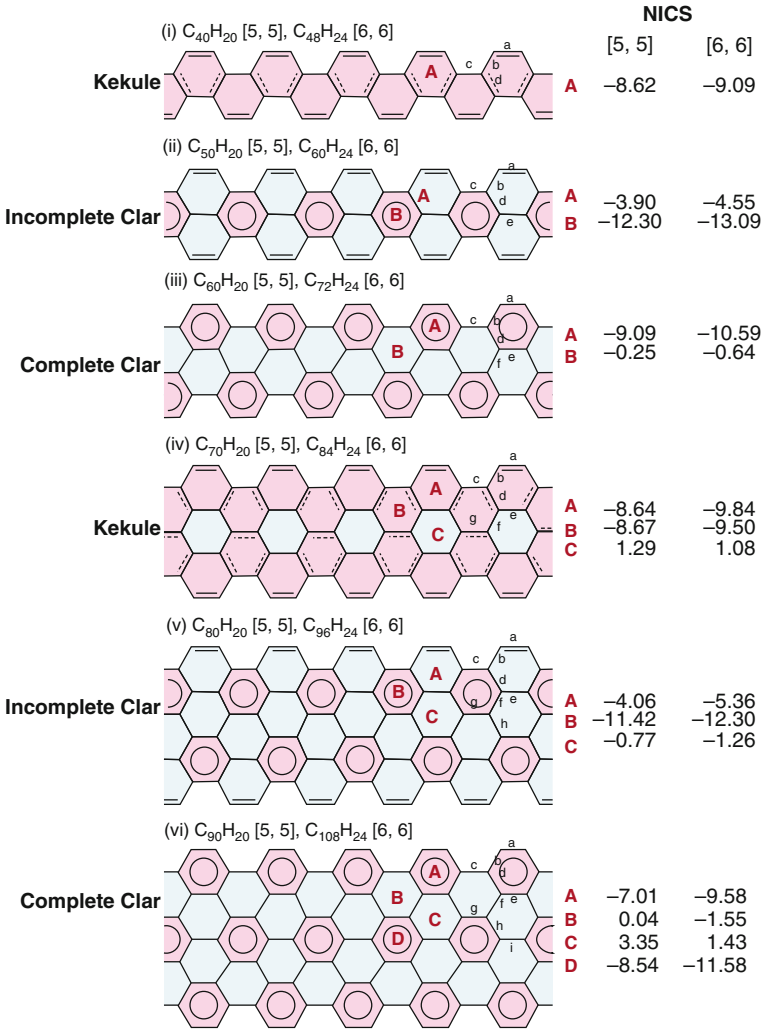

Fig. 38 Schematic structures and color-coded NICS maps of finite-length (5,5) and (6,6) SWCNTs. Hydrogen atoms are omitted for clarity. Chemical bonds are schematically represented by using single bond (*solid single line*; bond length > 1.43 Å), double bond (*solid double line*; bond length < 1.38 Å), single bond halfway to double bond (*solid dashed line*; 1.43 Å > bond length > 1.38 Å), and Clar structure (i.e., ideal benzene). NICS coding: *red*, aromatic < −4.5; *blue*, nonaromatic > −4.5 (Reprinted with permission from reference Matsuo et al. 2003. Copyright 2003 American Chemical Society)

radius (fullerene C_{240}) has the θ_P of about 9.7° (the hemisphere of fullerene C_{240} can be capped to (10,10) SWCNT) (Niyogi et al. 2002). Chen et al. mentioned that the pyramidalization angle of the C atoms of the sidewalls of SWCNTs is smaller compared to that of the fullerenes of same radius. As a consequence, the

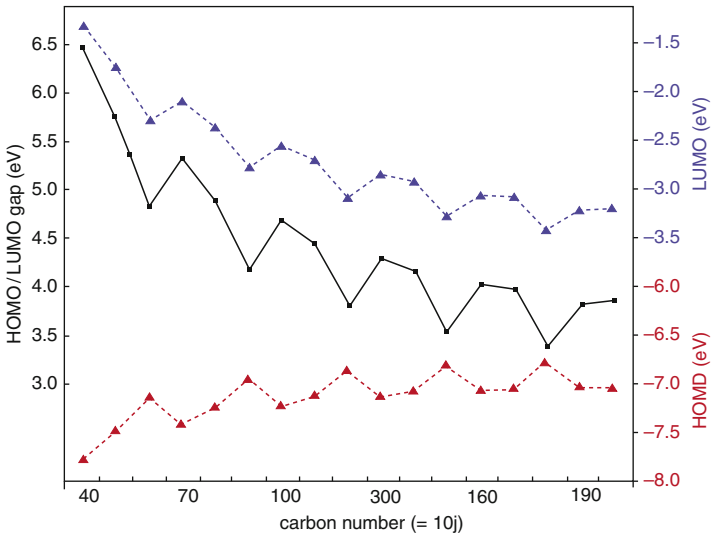

Fig. 39 Variation of HOMO–LUMO energies and HOMO–LUMO energy gap with increase in tube length of (5,5) armchair SWCNT ($C_{10j}H_{20}$) (Reprinted with permission from reference Matsuo et al. (2003). Copyright 2003 American Chemical Society)

covalent functionalization to SWCNTs is less favorable compared to fullerenes of same radius (Chen et al. 2003). The π-orbital misalignment is likely to be a main source of strain in the SWCNTs. For both armchair and zigzag SWCNTs, the pyramidalization angle and the π-orbital misalignment angle decrease with increase in diameter of the tube (Fig. 40; Niyogi et al. 2002).

Covalent Functionalization of SWCNTs: H and F Atom Chemisorptions

The covalent functionalization of SWCNTs, which modifies the properties of the tubes, has become a challenging field of research for the past few years (Bettinger 2006; Hirsch 2002; Niyogi et al. 2002; Vostrowsky and Hirsch 2004). Functionalization of tubes is considered to be promising to produce carbon nanotube-based materials for selective applications (Bettinger 2006; Cho et al. 2008; Denis et al. 2009). The binding of hydrogen with SWCNTs has generated a lot of experimental and theoretical interests due to their potential application in hydrogen storage (Dillon et al. 1997; Dinadayalane and Leszczynski 2009; Dinadayalane et al. 2007b; Kaczmarek et al. 2007; Nikitin et al. 2005; Ormsby and King 2007; Yang et al. 2006c; Zhang et al. 2006). Scientists have tried to obtain knowledge on the mechanism of hydrogen adsorption in SWCNTs. They attempted to design the viable nanotube-based hydrogen storage material to meet the Department of Energy (DOE) target of 6.5 wt% at ambient temperature (Dillon et al. 1997; Dinadayalane

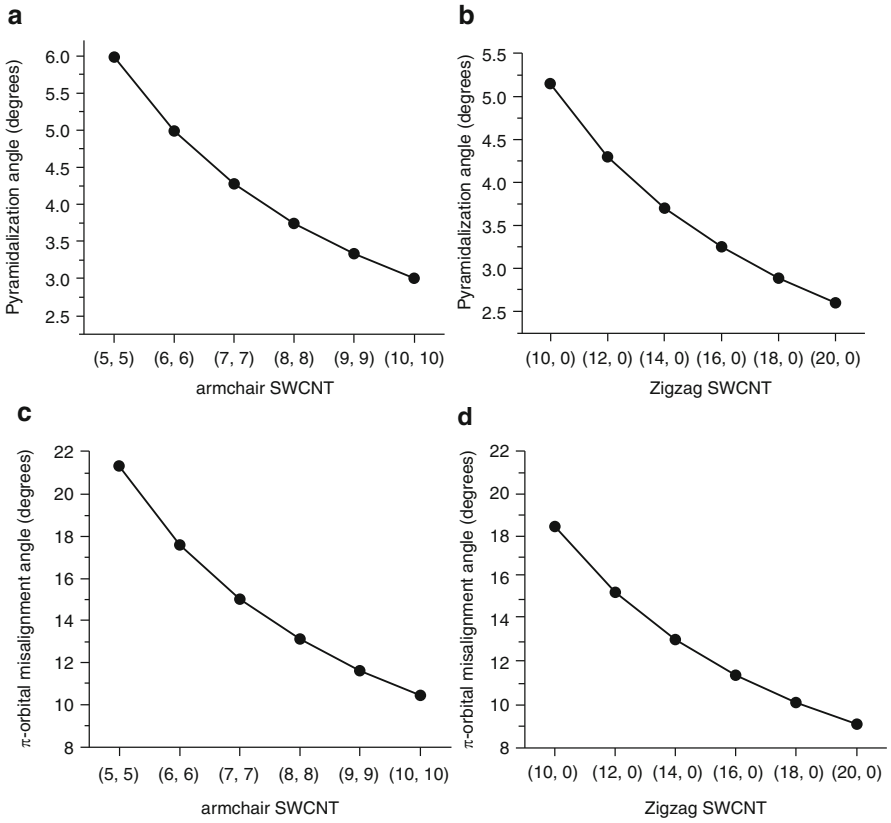

Fig. 40 The change of pyramidalization angle (**a**, **b**) at the carbon atom and the π-orbital misalignment angle (**c**, **d**) between two adjacent carbon atoms of armchair (**a**, **c**) and zigzag (**b**, **d**) SWCNTs. The π-orbital misalignment angle is zero for the carbon atoms of the circumferential bond in armchair tube and axial bond in zigzag tube (The data was taken from reference Niyogi et al. (2002))

and Leszczynski 2009; Dinadayalane et al. 2007b; Kaczmarek et al. 2007; Nikitin et al. 2005; Ormsby and King 2007; Yang et al. 2006c; Zhang et al. 2006). The experimental investigations reported the chemisorption of H atoms on the surface of SWCNTs as promising approach to meet DOE's target of hydrogen storage (Nikitin et al. 2005; Zhang et al. 2006). Chemisorptions of hydrogen atoms on the surface of SWCNTs were investigated (Dinadayalane and Leszczynski 2009; Dinadayalane et al. 2007b; Kaczmarek et al. 2007; Ormsby and King 2007; Yang et al. 2006c). The covalent functionalization of SWCNTs by H atoms is a hot topic. Thus, we discuss the quantum chemical studies of the hydrogen chemisorption on different types of SWCNTs.

Yang et al. studied, using DFT and ONIOM calculations, the chemisorption of atomic hydrogen(s) on the open-ended finite-sized (5,0), (7,0), and (9,0) zigzag and

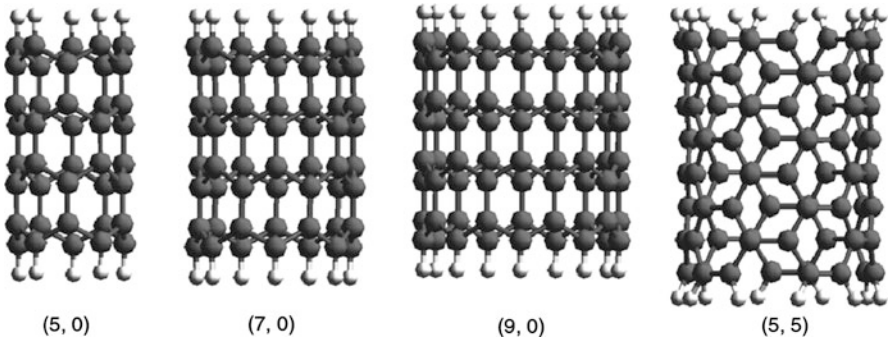

Fig. 41 Finite-sized small carbon nanotube models of (5,0), (7,0), and (9,0) zigzag and (5,5) armchair SWCNTs considered for low occupancy of H chemisorptions (Reprinted with permission from reference Yang et al. (2006c)). Copyright 2006 American Chemical Society)

(5,5) armchair SWCNTs (Fig. 41; Yang et al. 2006c). They compared the binding energies obtained for nanotubes with results of the model graphene sheet in order to examine the effect of curvature. It was reported that the chemisorptions of H atoms to the exterior wall of the SWCNTs are more favorable than the interior walls. The H chemisorption has strong dependence of tube diameter and helicity or chirality in both interior (endohedral) and exterior (exohedral) addition. In case of single H atom addition, the binding energy (chemisorption energy), which is the reaction energy for H chemisorption with SWCNT, decreases with increase in tube diameter. In the chemisorption of two hydrogen atoms in the interior and exterior walls of (5,0) and (7,0) SWCNTs, two hydrogen atoms prefer to bind at alternate positions rather than adjacent positions. This was attributed to the crowding effect when two hydrogen atoms occupy in the adjacent positions. In the case of (5,0) SWCNT, chemisorption of ten hydrogen atoms (33 % coverage) decreases the magnitude of chemisorption energy, which is further decreased by an increase in the coverage to 50 %. Similar to the situation in zigzag SWCNTs, two hydrogen atoms prefer to attach at alternate carbon sites rather than adjacent sites in the graphene sheet. Significantly large deviation of chemisorption energy between the graphene sheet and zigzag SWCNTs (H atoms chemisorbed on the exterior wall) was reported. It was found that the chemisorptions of H atoms with small diameter SWCNTs are much more favorable than with the graphene sheet (Yang et al. 2006c).

We investigated a single-hydrogen chemisorption, the preference of the positions (i.e., 1-2, 1-2', 1-3, or 1-4 positions) for the chemisorption of two hydrogen atoms considering (3,3), (4,4), (5,5), and (6,6) armchair SWCNTs of 9 and 15 carbon atom layers. The SWCNTs of 15 carbon layers considered in our study are shown in Fig. 42. The addition of H atoms on the outer wall of SWCNT (exohedral addition) has only been considered in our study. We performed DFT calculations using B3LYP/6-31G(d) level for full geometry optimizations. The finite-length SWCNTs were capped with hydrogen atoms to avoid dangling bonds. The reaction energies for hydrogen chemisorption (E_r) on the external surface of

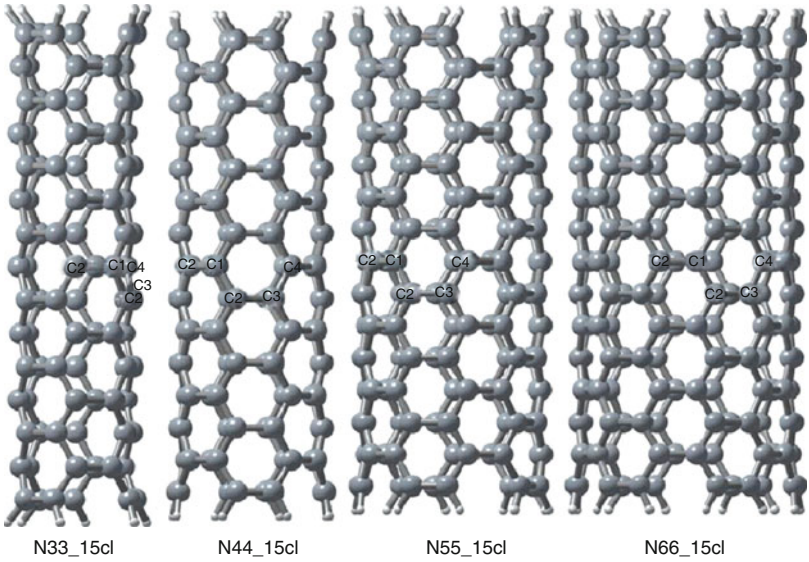

Fig. 42 Structures of (3,3), (4,4), (5,5), and (6,6) armchair SWCNTs of 15 carbon layers (15 cl) considered for the chemisorption of one and two H atoms. The carbon atom sites for attachment of H atoms are shown (Reprinted with permission from reference Dinadayalane et al. (2007b)). Copyright 2007 American Chemical Society)

SWCNTs have been calculated using the formula $E_r = E_{SWCNT+nH} - E_{SWCNT} - nE_H$, where $E_{SWCNT+nH}$ denotes the total energy of hydrogen-chemisorbed nanotube, n represents the number of hydrogen atoms chemisorbed, and E_{SWCNT} and E_H correspond to the energies of pristine nanotube and the hydrogen atom, respectively. The reaction energy E_r can also be considered as hydrogen chemisorption energy. The chemisorption of hydrogen is an exothermic process if the value of E_r is negative (Dinadayalane et al. 2007b).

We observed the rupture of circumferential C1−C2 bond when two hydrogen atoms were chemisorbed in the case of (3,3) SWCNT of 15 carbon layers. As shown in Fig. 43, the reactions of single as well as two hydrogen chemisorptions on the surface of armchair SWCNTs are highly exothermic. The reaction energy for the addition of two H atoms is more than two times that of one H chemisorption except for H(1,3) addition. Our computational study revealed a competition between H(1,2) and H(1,4) addition in the case of (5,5) and (6,6) SWCNTs, but such competition was not seen in the case of narrow diameter (3,3) and (4,4) SWCNTs. Increasing the length of the tube has pronounced effect on the reaction energy of hydrogen chemisorption. In case of armchair SWCNTs, the chemisorption of two hydrogen atoms at alternate positions is thermodynamically less favored compared to H(1,2) and H(1,2') additions regardless of the length and diameter of the tubes (Dinadayalane et al. 2007b). The least positional preference of H(1,3) for armchair SWCNTs is different compared to the results of zigzag-type nanotubes (Yang et al.

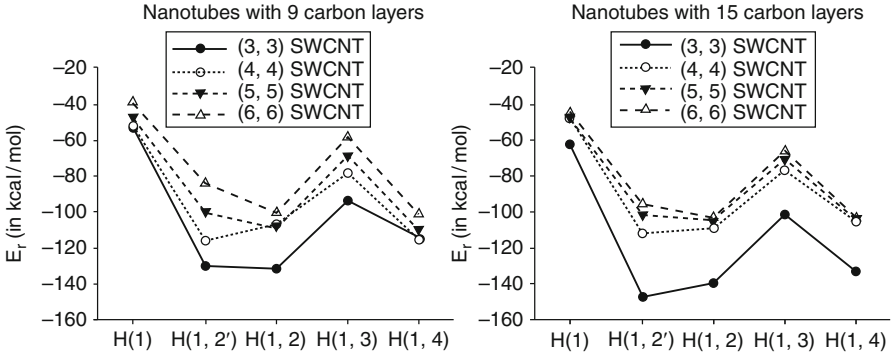

Fig. 43 The variation of reaction energies at the B3LYP/6-31G(d) level for the chemisorption of one and two hydrogen atoms on the external surface of (3,3), (4,4), (5,5), and (6,6) armchair single-walled carbon nanotubes (SWCNTs) (Reprinted with permission from reference Dinadayalane et al. (2007b)). Copyright 2007 American Chemical Society)

2006c; Dinadayalane et al. 2007b). We found that the H chemisorption on nanotubes of different diameters and the positions of two hydrogen atoms chemisorbed on the surface of armchair SWCNTs can be characterized by C−H stretching frequencies of chemisorbed hydrogen atoms (Dinadayalane et al. 2007b). In the investigation of chemisorption of H atoms with (3,3) and (4,4) SWCNTs of different lengths, we found that changing the length of the nanotube has significant effect on the reaction energy of hydrogen chemisorption and HOMO–LUMO gap of pristine and hydrogen-chemisorbed SWCNTs (Kaczmarek et al. 2007).

The reactivity pattern was predicted for the hydrogenation in chiral SWCNTs (Ormsby and King 2007). Investigations involving chiral SWCNTs are more challenging than for zigzag and armchair SWCNTs because single unit cell contains many atoms; consequently, more computational resources are required. Computational study demonstrated that hydrogenation of the fully benzenoid (12,9) SWCNT was significantly less energetic (by 8 kcal/mol per mol H_2) than the hydrogenation of (12,7) and (12,8) SWCNTs (Fig. 44). Furthermore, the hydrogenation at an internal Clar double bond or bonds was reported to be more exothermic than at randomly selected internal bonds. Like other polycyclic aromatic hydrocarbons, hydrogenation of double bonds is energetically preferred over hydrogenation of aromatic sextets. The frontier molecular orbitals (HOMO and LUMO) of chiral SWCNTs have maximum amplitude at the double bonds suggesting that Clar's model also predicts the kinetic reactivity. Thus, the frontier molecular orbitals are useful in predicting the favorable sites for hydrogenation in chiral SWCNTs (Ormsby and King 2007).

In the early 2000s, experimentalists found that partial fluorination of the SWCNTs could be used as a technique for cutting the nanotubes of varying lengths. However, the mechanism of cutting the nanotube is not clear (Gu et al. 2002). In a computational study, Bettinger observed a strong oscillation of reaction energy for

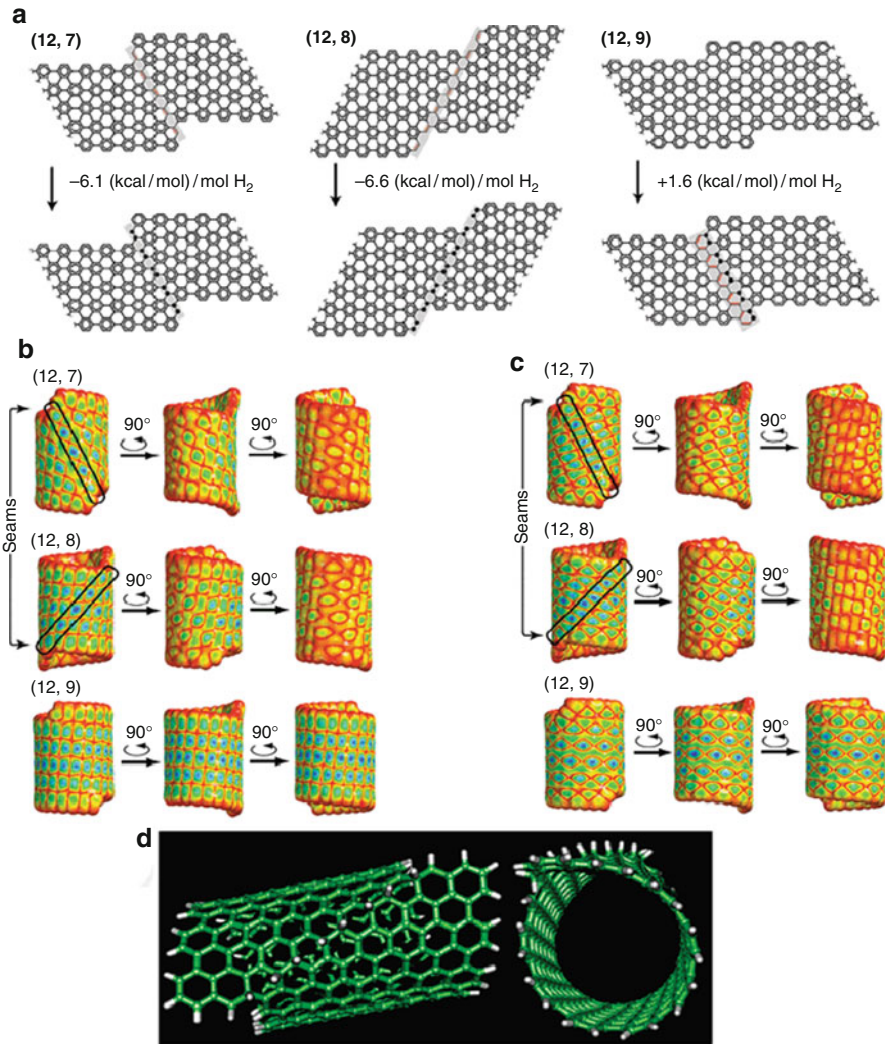

Fig. 44 (**a**) Hydrogenation of equivalent vectors of (12,7), (12,8), and (12,9) chiral SWCNT segments (planar representation). (**b**) HOMO plotted on the isodensity surface for (12,7), (12,8), and (12,9) chiral SWCNTs. (**c**) LUMO plotted on the isodensity surface for (12,7), (12,8), and (12,9) chiral SWCNTs. (**d**) The hydrogenated model chiral SWCNT (*side* and *top* views). The locations of double bond are indicated in (**b**) and (**c**). HOMO and LUMO isodensity surface structures generated at AM1 method (Reprinted with permission from reference Ormsby and King (2007). Copyright 2007 American Chemical Society)

the addition of F atom on the external surface of (5,5) SWCNT of varying lengths (Fig. 45). The computed reaction energy oscillation ranges from 43 to 68 kcal/mol at the UB3LYP/6-31G(d) level using UPBE/3-21G optimized geometries. The shortest tube exhibited the highest exothermicity. The energy oscillation was reported to be

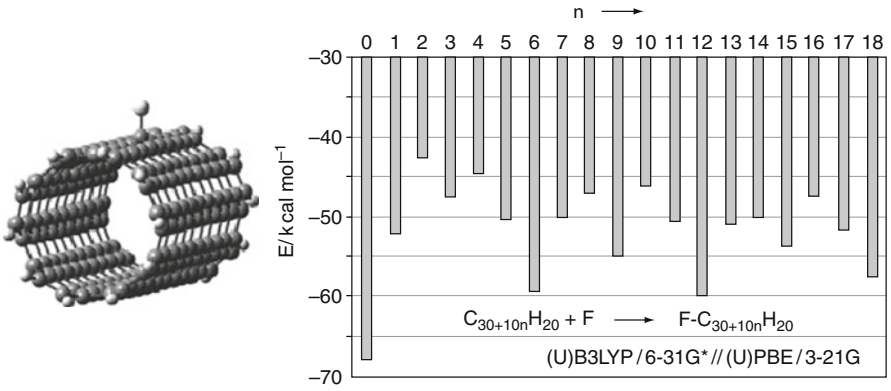

Fig. 45 Variation of reaction energy for the addition of F atom to (5,5) armchair SWCNT of different lengths (n – increasing number of carbon layers) (Reprinted with permission from reference Bettinger (2004)). Copyright 2004 American Chemical Society)

periodic with large exothermicity for the fully benzenoid frameworks, in agreement with their smaller band gaps compared to Kekule and incomplete Clar structures. Computational study demonstrated that the addition of F atom to the sidewall of SWCNT strongly depends on the length of the nanotube (Bettinger 2004). As observed in H atom addition (Dinadayalane et al. 2007b; Kaczmarek et al. 2007; Yang et al. 2006c), the F atom addition to the sidewalls of SWCNTs transforms the carbon atom hybridization from sp^2 to sp^3 (Bettinger 2004).

The chemical reactivity of carbon nanotubes is governed by the local atomic structure. As mentioned earlier, the pyramidalization angle is an important parameter in predicting the chemical reactivity of SWCNTs. Park et al. predicted the hydrogenation and fluorination energies of each carbon from its pyramidalization angle for zigzag SWCNTs (Fig. 46). They formulated the E_{total} for chemisorption of H and F atom on the external surface of zigzag tubes of different diameters as a function of pyramidalization angle of the binding site of tubes. They revealed that the metallic zigzag SWCNTs are slightly more reactive than the semiconducting SWCNTs. Furthermore, the fluorination is more viable than the hydrogenation (Park et al. 2003).

Theoretical Studies on Common Defects in SWCNTs

Investigating the atomic defects is important in tailoring the electronic properties of SWCNTs. Recent experimental study reported a method to selectively modify the electronic properties of semiconductor SWCNTs by the creation and annihilation of point defects on their surface with the tip of a scanning tunneling microscope (STM) (Berthe et al. 2007). Such experimental study motivates theoreticians to explore the structures, energetics, reactivities, and electronic properties of SWCNTs containing different types of defects.

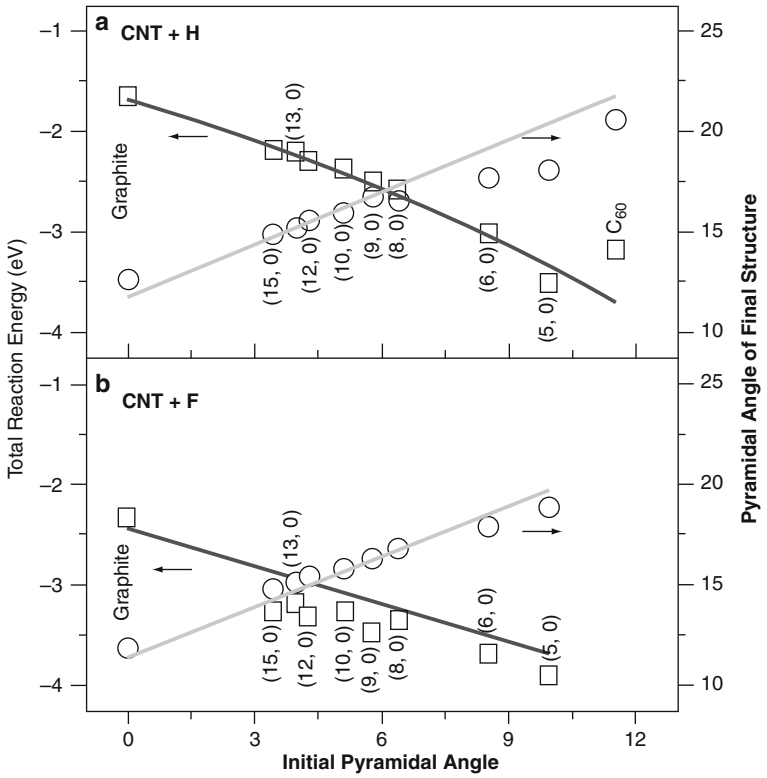

Fig. 46 DFT-computed E_{total} (□) and pyramidalization angle (θ_P) values (○) for fully relaxed configurations and their estimated values (*solid curves*) for (**a**) hydrogenation and (**b**) fluorination (Reprinted with permission from reference Park et al. (2003). Copyright 2003 American Chemical Society)

Stone–Wales Defect

The Stone–Wales defect can be created by 90° rotation of one of the C−C bonds in the hexagonal network of SWCNTs. Two types of C−C bonds exist in each of armchair and zigzag SWCNTs. Therefore, one can generate Stone–Wales defect in two different orientations in both armchair and zigzag SWCNTs (Fig. 47). DFT calculations revealed that the formation energies of (5,5) SWD_II and (10,0) SWD_II are lower than those of (5,5) SWD_I and (10,0) SWD_I. The computed formation energies of (5,5) SWD_I, (5,5) SWD_II, (10,0) SWD_I, and (10,0) SWD_II are 66.4 (2.88 eV), 57.0 (2.47 eV), 68.9 (2.99 eV), and 63.0 (2.73 eV) kcal/mol, respectively. The formation energy was calculated as the relative energy of the Stone–Wales defective tube with respect to the corresponding defect-free SWCNT. It was reported that the formation of Stone–Wales defect causes no change in the HOMO–LUMO gaps (Yang et al. 2006a, b).

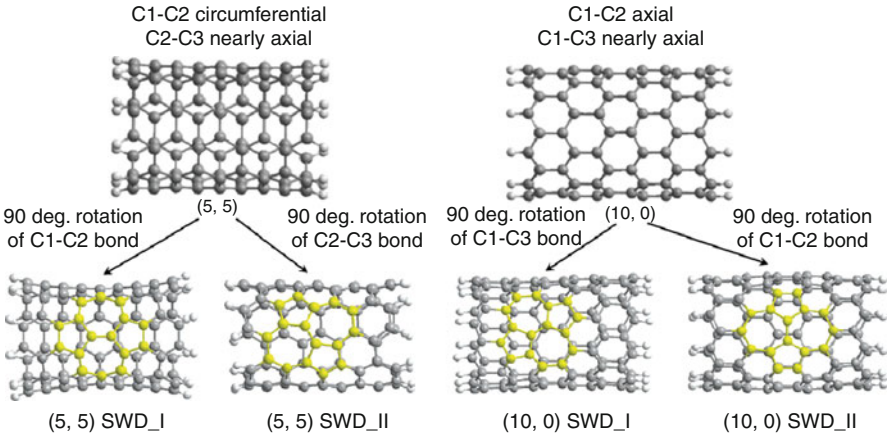

Fig. 47 Generation of Stone–Wales defect with different orientations in (5,5) armchair and (10,0) zigzag SWCNTs. The atoms in the Stone–Wales defect region are highlighted in *yellow color* (Reprinted with permission from reference Yang et al. (2006a). Copyright 2006 American Chemical Society. Reprinted with permission from Yang et al. (2006b). Copyright 2006, American Institute of Physics)

We investigated the structures, formation energies, and reactivities of Stone–Wales defect with two different orientations and different locations from the end of tube in armchair (5,5) SWCNTs of $C_{80}H_{20}$ (I) and $C_{100}H_{20}$ (II) (Fig. 48a; Dinadayalane and Leszczynski 2007b). We employed HF/4-31G, HF/6-31G(d), B3LYP/3-21G, and B3LYP/6-31G(d) levels of theory. HF/4-31G level overestimates the Stone–Wales defect formation energy compared to B3LYP/6-31G(d) level. Our study revealed that B3LYP/3-21G level, which provides reasonable energy estimation, may be employed for large nanotube systems to compute the defect formation energies when the calculations at the B3LYP functionals with large basis sets are prohibitive. Our study showed that the Stone–Wales defective (5,5) armchair SWCNTs generated by rotation of nearly axial bond (ABR) are more stable than those created by circumferential bond rotation (CBR) as shown in Fig. 48b. The SW defect structures generated by ABR show lower HOMO–LUMO gap than those created by CBR and the defect-free SWCNTs (Dinadayalane and Leszczynski 2007b).

Bettinger demonstrated in a comprehensive computational study that some of the bonds of SW defect show higher reactivity than pristine tube; others are less reactive (Bettinger 2005). Computational studies explained the reactivity of carbon atom sites based on the pyramidalization angles (Akdim et al. 2007; Bettinger 2005; Lu et al. 2005). Lu et al. investigated addition of O, CH_2, and O_3 across C−C bonds of SW defective and defect-free armchair SWCNTs. They showed that the central C−C bond of the SW defect in armchair SWCNT (SW defect generated by CBR) is chemically less reactive than that in the perfect tube, and it was attributed to small local curvature in the carbon atoms of central C−C bond of the SW defect (Lu et al. 2005). We found that the values of pyramidalization angles do not completely

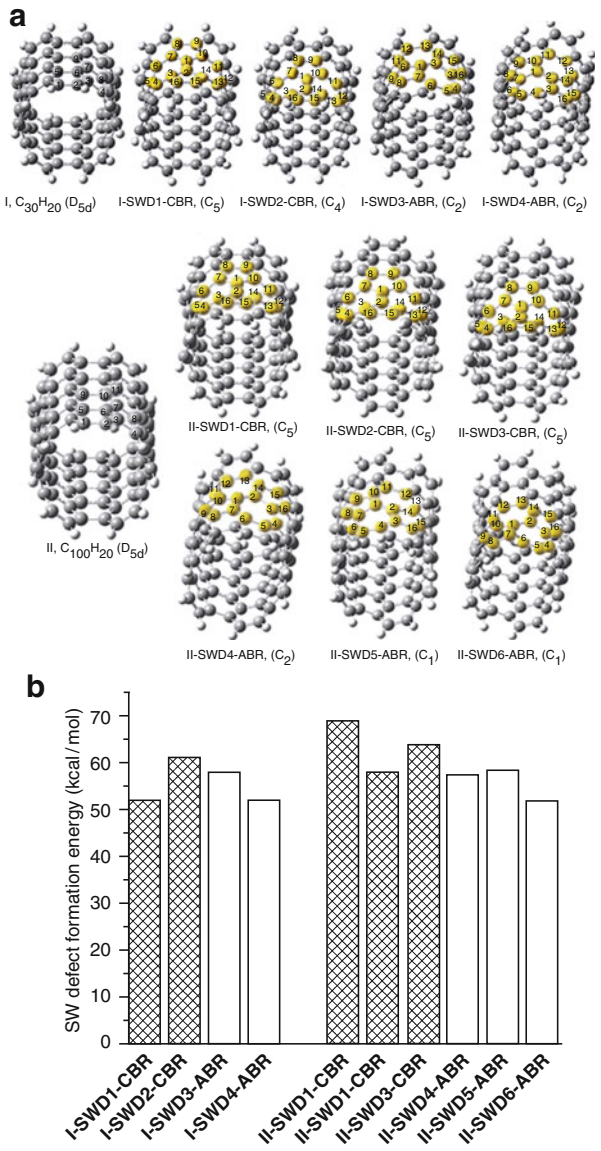

Fig. 48 (**a**) B3LYP/6-31G(d) level optimized structures of defect-free (5,5) armchair SWCNTs and the Stone–Wales defect tubes generated by the 90° rotation of circumferential and nearly axial C–C bonds. (**b**) The Stone–Wales defect formation energy obtained at the B3LYP/6-31G(d) level (Reprinted with permission from reference Dinadayalane and Leszczynski (2007b). Copyright 2007 Elsevier)

explain the reactivity of different bonds of SW defect region for cycloaddition reactions and the reactivity may arise from various other reasons, in addition to topology. We concluded that the cycloaddition reactions across the C–C bond

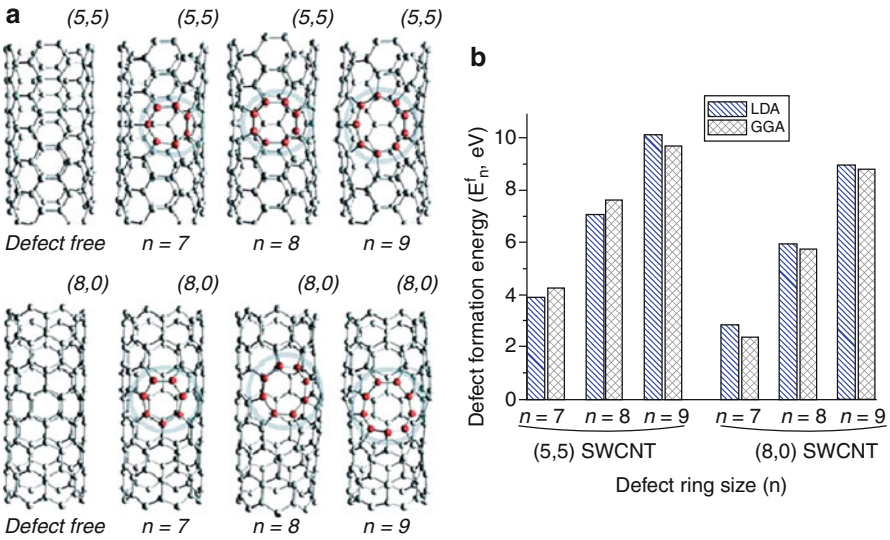

Fig. 49 (**a**) Fully relaxed structures of the defect-free and the defective (5,5) (*upper panel*) and (8,0) (*lower panel*) SWCNTs obtained by the GGA calculations. *Gray balls* and *rods* are the carbon atoms and bonds shorter than 1.5 Å, respectively. Carbon ring defects (given in *red color*) are indicated by the *thick circles*. (**b**) Defect formation energy (E_f^n) of n-membered carbon rings for (5,5) and (8,0) calculated using LDA and GGA (The pictures in (**a**) and the data for (**b**) were taken with permission from Nishidate and Hasegawa (2005). Copyright 2005 by the American Physical Society)

shared by two heptagons (7-7 ring fusion) need not always be less reactive than the corresponding bond in the pristine structure and the reactivity of that bond depends on the orientation of the SWD in the SWCNTs (Dinadayalane and Leszczynski 2007b).

Topological Ring Defects

Nishidate and Hasegawa calculated the formation energies of n-membered topological ring defects with $n = 7$ (heptagon), $n = 8$ (octagon), and $n = 9$ (enneagon) in (5,5) armchair and (8,0) zigzag SWCNTs (Fig. 49a). They used both local density approximation (LDA) and the generalized gradient approximation (GGA: PW91). The spin-polarized projector augmented-wave (PAW) implemented in VASP code was employed for calculations, and periodic boundary condition was used (Nishidate and Hasegawa 2005).

The defect formation energy (E_f^n) of n-membered rings was calculated as the energy difference between the total energy of defective SWCNT (E_{tot}^n) and that of the pristine SWCNT (E_{tot}); i.e., $E_f^n = E_{tot}^n - E_{tot}$. The number of atomsof each defective SWCNT is the same as that of the corresponding SWCNT. Computational

study showed that the defect formation energy increases with increase in defect ring size (n) (Fig. 49b). In general, LDA method yielded higher defect formation energy than generalized gradient approximation. The SWCNTs were reported to be more fragile than the graphene sheet for defect formation. Distortion of the SWCNTs became larger as the defect ring size increases (Nishidate and Hasegawa 2005).

Single- and Di-vacancy Defects

An ideal single vacancy (SV) with three dangling bonds (DBs) was generated by removing one carbon atom from the perfect (5,5) and (10,0) SWCNTs. Upon geometry optimization, an ideal SV with three dangling bonds rearranged into a pentagonal ring and one DB (Yang et al. 2006a). Hence, this defect is called a 5-1DB defect (Lu and Pan 2004; Yang et al. 2006a). In case of (5,5) SWCNT, the optimization of the ideal SV resulted in two different 5-1DB defects. The structures were named as (5,5) SV_I and (5,5) SV_II as shown in Fig. 50. The latter structure was reported to be energetically more favorable (by 1.20 eV) than the former one. A similar behavior was observed for (10,0) zigzag SWCNT. The bond length of

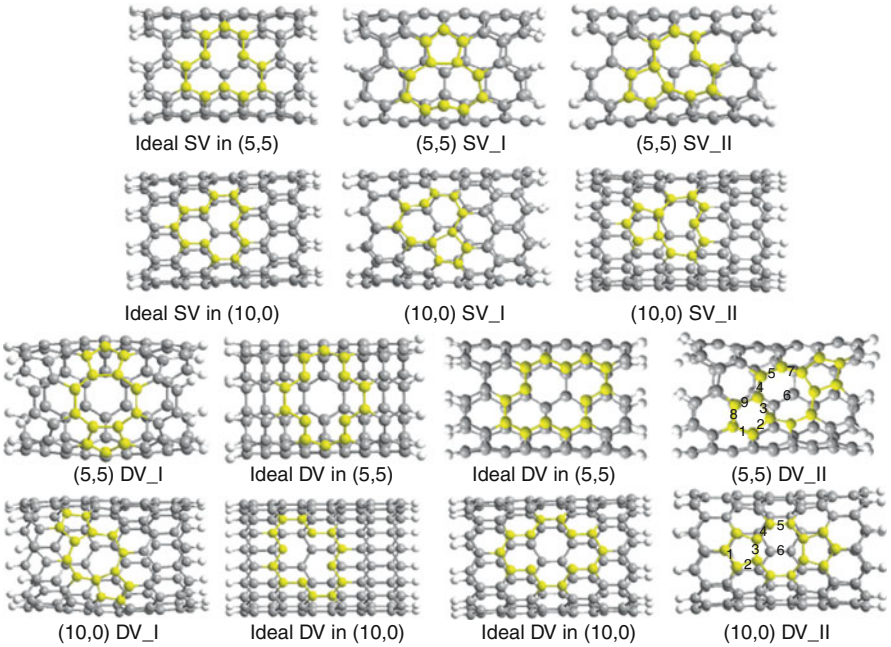

Fig. 50 Configurations of the single (SV) and double (DV) vacancies. Ideal SV and DV mean one and two carbon atoms removed from pristine SWCNT and the structures were not relaxed. Single and double vacancies in two different orientations (I and II) given for (5,5) and (10,0) SWCNTs. Carbon atoms in defect region are given in *yellow color* (Reprinted with permission form reference Yang et al. (2006a). Copyright 2006 American Chemical Society)

the new C−C bond forming five-membered ring is 1.64 Å in (5,5) SV_I, while that of 1.55 Å was obtained for (5,5) SV_II (Yang et al. 2006a). Lu and Pan found using tight-binding calculations that the single-vacancy defect formation energy for (n,n) armchair SWCNTs increases monotonically with increasing tube radii. The formation energy curve of single-vacancy defects in the zigzag (n,0) SWCNTs is periodic, which is mainly characterized by metallic (n,0) tubes (such as (6,0), (9,0), (12,0), (15,0), etc.) (Lu and Pan 2004).

An ideal di-vacancy can be generated by removing two carbon atoms. Two different orientations are possible because of the presence of two different types of bonds in both (5,5) armchair and (10,0) zigzag SWCNTs. Upon geometry optimizations, SWCNTs with ideal di-vacancies yielded 5-8-5 (five-eight-five-membered rings) defects in two different orientations in both armchair- and zigzag-type tubes. Computational study revealed that (5,5) DV_II and (10,0) DV_II configurations are energetically more favorable than (5,5) DV_I and (10,0) DV_I by 0.97 and 0.63 eV, respectively. (5,5) DV_II and (10,0) DV_II can be obtained by removing the carbon atoms with the dangling bond from (5,5) SV_II and (10,0) SV_II, which are the most stable configurations among the possible types of SVs in each type of tubes (Yang et al. 2006a).

The di-vacancy in graphene as well as SWCNTs generates structures possessing two pentagons side by side with an octagon (585 structure) as a result of geometry optimization. The 585 configuration can reconstruct further into a complex structure composed of three pentagons and three heptagons, called 555777 defect structure. In fact, 555777 configuration is more stable than 585 configuration in graphene. Amorim et al. investigated the stability of these types of configurations, derived by di-vacancies, in armchair and zigzag SWCNTs considering different tube diameters (Amorim et al. 2007). The 585 defect in SWCNTs has two possible orientations with respect to the tube axis: perpendicular and tilted in armchair and parallel and tilted in zigzag SWCNTs. For the (5,5) SWCNT, the perpendicular orientation is less stable than the tilted one by 3.5 eV. In case of (8,0) SWCNT, the tilted orientation is less stable by 2.7 eV than the parallel one. Only the tilted and the parallel orientations of defects were considered for armchair and zigzag SWCNTs, respectively (Fig. 51; Amorim et al. 2007).

In contrast to graphene, the 585 defect was predicted to be more stable than the 555777 defect in both armchair and zigzag SWCNTs. Both 585 and 555777 defects in nanotubes (both armchair and zigzag) are more stable than in graphene. The defect formation energy increases monotonically as the diameter of the armchair SWCNT increases (Fig. 52a). The energy difference between the 585 defect and the 555777 defect was computed to be 1.6 eV in case of zigzag tubes, while the difference was reported to be 0.7 eV for armchair SWCNTs. Zigzag SWCNTs exhibited oscillations in the formation energies and the oscillations were related to the alternation between semiconductor and metallic character of the (*n*,0) zigzag SWCNTs (Fig. 52b; Amorim et al. 2007).

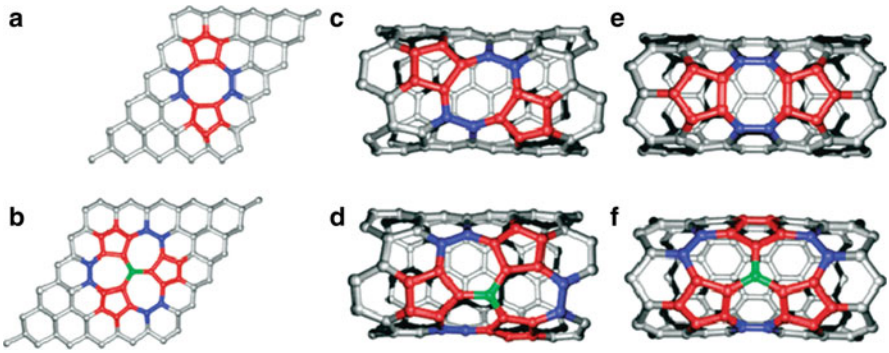

Fig. 51 Ball and stick models for the final geometries of the defects: (**a**) 585 and (**b**) 555777 in graphene; (**c**) 585 tilted and (**d**) 555777 in the (5,5) armchair SWCNT; (**e**) 585 parallel and (**f**) 555777 in the (8,0) zigzag SWCNT. The carbon atoms in pentagons are marked in *red*, the ones that complete either the octagons or the heptagons are colored in *blue*, and the ones at the center of the C_3 symmetry operation in the 555777 defects are colored in *green*. All the others are colored *gray* (Reprinted with permission from reference Amorim et al. (2007). Copyright 2007 American Chemical Society)

Outlook of Potential Applications of Carbon Nanostructures

Graphene is used as a base material for nanoelectromechanical systems (NEMS) due to its lightweight and stiffness properties (Bunch et al. 2007; Robinson et al. 2008). Functionalized graphene can be exploited for water splitting and hydrogen production. Scientists produce graphene-based materials with high structural and electronic quality for the preparation of transparent conducting electrodes for displays and touch screens. Solution processing and chemical vapor deposition are the ideal means to produce thin films that can be used as electrodes in energy devices such as solar panels, batteries, fuel cells, or in hydrogen storage (Bonaccorso et al. 2015). Graphene-based resonators have notable advantages in comparison with nanotubes. Reduced graphene oxide films are used to make drum resonators. The high Young's modulus, extremely low mass, and large surface area make the graphene-based resonators ideally suited for use as mass, force, and charge sensors (Ekinci et al. 2004; Knobel and Cleland 2003; Lavrik and Datskos 2003). Graphene can be used for metallic transistor applications and ballistic transport. One of the potential applications of graphene sheet is its use as membrane for separation (Jiang et al. 2009). Graphene may be useful for electro- and magneto-optics (Geim 2009). Graphane (fully hydrogenated graphene) nanoribbons have quite promising applications in optics and opto-electronics due to the wide band gap. Graphene may also be used for transistor applications (Novoselov et al. 2004). Research into applications for carbon graphene nanosheets has focused on their uses as platforms for next-wave microchips, active materials in field emitter arrays for flat panel screen displays; in gas sensors (Wang et al. 2015a), biological sensors, and medical imaging devices; in solar energy cells; and in high-surface area electrodes for use

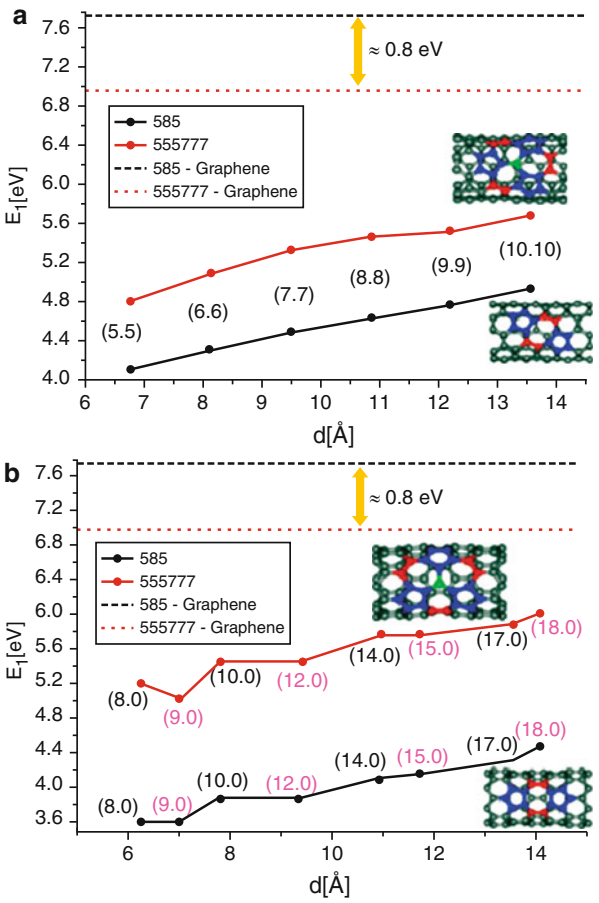

Fig. 52 Formation energy vs. diameter for the 585 and 555777 defects in (**a**) armchair and (**b**) zigzag SWCNTs. The limits for graphene were given in both graphs (Reprinted with permission from reference Amorim et al. (2007). Copyright 2007 American Chemical Society)

in bioscience. Graphene-based materials are known for energy and environmental applications (Bo et al. 2015; Chen et al. 2015; Yuan and He 2015). Graphene is a possible replacement material where carbon nanotubes are presently used (Xia et al. 2009). Graphene-based liquid crystal devices (LCD) show excellent performance with high contrast ratio. Thus, LCDs might be graphene's first realistic commercial application (Blake et al. 2008).

Fullerenes hold possibilities of application in many areas including antiviral activity, enzyme inhibition, DNA cleavage, photodynamic therapy, electron transfer, ball bearings, lightweight batteries, new lubricants, nanoscale electrical switches, new plastics, antitumor therapy for cancer patients, and combustion science and astrophysics (Dresselhaus et al. 1996; Lebedeva et al. 2015). The fullerene derivatives obtained by attachment of electron donor moieties are used as photovoltaic

devices. The supramolecular design of molecular assemblies involving fullerenes holds the possibility to reach new efficient photovoltaic devices (Hudhomme and Cousseau 2007). Fullerenes show promising biomedical applications (Bakry et al. 2007; Bosi et al. 2003; Mashino et al. 2003; Stoilova et al. 2007; Thrash et al. 1999). The fullerene derivatives showed antibacterial and antiproliferative activities; they inhibited bacteria and cancer cell growth effectively (Mashino et al. 2003). Cationic fullerenes were identified to work as antimicrobial photosensitizers. Bis-functionalized C_{60} derivatives have shown the activity against HIV-1 and HIV-2 strains (Bosi et al. 2003). The antiviral activity of fullerene derivatives is based on several biological properties including their unique molecular architecture and antioxidant activity (Bakry et al. 2007). Fullerenes derivatized by hydrophilic moieties are capable of carrying drugs and genes for the cellular delivery (Thrash et al. 1999). The localization of the metallofullerol in bone might be a useful chemotherapeutic agent for treatment of leukemia and bone cancer (Thrash et al. 1999).

Several potential applications have been proposed for carbon nanotubes, for example, conductive and high-strength composites, energy storage and energy conversion devices, sensors, field emission display and radiation sources, and nanotube-based semiconductor devices (Baughman et al. 2002; Sinha and Yeow 2005). Supercapacitors with carbon nanotube electrodes can be used for devices that require higher power capabilities than batteries. Nanotubes have potential application as hydrogen storage (Dinadayalane and Leszczynski 2009). CNTs can be added to aircraft to offer EMI (electromagnetic interference) shielding and lightning strike protection. They will also make the aircraft stronger and lighter, allowing for larger payloads and greater fuel efficiency. They may be used in commercial aircraft and in notebook computers to efficiently draw away generated heat without adding additional weight (Sinha and Yeow 2005). Nanotube films may be used by the automobile industry to make cars and trucks stronger yet lighter and, therefore, more fuel efficient. Three-dimensional graphene-CNT hollow fibers with radially aligned CNTs could be useful for efficient energy conversion and storage (Xue et al. 2015; Yu et al. 2014; Zhu et al. 2012).

MWCNTs show great potential for use in nanofluidic devices because of their high mechanical strength and fluid transport ability at near-molecular length scales (Sinha and Yeow 2005). Due to the advantages of miniature size of the nanotube and the small amount of material required, the carbon nanotubes are being explored for chemical sensing applications. SWCNTs are promising materials for building high-performance nano-sensors and devices (Close et al. 2008). Defects in SWCNTs play an important role in chemical sensing applications (Robinson et al. 2006). CNTs can be used as implanted sensors to monitor pulse, temperature, blood glucose, and heart's activity level and can also be used for repairing damaged cells or killing them by targeting tumors by chemical reactions (Sinha and Yeow 2005). Some of the selected applications of carbon nanotubes are shown in Fig. 53.

Potential biological and biomedical applications of CNTs are under investigation (Dhar et al. 2008; Karousis et al. 2009; Liu et al. 2007; Sinha and Yeow 2005). Carbon nanotubes have potential to make miniature biological electronic devices,

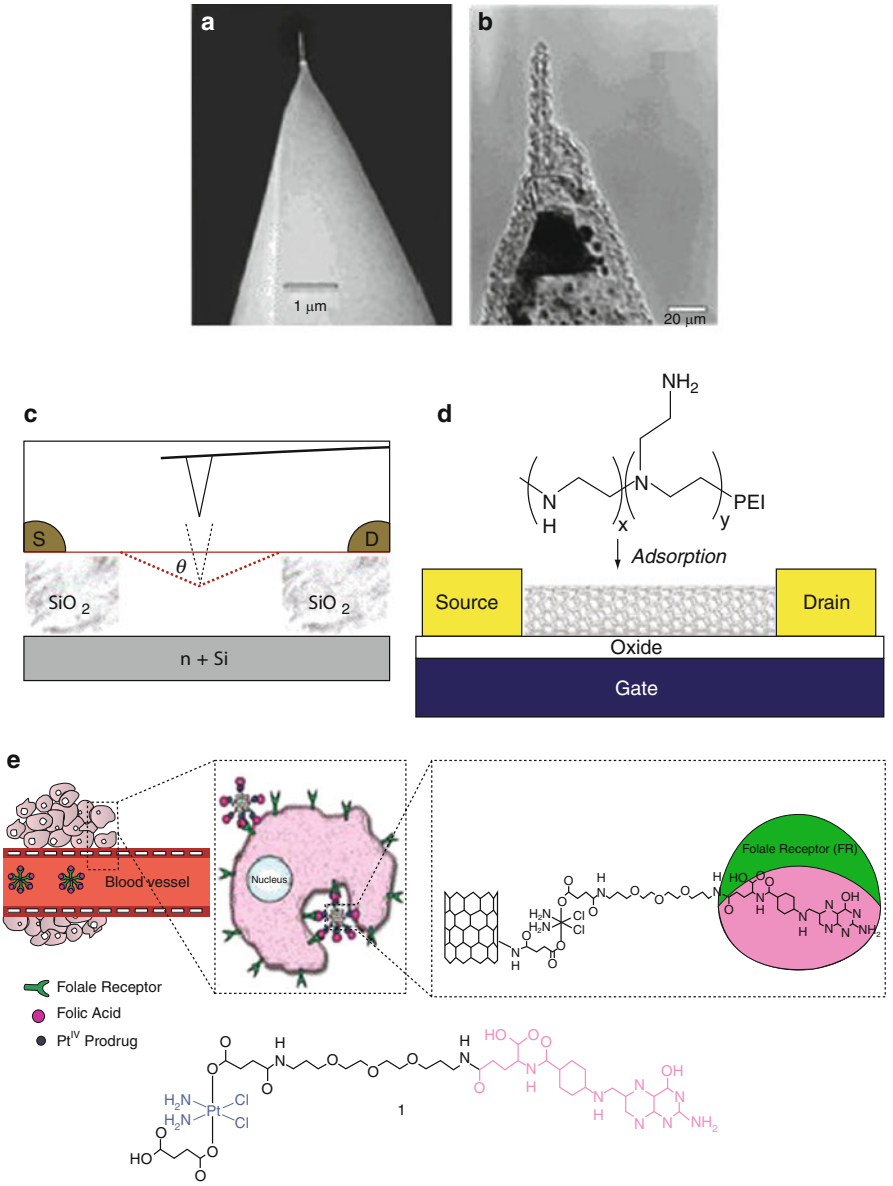

Fig. 53 (**a**) and (**b**) Electron micrographs of two different AFM cantilever tips, each with a nanotube attached; (**a**) an SEM (scanning electron microscope) micrograph of a nanotube. (**b**) A TEM (transmission electron microscope) micrograph of a nanotube (Reprinted with permission from reference Stevens et al. (2000). Copyright 2000 Institute of Physics). (**c**) Nanoelectromechanics of suspended nanotubes – experimental scheme for measuring the electromechanical property of the nanotube. (**d**) The SWCNT evolves into an n-type FET (field-effect transistor) after adsorption of PEI (polyethyleneimine). Pictures (**c**) and (**d**) were reprinted with permission from reference Dai (2002). Copyright 2002 American Chemical Society). (**e**) Folate receptor (FR)-mediated targeting and SWCNT-mediated delivery of Pt-containing complex (Reprinted with permission from reference Dhar et al. (2008). Copyright 2008 American Chemical Society)

including probes and sensors (Sotiropoulou and Chaniotakis 2003; Stevens et al. 2000, 2004). Water-soluble peptidomimetic-functionalized carbon nanotubes have been reported to have antitrypsin activity (Dhar et al. 2008). Functionalized and water-soluble SWCNTs have been explored to find biological applications in the area of drug delivery (Dhar et al. 2008; Karousis et al. 2009; Liu et al. 2007). CNTs could be used as potential delivery tools for peptide-based synthetic vaccines. CNTs are currently being considered as suitable substrate for neuronal growth, as ion channel blockers, and as vectors for gene transfection (Sinha and Yeow 2005). Carbon nanotubes have provided possibilities for applications in nanotechnology. Continuous and optimistic research efforts in the area of carbon nanotubes are required to realize a lot of breakthrough commercial applications.

Summary and Outlook

In this chapter, we provided vital information and up-to-date research on carbon nanostructures, particularly graphene, fullerenes, and carbon nanotubes, which are critical in the nanotechnology revolution. This chapter also covered the modeling aspects, especially the current trends of computational chemistry applications in understanding the structures, reactivity, and other properties of abovementioned carbon nanostructures, and their importance in supporting the experimental results. Many aspects of basic research and practical application requirements have been motivating both theoreticians and experimentalists to gain better understanding about the carbon nanostructures. Obtaining knowledge on a specific class of chemical reactions with graphene, fullerenes, and SWCNTs is required for making novel materials as well as producing carbon-based nanomaterials for specific applications. Computational investigations provide opportunity to understand the structures, binding of atoms/molecules with the carbon nanotubes. A systematic and careful computational chemistry approaches could have important implications for the rational design of novel CNT composite materials, novel nanotube-based sensors, as well as for the development of new chemical strategies for SWCNT functionalization. Strong interactions between experimentalists and theoreticians working in the area of carbon nanostructures will enhance the real-time applications rapidly. Future efforts should not only provide high-tech nano-devices but also address fundamental scientific questions. Further exciting developments in nanoscience and nanotechnology are expected.

Acknowledgments This work was supported by the High Performance Computational Design of Novel Materials (HPCDNM) Project funded by the Department of Defense (DoD) through the US Army Engineer Research and Development Center (Vicksburg, MS) Contract # W912HZ-06-C-0057 and by the Office of Naval Research (ONR) grant 08PRO2615-00/N00014-08-1-0324. JL acknowledges the support from the National Science Foundation (NSF) for the Interdisciplinary Center for Nanotoxicity (ICN) through CREST grant HRD-0833178. TCD acknowledges the start up support provided by the Clark Atlanta University.

Bibliography

Abanin, D. A., Lee, P. A., & Levitov, L. S. (2006). Spin-filtered edge states and quantum hall effect in graphene. *Physical Review Letters, 96*, 176803-1–176803-4.

Achiba, Y., Kikuchi, K., Aihara, Y., Wakabayashi, Y., Miyake, Y., & Kainosho, M. (1995). In P. Bernier, D. S. Bethune, L. Y. Chiang, T. W. Ebbesen, R. M. Metzger, & J. W. Mintmire, J. W. (Eds.), *Higher fullerenes: Structure and properties* (Materials Research Society symposium proceedings, Vol. 359, p. 3). Pittsburgh, PA: Materials Research Society.

Achiba, Y., Kikuchi, K., Aihara, Y., Wakabayashi, T., Miyake, Y., & Kainosho, M. (1996). Fullerenes and Endofullerenes: Model Substances?. In W. Andreoni (Ed.), *The chemical physics of fullerenes 10 (and 5) years later: the far-reaching impact of the discovery of C60* (p. 139). Dordrecht: Kluwer.

Akdim, B., Kar, T., Duan, X., & Pachter, R. (2007). Density functional theory calculations of ozone adsorption on sidewall single-wall carbon nanotubes with Stone-Wales defects. *Chemical Physics Letters, 445*, 281–287.

Amorim, R. G., Fazzio, A., Antonelli, A., Novaes, F. D., & da Silva, A. J. R. (2007). Divacancies in graphene and carbon nanotubes. *Nano Letters, 7*, 2459–2462.

Amsharov, K. Y., & Jensen, M. (2008). A C_{78} fullerene precursor: Toward the direct synthesis of higher fullerenes. *Journal of Organic Chemistry, 73*, 2931–2934.

An, W., Gao, Y., Bulusu, S., & Zeng, X. C. (2005). Ab initio calculation of bowl, cage, and ring isomers of C_{20} and C_{20}^-. *Journal of Chemical Physics, 122*, 204109-1–204109-8.

Andzelm, J., Govind, N., & Maiti, A. (2006). Nanotube-based gas sensors – Role of structural defects. *Chemical Physics Letters, 421*, 58–62.

Arnold, M. S., Green, A. A., Hulvat, J. F., Stupp, S. I., & Hersam, M. C. (2006). Sorting carbon nanotubes by electronic structure using density differentiation. *Nature Nanotechnology, 1*, 60–65.

Austin, S. J., Fowler, P. W., Manolopoulos, D. E., & Zerbetto, F. (1995). The Stone-Wales map forC_{60}. *Chemical Physics Letters, 235*, 146–151.

Avila, A. F., & Lacerda, G. S. R. (2008). Molecular mechanics applied to single-walled carbon nanotubes. *Materials Research, 11*, 325–333.

Avouris, P., Chen, Z. H., & Perebeinos, V. (2007). Carbon-based electronics. *Nature Nanotechnology, 2*, 605–615.

Bakry, R., Vallant, R. M., Najam-ul-Haq, M., Rainer, M., Szabo, Z., Huck, C. W., & Bonn, G. K. (2007). Medicinal applications of fullerenes. *International Journal of Nanomedicine, 2*, 639–649.

Balandin, A. A., Ghosh, S., Bao, W., Calizo, I., Teweldebrhan, D., Miao, F., & Lau, C. N. (2008). Superior thermal conductivity of single-layer graphene. *Nano Letters, 8*, 902–907.

Barth, W. E., & Lawton, R. G. (1966). Dibenzo[ghi, mno]fluoranthene. *Journal of the American Chemical Society, 88*, 380–381.

Baughman, R. H., Zakhidov, A. A., & de Heer, W. A. (2002). Carbon nanotubes-the route toward applications. *Science, 297*, 787–792.

Beavers, C. M., Zuo, T., Duchamp, J. C., Harich, K., Dorn, H. C., Olmstead, M. M., & Balch, A. L. (2006). $Tb_3N@C_{84}$: An improbable, egg-shaped endohedral fullerene that violates the isolated pentagon rule. *Journal of the American Chemical Society, 128*, 11352–11353.

Becke, A. D. (1993). Density-functional thermochemistry. III. The role of exact exchange. *Journal of Chemistry Physics, 98*, 5648–5652.

Becker, L., Bada, J. L., Winans, R. E., Hunt, J. E., Bunch, T. E., & French, B. M. (1994). Fullerenes in the 1.85-billion-year-old Sudbury impact structure. *Science, 265*, 642–645.

Berthe, M., Yoshida, S., Ebine, Y., Kanazawa, K., Okada, A., Taninaka, A., Takeuchi, O., Fukui, N., Shinohara, H., Suzuki, S., Sumitomo, K., Kobayashi, Y., Grandidier, B., Stievenard, D., & Shigekawa, H. (2007). Reversible defect engineering of single-walled carbon nanotubes using scanning tunneling microscopy. *Nano Letters, 7*, 3623–3627.

Bethune, D. S., Klang, C.-H., de Vries, M. S., Gorman, G., Savoy, R., Vazquez, J., & Beyers, R. (1993). Cobalt-catalysed growth of carbon nanotubes with single-atomic-layer walls. *Nature, 363*, 605–607.

Bettinger, H. F. (2004). Effects of finite carbon nanotube length on sidewall addition of fluorine atom and methylene. *Organic Letters, 6*, 731–734.

Bettinger, H. F. (2005). The reactivity of defects at the sidewalls of single-walled carbon nanotubes: The Stone−Wales defect. *Journal of Physical Chemistry B, 109*, 6922–6924.

Bettinger, H. F. (2006). Addition of carbenes to the sidewalls of single-walled carbon nanotubes. *Chemistry – A European Journal, 12*, 4372–4379.

Bettinger, H. F., Yakobson, B. I., & Scuseria, G. E. (2003). Scratching the surface of buckminsterfullerene: The barriers for Stone-Wales transformation through symmetric and asymmetric transition states. *Journal of the American Chemical Society, 125*, 5572–5580.

Blake, P., Brimicombe, P. D., Nair, R. R., Booth, T. J., Jiang, D., Schedin, F., Ponomarenko, L. A., Morozov, S. V., Gleeson, H. F., Hill, E. W., Geim, A. K., & Novoselov, K. S. (2008). Graphene-based liquid crystal device. *Nano Letters, 8*, 1704–1708.

Bo, Z., Mao, S., Han, Z. J., Cen, K., Chen, J., & Ostrikov, K. (2015). Emerging energy and environmental applications of vertically-oriented graphenes. *Chemical Society Reviews, 44*, 2108–2121.

Bonaccorso, F., Colombo, L., Yu, G., Stoller, M., Tozzini, V., Ferrari, A. C., Ruoff, R. S., & Vittorio Pellegrini, V. (2015). Graphene, related two-dimensional crystals, and hybrid systems for energy conversion and storage. *Science, 347*, 1246501.

Bosi, S., Ros, T. D., Spalluto, G., Balzarini, J., & Pratoa, M. (2003). Synthesis and anti-HIV properties of new water-soluble bis-functionalized[60]fullerene derivatives. *Bioorganic and Medicinal Chemistry Letters, 13*, 4437–4440.

Boukhvalov, D. W., & Katsnelson, M. I. (2008). Chemical functionalization of graphene with defects. *Nano Letters, 8*, 4373–4379.

Boukhvalov, D. W., Katsnelson, M. I., & Lichtenstein, A. I. (2008). Hydrogen on graphene: Electronic structure, total energy, structural distortions and magnetism from first-principles calculations. *Physical Review B, 77*, 035427-1–035427-7.

Bunch, J. S., van der Zande, A. M., Verbridge, S. S., Frank, I. W., Tanenbaum, D. M., Parpia, J. M., Craighead, H. G., & McEuen, P. L. (2007). Electromechanical resonators from graphene sheets. *Science, 315*, 490–493.

Burda, C., Samia, A. C. S., Hathcock, D. J., Huang, H., & Yang, S. (2002). Experimental evidence for the photoisomerization of higher fullerenes. *Journal of the American Chemical Society, 124*, 12400–12401.

Buseck, P. R., Tsipursky, S. J., & Hettich, R. (1992). Fullerenes from the geological environment. *Science, 257*, 215–217.

Cabrera-Sanfelix, P., & Darling, G. R. (2007). Dissociative adsorption of water at vacancy defects in graphite. *The Journal of Physical Chemistry C, 111*, 18258–18263.

Calaminici, P., Geudtner, G., & Koster, A. M. (2009). First-principle calculations of large fullerenes. *Journal of Chemical Theory and Computation, 5*, 29–32.

Carlson, J. M., & Scheffler, M. (2006). Structural, electronic, and chemical properties of nanoporous carbon. *Physical Review Letters, 96*, 046806-1–046806-4.

Carpio, A., Bonilla, L. L., de Juan, F., & Vozmediano, M. A. H. (2008). Dislocations in graphene. *New Journal of Physics, 10*, 053021-1–053021-13.

Chakraborty, A. K., Woolley, R. A. J., Butenko, Y. V., Dhanak, V. R., Šiller, L., & Hunt, M. R. C. (2007). A photoelectron spectroscopy study of ion-irradiation induced defects in single-wall carbon nanotubes. *Carbon, 45*, 2744–2750.

Chandra, N., Namilae, S., & Shet, C. (2004). Local elastic properties of carbon nanotubes in the presence of Stone-Wales defects. *Physical Review B, 69*, 094101-1–094101-12.

Charlier, J.-C. (2002). Defects in carbon nanotubes. *Accounts of Chemical Research, 35*, 1063–1069.

Charlier, J.-C., Ebbesen, T. W., & Lambin, P. (1996). Structural and electronic properties of pentagon- heptagon pair defects in carbon nanotubes. *Physical Review B, 53*, 11108–11113.

Chaur, M. N., Valencia, R., Rodríguez-Fortea, A., Poblet, J. M., & Echegoyen, L. (2009a). Trimetallic nitride endohedral fullerenes: Experimental and theoretical evidence for the $M_3N^{6+}@C_{2n}^{6-}$ model. *Angewandte Chemie, International Edition, 48*, 1425–1428.

Chaur, M. N., Melin, F., Ortiz, A. L., & Echegoyen, L. (2009b). Chemical, electrochemical, and structural properties of endohedral metallofullerenes. *Angewandte Chemie, International Edition, 48*, 7514–7538.

Chen, Z. (2004). The smaller fullerene C_{50}, isolated as $C_{50}Cl_{10}$. *Angewandte Chemie, International Edition, 43*, 4690–4691.

Chen, Z., Thiel, W., & Hirsch, A. (2003). Reactivity of the convex and concave surfaces of single-walled carbon nanotubes (SWCNTs) towards addition reactions: Dependence on the carbon-atom pyramidalization. *Chemical Physics and Physical Chemistry, 4*, 93–97.

Chen, K., Song, S., Liu, F., & Xue, D. (2015). Structural design of graphene for use in electrochemical energy storage devices. *Chemical Society Reviews, 44*, 6230–6257.

Chico, L., Crespi, V. H., Benedict, L. X., Louie, S. G., & Cohen, M. L. (1996). Pure carbon nanoscale devices: Nanotube heterojunctions. *Physical Review Letters, 76*, 971–974.

Cho, E., Shin, S., & Yoon, Y.-G. (2008). First-principles studies on carbon nanotubes functionalized with azomethine ylides. *The Journal of Physical Chemistry C, 112*, 11667–11672.

Christian, J. F., Wan, Z., & Anderson, S. L. (1992). $O^+ + C_{60} \cdot C_{60}O^+$ production and decomposition, charge transfer, and formation of $C_{59}O^+$. Dopeyball or $[CO@C_{58}{}^+]$. *Chemical Physics Letters, 199*, 373–378.

Chun, H., Hahm, M. G., Homma, Y., Meritz, R., Kuramochi, K., Menon, L., Ci, L., Ajayan, P. M., & Jung, Y. J. (2009). Engineering low-aspect ratio carbon nanostructures: Nanocups, nanorings, and nanocontainers. *ACS Nano, 3*, 1274–1278.

Chuvilin, A., Kaiser, U., Bichoutskaia, E., Besley, N. A., & Khlobystov, A. N. (2010). Direct transformation of graphene to fullerene. *Nature Chemistry, 2*, 450–453.

Cioslowski, J., Rao, N., & Moncrieff, D. (2002). Electronic structures and energetics of [5,5] and [9,0] single-walled carbon nanotubes. *Journal of the American Chemical Society, 124*, 8485–8489.

Close, G. F., Yasuda, S., Paul, B., Fujita, S., & Wong, H. S. P. (2008). A 1 GHz integrated circuit with carbon nanotube interconnects and silicon transistors. *Nano Letters, 8*, 706–709.

Cohen, M. L. (1993). Predicting useful materials. *Science, 261*, 307–308.

Crassous, J., Rivera, J., Fender, N. S., Shu, L., Echegoyen, L., Thilgen, C., Herrmann, A., & Diederich, F. (1999). Chemistry of C_{84}: Separation of three constitutional isomers and optical resolution of D_2-C_{84} by using the "Bingel-Retro-Bingel" strategy. *Angewandte Chemie, International Edition, 38*, 1613–1617.

Cuesta, I. G., Pedersen, T. B., Koch, H., & de Meras, A. S. (2006). Carbon nanorings: A challenge to theoretical chemistry. *Chemical Physics and Physical Chemistry, 7*, 2503–2507.

Cyranski, M. K., Howard, S. T., & Chodkiewicz, M. L. (2004). Bond energy, aromatic stabilization energy and strain in IPR fullerenes. *Chemical Communications*, 2458–2459

Dai, H. (2002). Carbon nanotubes: Synthesis, integration, and properties. *Accounts of Chemical Research, 35*, 1035–1044.

David, W. I. F., Ibberson, R. M., Matthewman, J. C., Prassides, K., Dennis, T. J. S., Hare, J. P., Kroto, H. W., Taylor, R., & Walton, D. R. M. (1991). Crystal structure and bonding of ordered C_{60}. *Nature, 353*, 147–149.

David, V. P., Lin, X., Zhang, H., Liu, S., & Kappes, M. M. (1992). Transmission electron microscopy of C_{70} single crystals at room temperature. *Journal of Materials Research, 7*, 2440–2446.

Deng, J.-P., Ju, D.-D., Her, G.-R., Mou, C.-Y., Chen, C.-J., Lin, Y.-Y., & Han, C.-C. (1993). Odd-numbered fullerene fragment ions from C_{60} oxides. *Journal of Physical Chemistry, 97*, 11575–11577.

Denis, P. A., Iribarne, F., & Faccio, R. (2009). Hydrogenated double wall carbon nanotubes. *Journal of Chemical Physics, 130*, 194704-1–194704-10.

Dennis, T. J. S., & Shinohara, H. (1998). Isolation and characterisation of the two major isomers of [84]fullerene (C_{84}). *Chemical Communications*, 619–620.

Dereli, G., & Sungu, B. (2007). Temperature dependence of the tensile properties of single-walled carbon nanotubes: O(N) tight-binding molecular-dynamics simulations. *Physical Review B, 75*, 184104-1–184104-6.

Dewar, M. J. S., & Thiel, W. (1977). Ground states of molecules. 38. The MNDO method. Approximations and parameters. *Journal of the American Chemical Society, 99*, 4899–4907.

Dewar, M. J. S., Zoebisch, E. G., Healy, E. F., & Stewart, J. J. P. (1985). Development and use of quantum mechanical molecular models. 76. AM1: A new general purpose quantum mechanical molecular model. *Journal of the American Chemical Society, 107*, 3902–3909.

Dewar, M. J. S., Jie, C., & Yu, J. (1993). SAM1; The first of a new series of general purpose quantum mechanical molecular models. *Tetrahedron, 49*, 5003–5038.

Dhar, S., Liu, Z., Thomale, J., Dai, H., & Lippard, S. J. (2008). Targeted single-wall carbon nanotube- mediated Pt(IV) prodrug delivery using folate as a homing device. *Journal of the American Chemical Society, 130*, 11467–11476.

Diederich, F., Ettl, R., Rubin, Y., Whetten, R. L., Beck, R., Alvarez, M., Anz, S., Sensharma, D., Wudl, F., Khemani, K. C., & Koch, A. (1991a). The higher fullerenes: Isolation and characterization of C_{76}, C_{84}, C_{90}, C_{94}, and $C_{70}O$, an oxide of D_{5h}-C_{70}. *Science, 252*, 548–551.

Diederich, F., Whetten, R. L., Thilgen, C., Ettl, R., Chao, I., & Alvarez, M. M. (1991b). Fullerene isomerism: Isolation of C_{2v}-C_{78} and D_3-C_{78}. *Science, 254*, 1768–1770.

Dillon, A. C., Jones, K. M., Bekkedahl, T. A., Kiang, C. H., Bethune, D. S., & Heben, M. J. (1997). Storage of hydrogen in single-walled carbon nanotubes. *Nature, 386*, 377–379.

Dinadayalane, T. C., & Leszczynski, J. (2007a). Toward nanomaterials: Structural, energetic and reactivity aspects of single-walled carbon nanotubes. In P. B. Balbuena & J. M. Seminario (Eds.), *Nanomaterials: Design and simulation* (Theoretical and computational chemistry, Vol. 18, pp. 167–199). Amsterdam: Elsevier.

Dinadayalane, T. C., & Leszczynski, J. (2007b). StoneWales defects with two different orientations in (5, 5) single-walled carbon nanotubes: A theoretical study. *Chemical Physics Letters, 434*, 86–91.

Dinadayalane, T. C., & Leszczynski, J. (2009). Toward understanding of hydrogen storage in single-walled carbon nanotubes by chemisorption mechanism. In J. Leszczynski & M. K. Shukla (Eds.), *Practical aspects of computational chemistry: Methods, concepts and applications* (pp. 297–313). Dordrecht: Springer.

Dinadayalane, T. C., & Sastry, G. N. (2001). Synthetic strategies toward buckybowls and C_{60}: Benzannulation is remarkably facile compared to cyclopentannulation. *Tetrahedron Letters, 42*, 6421–6423.

Dinadayalane, T. C., & Sastry, G. N. (2002a). Structure-energy relationships in curved polycyclic aromatic hydrocarbons: Study of benzocorannulenes. *Journal of Organic Chemistry, 67*, 4605–4607.

Dinadayalane, T. C., & Sastry, G. N. (2002b). An assessment of semiempirical (MNDO, AM1 and PM3) methods to model buckybowls. *Journal of Molecular Structure (THEOCHEM), 579*, 63–72.

Dinadayalane, T. C., & Sastry, G. N. (2003). Isolated pentagon rule in buckybowls: A computational study on thermodynamic stabilities and bowl-to-bowl inversion barriers. *Tetrahedron, 59*, 8347–8351.

Dinadayalane, T. C., Priyakumar, U. D., & Sastry, G. N. (2001). Theoretical studies on the effect of sequential benzannulation to corannulene. *Journal of Molecular Structure (THEOCHEM), 543*, 1–10.

Dinadayalane, T. C., Priyakumar, U. D., & Sastry, G. N. (2002). Ring closure synthetic strategies toward buckybowls: Benzannulation versus cyclopentannulation. *Journal of the Chemical Society, Perkin Transactions, 2*, 94–101.

Dinadayalane, T. C., Deepa, S., & Sastry, G. N. (2003). Is peri hydrogen repulsion responsible for flattening buckybowls? The effect of ring annelation to the rim of corannulene. *Tetrahedron Letters, 44*, 4527–4529.

Dinadayalane, T. C., Deepa, S., Reddy, A. S., & Sastry, G. N. (2004). Density functional theory study on the effect of substitution and ring annelation to the rim of corannulene. *Journal of Organic Chemistry, 69*, 8111–8114.

Dinadayalane, T. C., Gorb, L., Simeon, T., & Dodziuk, H. (2007a). Cumulative p-p interaction triggers unusually high stabilization of linear hydrocarbons inside the single-walled carbon nanotube. *International Journal of Quantum Chemistry, 107*, 2204–2210.

Dinadayalane, T. C., Kaczmarek, A., Łukaszewicz, J., & Leszczynski, J. (2007b). Chemisorption of hydrogen atoms on the sidewalls of armchair single-walled carbon nanotubes. *Journal of Physical Chemistry C, 111*, 7376–7383.

Ding, F. (2005). Theoretical study of the stability of defects in single-walled carbon nanotubes as a function of their distance from the nanotube end. *Physical Review B, 72*, 245409-1–245409-7.

Dresselhaus, M. S., Dresselhaus, G., & Eklund, P. C. (1996). *Science of fullerenes and carbon nanotubes: Their properties and applications*. San Diego: Academic.

Dresselhaus, M. S., Dresselhaus, G., & Avouris, P. (Eds.). (2001). *Carbon nanotubes: Synthesis, structure, properties, and applications*. Berlin: Springer.

Dresselhaus, M. S., Dresselhaus, G., Jorio, A., Filho, A. G. S., Pimenta, M. A., & Saito, R. (2002). Single nanotube Raman spectroscopy. *Accounts of Chemical Research, 35*, 1070–1078.

Dresselhaus, M. S., Dresselhaus, G., Saito, R., & Jorio, A. (2005). Raman spectroscopy of carbon nanotubes. *Physics Reports, 409*, 47–99.

Dresselhaus, M. S., Dresselhaus, G., & Jorio, A. (2007). Raman spectroscopy of carbon nanotubes in 1997 and 2007. *The Journal of Physical Chemistry C, 111*, 17887–17893.

Dulap, B. I., & Zope, R. R. (2006). Efficient quantum-chemical geometry optimization and the structure of large icosahedral fullerenes. *Chemical Physics Letters, 422*, 451–454.

Dunlap, B. I., Brenner, D. W., Mintmire, J. W., Mowrey, R. C., & White, C. T. (1991). Local density functional electronic structures of three stable icosahedral fullerenes. *Journal of Physical Chemistry, 95*, 8737–8741.

Duplock, E. J., Scheffler, M., & Lindan, P. J. D. (2004). Hallmark of perfect graphene. *Physical Review Letters, 92*, 225502-1–225502-4.

Eggen, B. R., Heggie, M. I., Jungnickel, G., Latham, C. D., Jones, R., & Briddon, P. R. (1996). Autocatalysis during fullerene growth. *Science, 272*, 87–89.

Ekinci, K. L., Huang, X. M. H., & Roukes, M. L. (2004). Ultrasensitive nanoelectromechanical mass detection. *Applied Physics Letters, 84*, 4469–4471.

Elias, D. C., Nair, R. R., Mohiuddin, T. M. G., Morozov, S. V., Blake, P., Halsall, M. P., Ferrari, A. C., Boukhvalov, D. W., Katsnelson, M. I., Geim, A. K., & Novoselov, K. S. (2009). Control of graphene's properties by reversible hydrogenation: Evidence for graphene. *Science, 323*, 610–613.

Ertekin, E., Chrzan, D. C., & Daw, M. S. (2009). Topological description of the Stone-Wales defect formation energy in carbon nanotubes and graphene. *Physical Review B, 79*, 155421-1–155421-17.

Esquivel, E. V., & Murr, L. E. (2004). A TEM analysis of nanoparticulates in a polar ice core. *Materials Characterization, 52*, 15–25.

Feng, X., Irle, S., Witek, H., Morokuma, K., Vidic, R., & Borguet, E. (2005). Sensitivity of ammonia interaction with single-walled carbon nanotube bundles to the presence of defect sites and functionalities. *Journal of the American Chemical Society, 127*, 10533–10538.

Fischer, J. E., Heiney, P. A., McGhie, A. R., Romanow, W. J., Denenstein, A. M., McCauley, J. P., Jr., & Smith, A. B., III. (1991). Compressibility of solid C_{60}. *Science, 252*, 1288–1290.

Fowler, P. W., & Heine, T. (2001). Stabilisation of pentagon adjacencies in the lower fullerenes by functionalisation. *Journal of the Chemical Society, Perkin Transactions, 2*, 487–490.

Fowler, P. W., & Manolopoulos, D. E. (1995). *An atlas of fullerenes*. New York: Oxford University Press.

Frisch, M. J. et al. (2003). *Gaussian 03, revision E.1*. Pittsburg, PA: Gaussian.

Fu, W., Xu, L., Azurmendi, H., Ge, J., Fuhrer, T., Zuo, T., Reid, J., Shu, C., Harich, K., & Dorn, H. C. (2009). ^{89}Y and ^{13}C NMR cluster and carbon cage studies of an yttrium metallofullerene

family, $Y_3N@C_{2n}$ ($n = 40 - 43$). *Journal of the American Chemical Society, 131*, 11762–11769.

Galano, A. (2006). On the influence of diameter and length on the properties of armchair single-walled carbon nanotubes: A theoretical chemistry approach. *Chemical Physics, 327*, 159–170.

Geim, A. K. (2009). Graphene: Status and prospects. *Science, 324*, 1530–1534.

Geim, A. K., & Novoselov, K. S. (2007). The rise of graphene. *Nature Materials, 6*, 183–191.

Govind, N., Andzelm, J., & Maiti, A. (2008). Dissociation chemistry of gas molecules on carbon nanotubes applications to chemical sensing. *IEEE Sensors Journal, 8*, 837–841.

Gu, Z., Peng, H., Hauge, R. H., Smalley, R. E., & Margrave, J. L. (2002). Cutting single-wall carbon nanotubes through fluorination. *Nano Letters, 2*, 1009–1013.

Gueorguiev, G. K., Pacheco, J. M., & Tomanek, D. (2004). Quantum size effects in the polarizability of carbon fullerenes. *Physical Review Letters, 92*, 215501-1–215501-4.

Guo, T., Diener, M. D., Chai, Y., Alford, M. J., Haufler, R. E., McClure, S. M., Ohno, T., Weaver, J. H., Scuseria, G. E., & Smalley, R. E. (1992). Uranium stabilization of C_{28}: A tetravalent fullerene. *Science, 257*, 1661–1663.

Haddon, R. C. (1993). Chemistry of the fullerenes: The manifestation of strain in a class of continuous aromatic molecules. *Science, 261*, 1545–1550.

Haddon, R. C., & Scott, L. T. (1986). π-Orbital conjugation and rehybridization in bridged annulenes and deformed molecules in general: π-orbital axis vector analysis. *Pure and Applied Chemistry, 58*, 137–142.

Hamada, N., Sawada, S., & Oshiyama, A. (1992). New one-dimensional conductors: Graphitic microtubules. *Physical Review Letters, 68*, 1579–1581.

Harutyunyan, A. R., Chen, G., Paronyan, T. M., Pigos, E. M., Kuznetsov, O. A., Hewaparakrama, K., Kim, S. M., Zakharov, D., Stach, E. A., & Sumanasekera, G. U. (2009). Preferential growth of single-walled carbon nanotubes with metallic conductivity. *Science, 326*, 116–120.

He, H. Y., & Pan, B. C. (2009). Electronic structures and Raman features of a carbon nanobud. *The Journal of Physical Chemistry C, 113*, 20822–20826.

Heath, J. R. (1991). Synthesis of C60 from small carbon clusters: a model based on experiment and theory. *ACS Symposium Series, 481*, 1–23.

Helden, G. v., Gotts, N. G., & Bowers, M. T. (1993). Experimental evidence for the formation of fullerenes by collisional heating of carbon rings in the gas phase. *Nature, 363*, 60–63.

Hernández, E., Ordejón, P., & Terrones, H. (2001). Fullerene growth and the role of nonclassical isomers. *Physical Review B, 63*, 193403-1–193403-4.

Heymann, D., Chibante, L. P. F., Brooks, R. R., Wolbach, W. S., & Smalley, R. E. (1994). Fullerenes in the cretaceous-tertiary boundary layer. *Science, 265*, 645–647.

Heymann, D., Jenneskens, L. W., Jehlička, J., Koper, C., & Vlietstra, E. (2003). Terrestrial and extraterrestrial fullerenes. *Fullerenes, Nanotubes, and Carbon Nanostructures, 11*, 333–370.

Hirahara, K., Suenaga, K., Bandow, S., Kato, H., Okazaki, T., Shinohara, H., & Iijima, S. (2000). One-dimensional metallofullerene crystal generated inside single-walled carbon nanotubes. *Physical Review Letters, 85*, 5384–5387.

Hirsch, A. (2002). Functionalization of single-walled carbon nanotubes. *Angewandte Chemie, International Edition, 41*, 1853–1859.

Howard, J. B., Mckinnon, J. T., Makarovsky, Y., Lafleur, A. L., & Johnson, M. E. (1991). Fullerenes C_{60} and C_{70} in flames. *Nature, 352*, 139–141.

http://www.nndc.bnl.gov/content/elements.html

Hu, Y. H., & Ruckenstein, E. (2003). Ab initio quantum chemical calculations for fullerene cages with large holes. *Journal of Chemical Physics, 119*, 10073–10080.

Hu, Y. H., & Ruckenstein, E. (2004). Quantum chemical density-functional theory calculations of the structures of defect C_{60} with four vacancies. *Journal of Chemical Physics, 120*, 7971–7975.

Hudhomme, P., & Cousseau, J. (2007). Plastic solar cells using fullerene derivatives in the photoactive layer. In F. Langa & J.-F. Nierengarten (Eds.), *Fullerenes: Principles and applications*. London: Royal Society of Chemistry.

Hutter, J., et al. Computer code CPMD, version 3.11 (The CPMD program is © 2000–2016 jointly by IBM Corp. and by Max Planck Institute, Stuttgart.), http://www.cpmd.org/.

Iijima, S. (1991). Helical microtubules of graphitic carbon. *Nature, 354*, 56–58.
Iijima, S. (2007). A career in carbon. *Nature Nanotechnology, 2*, 590–591.
Iijima, S., & Ichihashi, T. (1993). Single-shell carbon nanotubes of 1-nm diameter. *Nature, 363*, 603–605.
Iijima, S., Yudasaka, M., Yamada, R., Bandow, S., Suenaga, K., Kokai, F., & Takahashi, K. (1999). Nano-aggregates of single-walled graphitic carbon nano-horns. *Chemical Physics Letters, 309*, 165–170.
Ioffe, I. N., Goryunkov, A. A., Tamm, N. B., Sidorov, L. N., Kemnitz, E., & Troyanov, S. I. (2009). Fusing pentagons in a fullerene cage by chlorination: IPR D_2-C_{76} Rearranges into non-IPR $C_{76}Cl_{24}$. *Angewandte Chemie, International Edition, 48*, 5904–5907.
Jia, T.-T., Zheng, M.-M., Fan, X.-Y., Su, Y., Li, S.-J., Liu, H.-Y., Chen, G., & Kawazoe, Y. (2016). Dirac cone move and bandgap on/off switching of graphene superlattice. *Scientific Reports, 6*, 18869.
Jiang, H., Nasibulin, A. G., Brown, D. P., & Kauppinen, E. I. (2007). Unambiguous atomic structural determination of single-walled carbon nanotubes by electron diffraction. *Carbon, 45*, 662–667.
Jiang, D., Cooper, V. R., & Dai, S. (2009). Porous graphene as the ultimate membrane for gas separation. *Nano Letters, 9*, 4019–4024.
Kaczmarek, A., Dinadayalane, T. C., Łukaszewicz, J., & Leszczynski, J. (2007). Effect of tube length on the chemisorptions of one and two hydrogen atoms on the sidewalls of (3,3) and (4,4) single-walled carbon nanotubes: A theoretical study. *International Journal of Quantum Chemistry, 107*, 2211–2219.
Kadish, K. M., & Ruoff, R. S. (Eds.). (2002). *Fullerene: Chemistry physics and technology*. New York: Wiley.
Kar, T., Bettinger, H. F., Scheiner, S., & Roy, A. K. (2008). Noncovalent $\pi - \pi$ stacking and CH-π interactions of aromatics on the surface of single-wall carbon nanotubes: An MP2 study. *The Journal of Physical Chemistry C, 112*, 20070–20075.
Karousis, N., Papi, R. M., Siskos, A., Vakalopoulou, P., Glezakos, P., Sarigiannis, Y., Stavropoulos, G., Kyriakidis, D. A., & Tagmatarchis, N. (2009). Peptidomimetic–functionalized carbon nanotubes with antitrypsin activity. *Carbon, 47*, 3550–3558.
Kessler, B., Bringer, A., Cramm, S., Schlebusch, C., Eberhardt, W., Suzuki, S., Achiba, Y., Esch, F., Barnaba, M., & Cocco, D. (1997). Evidence for incomplete charge transfer and La-derived states in the valence bands of endohedrally doped La@C_{82}. *Physical Review Letters, 79*, 2289–2292.
Kikuchi, K., Nakahara, N., Wakabayashi, T., Suzuki, S., Shiromaru, H., Miyake, Y., Saito, K., Ikemoto, I., Kainosho, M., & Achiba, Y. (1992a). NMR characterization of isomers of C_{78}, C_{82} and C_{84} fullerenes. *Nature, 357*, 142–145.
Kikuchi, K., Nakahara, N., Wakabayashi, T., Honda, M., Matsumiya, H., Moriwaki, T., Suzuki, S., Shiromaru, H., Saito, K., Yamauchi, K., Ikemoto, I., & Achiba, Y. (1992b). Isolation and identification of fullerene family: C_{76}, C_{78}, C_{82}, C_{84}, C_{90} and C_{96}. *Chemical Physics Letters, 188*, 177–180.
Kimura, T., Sugai, T., Shinohara, H., Goto, T., Tohji, K., & Matsuoka, I. (1995). Preferential arc-discharge production of higher fullerenes. *Chemical Physics Letters, 246*, 571–576.
Klein, D. J., & Schmalz, T. G. (1990). In I. Hargittai (Ed.), *Quasicrystals, networks, and molecules of fivefold symmetry* (p. 239). New York: VCH.
Knobel, R. G., & Cleland, A. N. (2003). Nanometre-scale displacement sensing using a single electron Transistor. *Nature, 424*, 291–293.
Kostov, M. K., Santiso, E. E., George, A. M., Gubbins, K. E., & Nardelli, M. B. (2005). Dissociation of water on defective carbon substrates. *Physical Review Letters, 95*, 136105-1–136105-4.
Krätschmer, W., Lamb, L. D., Fostiropoulos, K., & Huffman, D. R. (1990). Solid C_{60}: A new form of carbon. *Nature, 347*, 354–358.
Kresse, G., & Furthmuller, J. (1996a). Efficient iterative schemes for ab initio total-energy calculations using a plane-wave basis set. *Physical Review B, 54*, 11169–11186.

Kresse, G., & Furthmuller, J. (1996b). Efficiency of ab-initio total energy calculations for metals and semiconductors using a plane-wave basis set. *Computational Materials Science, 6*, 15–50.

Kroto, H. W. (1987). The stability of the fullerenes C_n, with n = 24, 28, 32, 36, 50, 60 and 70. *Nature, 329*, 529–531.

Kroto, H. W., Heath, J. R., O'Brien, S. C., Curl, R. F., & Smalley, R. E. (1985). Buckminsterfullerene. *Nature, 318*, 162–163.

Kubozono, Y., Maeda, H., Takabayashi, Y., Hiraoka, K., Nakai, T., Kashino, S., Emura, S., Ukita, S., & Sogabe, T. (1996). Extractions of Y@C_{60}, Ba@C_{60}, La@C_{60}, Ce@C_{60}, Pr@C_{60}, Nd@C_{60}, and Gd@C_{60} with aniline. *Journal of the American Chemical Society, 118*, 6998–6999.

Launois, P., Chorro, M., Verberck, B., Albouy, P.-A., Rouziere, S., Colson, D., Foget, A., Noe, L., Kataura, H., Monthioux, M., & Cambedouzou, J. (2010). Transformation of C_{70} peapods into double walled carbon nanotubes. *Carbon, 48*, 89–98.

Lavrik, N. V., & Datskos, P. G. (2003). Femtogram mass detection using photothermally actuated nanomechanical resonators. *Applied Physics Letters, 82*, 2697–2699.

Lebedeva, M. A., Chamberlain, T. W., & Khlobystov, A. N. (2015). Harnessing the synergistic and complementary properties of fullerene and transition-metal compounds for nanomaterial applications. *Chemical Reviews, 115*, 11301–11351.

Lee, S. U., & Han, Y.-K. (2004). Structure and stability of the defect fullerene clusters of C_{60}: C_{59}, C_{58}, and C_{57}. *Journal of Chemical Physics, 121*, 3941–3942.

Lee, C., Yang, W., & Parr, R. G. (1988). Development of the Colle-Salvetti correlation-energy formula into a functional of the electron density. *Physical Review B, 37*, 785–789.

Lee, C., Kim, D., Jurecka, P., Tarakeshwar, P., Hobza, P., & Kim, K. S. (2007). Understanding of assembly phenomena by aromatic ─ aromatic interactions: Benzene dimer and the substituted systems. *The Journal of Physical Chemistry. A, 111*, 3446–3457.

Lee, C., Wei, X., Kysar, J. W., & Hone, J. (2008). Measurement of the elastic properties and intrinsic strength of monolayer grapheme. *Science, 321*, 385–388.

Lherbier, A., Blase, X., Niquet, Y. M., Triozon, N., & Roche, S. (2008). Charge transport in chemically doped 2D graphene. *Physical Review Letters, 101*, 036808-1–036808-4.

Li, L., Reich, S., & Robertson, J. (2005). Defect energies of graphite: Density-functional calculations. *Physical Review B, 72*, 184109-1–184109-10.

Li, J., Wu, C., & Guan, L. (2009a). Lithium insertion/extraction properties of nanocarbon materials. *The Journal of Physical Chemistry C, 113*, 18431–18435.

Li, Y., Zhou, Z., Shen, P., & Chen, Z. (2009b). Structural and electronic properties of graphane nanoribbons. *The Journal of Physical Chemistry, 113*, 15043–15045.

Li, Y., Liu, S., Datta, D., & Li, Z. (2015). Surface hydrogenation regulated wrinkling and torque capability of hydrogenated graphene annulus under circular shearing. *Scientific Reports, 5*, 16556.

Liu, J., Dai, H., Hafner, J. H., Colbert, D. T., Smalley, R. E., Tans, S. J., & Dekker, C. (1997). Fullerene 'crop circles'. *Nature, 385*, 780–781.

Liu, Z., Sun, X., Nakayama-Ratchford, N., & Dai, H. (2007). Supramolecular chemistry on water-soluble carbon nanotubes for drug loading and delivery. *ACS Nano, 1*, 50–56.

Lopez-Urias, F., Terrones, M., & Terrones, H. (2003). Electronic properties of giant fullerenes and complex graphitic nanostructures with novel morphologies. *Chemical Physics Letters, 381*, 683–690.

Lu, X., & Chen, Z. (2005). Curved pi-conjugation, aromaticity, and the related chemistry of small fullerenes (< C_{60}) and single-walled carbon nanotubes. *Chemical Reviews, 105*, 3643–3696.

Lu, A. J., & Pan, B. C. (2004). Nature of single vacancy in achiral carbon nanotubes. *Physical Review Letters, 92*, 105504-1–105504-4.

Lu, J., Zhang, X., & Zhao, X. (2000). Metal-cage hybridization in endohedral La@C_{60}, Y@C_{60} and Sc@C_{60}. *Chemical Physics Letters, 332*, 51–57.

Lu, X., Chen, Z., Thiel, W., von Rague Schleyer, P., Huang, R., & Zheng, L. (2004). Properties of fullerene[50] and D_{5h} decachlorofullerene[50]: A computational study. *Journal of the American Chemical Society, 126*, 14871–14878.

Lu, X., Chen, Z., & von Rague Schleyer, P. (2005). Are Stone − Wales defect sites always more reactive than perfect sites in the sidewalls of single-wall carbon nanotubes? *Journal of the American Chemical Society, 127*, 20–21.

Lu, J., Yuan, D., Liu, J., Leng, W., & Kopley, T. E. (2008). Three dimensional single-walled carbon nanotubes. *Nano Letters, 8*, 3325–3329.

Ma, J., Alfe, D., Michaelides, A., & Wang, E. (2009). Stone-Wales defects in graphene and other planar sp^2-bonded materials. *Physical Review B, 80*, 033407-1–033407-4.

MacKenzie, K. J., See, C. H., Dunens, O. M., & Harris, A. T. (2008). Do single-walled carbon nanotubes occur naturally? *Nature Nanotechnology, 3*, 310.

Malyi, O. I., Sopiha, K., Kulish, V. V., Tan, T. L., Manzhos, S., & Persson, C. (2015). A computational study of Na behavior on graphene. *Applied Surface Science, 333*, 235–243.

Manolopoulos, D. E., & Fowler, P. W. (1991). Structural proposals for endohedral metal-fullerene Complexes. *Chemical Physics Letters, 187*, 1–7.

Manolopoulos, D. E., & Fowler, P. W. (1992). Molecular graphs, point groups, and fullerenes. *Journal of Chemical Physics, 96*, 7603–7614.

Maruyama, S., & Yamaguch, Y. (1998). A molecular dynamics demonstration of annealing to a perfect C_{60} Structure. *Chemical Physics Letters, 286*, 343–349.

Maseras, F., & Morokuma, K. (1995). IMOMM: A new integrated ab initio + molecular mechanics geometry optimization scheme of equilibrium structures and transition states. *Journal of Computational Chemistry, 16*, 1170–1179.

Mashino, T., Nishikawa, D., Takahashi, K., Usui, N., Yamori, T., Seki, M., Endo, T., & Mochizuki, M. (2003). Antibacterial and antiproliferative activity of cationic fullerene derivatives. *Bioorganic and Medicinal Chemistry Letters, 13*, 4395–4397.

Matsuo, Y., Tahara, K., & Nakamura, E. (2003). Theoretical studies on structures and aromaticity of finite-length armchair carbon nanotubes. *Organic Letters, 5*, 3181–3184.

McKenzie, D. R., Davis, C. A., Cockayne, D. J. H., Muller, D. A., & Vassallo, A. M. (1992). The structure of the C_{70} molecule. *Nature, 355*, 622–624.

Mehta, G., & Rao, H. S. P. (1998). Synthetic studies directed towards bucky-balls and bucky-bowls. *Tetrahedron, 54*, 13325–13370.

Mehta, G., Panda, G., Yadav, R. D., & Kumar, K. R. (1997). A synthetic approach towards Pinakene, a $C_{28}H_{14}$ fragment of [70]-fullerene. *Indian Journal of Chemistry Section B, 36*, 301–302.

Melin, F., Chaur, M. N., Engmann, S., Elliott, B., Kumbhar, A., Athans, A. J., & Echegoyen, L. (2007). The large $Nd_3N@C_{2n}$ ($40 \leq n \leq 49$) cluster fullerene family: Preferential templating of a C_{88} cage by a trimetallic nitride cluster. *Angewandte Chemie, International Edition, 46*, 9032–9035.

Menon, M., & Srivastava, D. (1997). Carbon nanotube T junctions: Nanoscale metal-semiconductor-metal contact devices. *Physical Review Letters, 79*, 4453–4456.

Meyer, J. C., Kisielowski, C., Erni, R., Rossell, M. D., Crommine, M. F., & Zettl, A. (2008). Direct imaging of lattice atoms and topological defects in graphene membranes. *Nano Letters, 8*, 3582–3586.

Mielke, S. L., Troya, D., Zhang, S., Li, J.-L., Xiao, S., Car, R., Ruoff, R. S., Schatz, G. C., & Belytschko, T. (2004). The role of vacancy defects and holes in the fracture of carbon nanotubes. *Chemical Physics Letters, 390*, 413–420.

Mintmire, J. W., Dunlap, B. I., & White, C. T. (1992). Are fullerene tubules metallic? *Physical Review Letters, 68*, 631–634.

Miwa, R. H., Martins, T. B., & Fazzio, A. (2008). Hydrogen adsorption on boron doped graphene: An ab initio study. *Nanotechnology, 19*, 155708-1–155708-7.

Miyake, Y., Minami, T., Kikuchi, K., Kainosho, M., & Achiba, Y. (2000). Trends in structure and growth of higher fullerenes isomer structure of C_{86} and C_{88}^-. *Molecular Crystals and Liquid Crystals, 340*, 553–558.

Miyamoto, Y., Rubio, A., Berber, S., Yoon, M., & Tomanek, D. (2004). Spectroscopic characterization of Stone-Wales defects in nanotubes. *Physical Review B, 69*, 121413-1–121413-4.

Mizorogi, N., & Aihara, J. (2003). PM3 localization energies for the isolated-pentagon isomers of the C_{84} Fullerene. *Physical Chemistry Chemical Physics, 5*, 3368–3371.

Monthioux, M., & Kuznetsov, V. L. (2006). Who should be given the credit for the discovery of carbon nanotubes? *Carbon, 44*, 1621–1623.

Moothi, K., Simate, G. S., Falcon, R., Iyuke, S. E., & Meyyappan, M. (2015). Carbon nanotube synthesis using coal pyrolysis. *Langmuir, 31*, 9464–9472.

Moro, L., Ruoff, R. S., Becker, C. H., Lorents, D. C., & Malhotra, R. (1993). Studies of metallofullerene primary soots by laser and thermal desorption mass spectrometry. *Journal of Physical Chemistry, 97*, 6801–6805.

Morokuma, K., Wang, Q., & Vreven, T. (2006). Performance evaluation of the three-layer ONIOM method: Case study for a zwitterionic peptide. *Journal of Chemical Theory and Computation, 2*, 1317–1324.

Murry, R. L., Strout, D. L., Odom, G. K., & Scuseria, G. E. (1993). Role of sp^3 carbon and 7-membered rings in fullerene annealing and fragmentation. *Nature, 366*, 665–667.

Nasibulin, A. G., Pikhitsa, P. V., Jiang, H., Brown, D. P., Krasheninnikov, A. V., Anisimov, A. S., Queipo, P., Moisala, A., Gonzalez, D., Lientschnig, G., Hassanien, A., Shandakov, S. D., Lolli, G., Resasco, D. E., Choi, M., Tomanek, D., & Kauppinen, E. I. (2007a). A novel hybrid carbon material. *Nature Nanotechnology, 2*, 156–161.

Nasibulin, A. G., Anisimov, A. S., Pikhitsa, P. V., Jiang, H., Brown, D. P., Choi, M., & Kauppinen, E. I. (2007b). Investigations of nanobud formation. *Chemical Physics Letters, 446*, 109–114.

Neto, A. H. C. (2010). The carbon new age. *Materials Today, 13*(3), 12–17.

Neto, A. H. C., Guinea, F., Peres, N. M. R., Novoselov, K. S., & Geim, A. K. (2009). The electronic properties of graphene. *Reviews of Modern Physics, 81*, 109–162.

Nikitin, A., Ogasawara, H., Mann, D., Denecke, R., Zhang, Z., Dai, H., Cho, K., & Nilsson, A. (2005). Hydrogenation of single-walled carbon nanotubes. *Physical Review Letters, 95*, 225507-1–225507-1.

Nishidate, K., & Hasegawa, M. (2005). Energetics of lithium ion adsorption on defective carbon nanotubes. *Physical Review B, 71*, 245418-1–245418-6.

Niyogi, S., Hamon, M. A., Hu, H., Zhao, B., Bhowmik, P., Sen, R., Itkis, M. E., & Haddon, R. C. (2002). Chemistry of single-walled carbon nanotubes. *Accounts of Chemical Research, 35*, 1105–1113.

Novoselov, K. S., Geim, A. K., Morozov, S. V., Jiang, D., Zhang, Y., Dubonos, S. V., Grigorieva, I. V., & Firsov, A. A. (2004). Electric field effect in atomically thin carbon films. *Science, 306*, 666–669.

Novoselov, K. S., Jiang, D., Schedin, F., Booth, T. J., Khotkevich, V. V., Morozov, S. V., & Geim, A. K. (2005a). Two-dimensional atomic crystals. *Proceedings of the National Academy of Sciences of the United State of America, 102*, 10451–10453.

Novoselov, K. S., Geim, A. K., Morozov, S. V., Jiang, D., Katsnelson, M. I., Grigorieva, I. V., Dubonos, S. V., & Firsov, A. A. (2005b). Two-dimensional gas of massless Dirac fermions in graphene. *Nature, 438*, 197–200.

Oberlin, A., Endo, M., & Koyama, T. (1976). Filamentous growth of carbon through benzene Decomposition. *Journal of Crystal Growth, 32*, 335–349.

O'Brien, S. C., Heath, J. R., Curl, R. F., & Smalley, R. E. (1988). Photophysics of buckminsterfullerene and other carbon cluster ions. *Journal of Chemical Physics, 88*, 220–230.

Okada, S. (2007). Radial-breathing mode frequencies for nanotubes encapsulating fullerenes. *Chemical Physics Letters, 438*, 59–62.

Okada, S., & Saito, S. (1996). Number of extractable fullerene isomers and speciality of C_{84}. *Chemical Physical Letters, 252*, 94–100.

Ormsby, J. L., & King, B. T. (2007). The regioselectivity of addition to carbon nanotube segments. *Journal of Organic Chemistry, 72*, 4035–4038.

Osawa, E. (1970). Superaromaticity. *Kagaku (Kyoto), 25*, 854–863.

Osuna, S., Morera, J., Cases, M., Morokuma, K., & Sola, M. (2009). Diels ─ Alder reaction between cyclopentadiene and C_{60}: An analysis of the performance of the ONIOM method for

the study of chemical reactivity in fullerenes and nanotubes. *The Journal of Physical Chemistry. A, 113*, 9721–9726.

Ouyang, M., Huang, J.-L., & Lieber, C. M. (2002). Fundamental electronic properties and applications of single-walled carbon nanotubes. *Accounts of Chemical Research, 35*, 1018–1025.

Palkar, A., Kumbhar, A., Athans, A. J., & Echegoyen, L. (2008). Pyridyl-functionalized and water-soluble carbon nano onions: First supramolecular complexes of carbon nano onions. *Chemistry of Materials, 20*, 1685–1687.

Park, S., Srivastava, D., & Cho, K. (2003). Generalized chemical reactivity of curved surfaces: Carbon Nanotubes. *Nano Letters, 3*, 1273–1277.

Park, S. S., Liu, D., & Hagelberg, F. (2005). Comparative investigation on non-IPR C_{68} and IPR C_{78} fullerenes encaging Sc_3N molecules. *The Journal of Physical Chemistry. A, 109*, 8865–8873.

Peng, X., Komatsu, N., Bhattacharya, S., Shimawaki, T., Aonuma, S., Kimura, T., & Osuka, A. (2007). Optically active single-walled carbon nanotubes. *Nature Nanotechnology, 2*, 361–365.

Perdew, J. P., Burke, K., & Ernzerhof, M. (1996). Generalized gradient approximation made simple. *Physical Review Letters, 77*, 3865–3868.

Pereira, V. M., Neto, A. H. C., & Peres, N. M. R. (2009). Tight-binding approach to uniaxial strain in graphene. *Physical Review B, 80*, 045401-1–045401-8.

Pierson, H. O. (1993). *Handbook of carbon, graphite, diamonds and fullerenes: Processing, properties and applications*. New Jersey: Noyes.

Piskoti, C., Yarger, J., & Zettl, A. (1998). C_{36}, a new carbon solid. *Nature, 393*, 771–774.

Ponomarenko, L. A., Schedin, F., Katsnelson, M. I., Yang, R., Hill, E. W., Novoselov, K. S., & Geim, A. K. (2008). Chaotic Dirac billiard in graphene quantum dots. *Science, 320*, 356–358.

Poonjarernsilp, C., Sano, N., Tamon, H., & Charinpanitkul, T. (2009). A model of reaction field in gas- injected arc-in-water method to synthesize single-walled carbon nanohorns: Influence of water temperature. *Journal of Applied Physics, 106*, 104315-1–104315-7.

Prinzbach, H., Weiler, A., Landenberger, P., Wahl, F., Worth, J., Scott, L. T., Gelmont, M., Olevano, D., & Issendorff, B. v. (2000). Gas-phase production and photoelectron spectroscopy of the smallest fullerene, C20. *Nature, 407*, 60–63.

Priyakumar, U. D., & Sastry, G. N. (2001a). Heterobuckybowls: A theoretical study on the structure, bowl- to-bowl inversion barrier, bond length alternation, structure-inversion barrier relationship, stability, and synthetic feasibility. *Journal of Organic Chemistry, 66*, 6523–6530.

Priyakumar, U. D., & Sastry, G. N. (2001b). Tailoring the curvature, bowl rigidity and stability of heterobuckybowls: Theoretical design of synthetic strategies towards heterosumanenes. *Journal of Molecular Graphics and Modelling, 19*, 266–269.

Priyakumar, U. D., & Sastry, G. N. (2001c). Theory provides a clue to accomplish the synthesis of sumanene, $C_{21}H_{12}$, the prototypical C_{3v}-buckybowl. *Tetrahedron Letters, 42*, 1379–1381.

Qin, L.-C. (2007). Determination of the chiral indices (n, m) of carbon nanotubes by electron diffraction. *Physical Chemistry Chemical Physics, 9*, 31–48.

Radushkevich, L. V., & Lukyanovich, V. M. (1952). O strukture ugleroda, obrazujucegosja pri termiceskom razlozenii okisi ugleroda na zeleznom kontakte. *Zurn Fisic Chim, 26*, 88–95.

Rao, C. N. R., Voggu, R., & Govindaraj, A. (2009a). Selective generation of single-walled carbon nanotubes with metallic, semiconducting and other unique electronic properties. *Nanoscale, 1*, 96–105.

Rao, F., Li, T., & Wang, Y. (2009b). Growth of all-carbon single-walled carbon nanotubes from diamonds and Fullerenes. *Carbon, 47*, 3580–3584.

Robertson, D. H., Brenner, D. W., & Mintmire, J. W. (1992). Energetics of nanoscale graphitic tubules. *Physical Review B, 45*, 12592–12595.

Robinson, J. A., Snow, E. S., Badescu, S. C., Reinecke, T. L., & Perkins, F. K. (2006). Role of defects in single-walled carbon nanotube chemical sensors. *Nano Letters, 6*, 1747–1751.

Robinson, J. T., Perkins, F. K., Snow, E. S., Wei, Z., & Sheehan, P. E. (2008). Reduced graphene oxide molecular sensors. *Nano Letters, 8*, 3137–3140.

Rohlfing, E. A., Cox, D. M., & Kaldor, A. (1994). Production and characterization of supersonic carbon cluster Beams. *Journal of Chemical Physics, 81*, 3322–3330.

Rojas, A., Martínez, M., Amador, P., & Torres, L. A. (2007). Increasing stability of the fullerenes with the number of carbon atoms: The experimental evidence. *The Journal of Physical Chemistry B, 111*, 9031–9035.

Saito, M., & Miyamoto, Y. (2001). Theoretical identification of the smallest fullerene, C_{20}. *Physical Review Letters, 87*, 035503-1–035503-4.

Saito, R., Fujita, M., Dresselhaus, G., & Dresselhaus, M. S. (1992). Electronic structure of chiral graphene tubules. *Applied Physics Letters, 60*, 2204–2206.

Saito, R., Dresselhaus, G., & Dresselhaus, M. S. (1998). *Physical properties of carbon nanotubes*. London: Imperial College Press.

Sakurai, H., Daiko, T., & Hirao, T. (2003). A synthesis of sumanene, a fullerene fragment. *Science, 301*, 1878.

Sano, M., Kamino, A., Okamura, J., & Shinkai, S. (2001). Ring closure of carbon nanotubes. *Science, 293*, 1299–1301.

Sastry, G. N., & Priyakumar, U. D. (2001). The role of heteroatom substitution in the rigidity and curvature of buckybowls. A theoretical study. *Journal of the Chemical Society, Perkin Transactions, 2*, 30–40.

Sastry, G. N., Jemmis, E. D., Mehta, G., & Shah, S. R. (1993). Synthetic strategies towards C_{60}. Molecular mechanics and MNDO study on sumanene and related structures. *Journal of the Chemical Society, Perkin Transactions, 2*, 1867–1871.

Sastry, G. N., Rao, H. S. P., Bednarek, P., & Priyakumar, U. D. (2000). Effect of substitution on the curvature and bowl-to-bowl inversion barrier of bucky-bowls. Study of mono-substituted corannulenes ($C_{19}XH_{10}$, $X = B^-$, N^+, P^+ and Si). *Chemical Communications*, 843–844.

Saunders, M., Jiménez-Vázquez, H. A., Cross, R. J., & Poreda, R. J. (1993). Stable compounds of helium and neon: $He@C_{60}$ and $Ne@C_{60}$. *Science, 259*, 1428–1430.

Scheina, S., & Friedrich, T. (2008). A geometric constraint, the head-to-tail exclusion rule, may be the basis for the isolated-pentagon rule in fullerenes with more than 60 vertices. *Proceeding of the National Academy of Sciences of the United States of America, 105*, 19142–19147.

Scott, L. T., Boorum, M. M., McMahon, B. J., Hagen, S., Mack, J., Blank, J., Wegner, H., & de Meijere, A. (2002). A rational chemical synthesis of C_{60}. *Science, 295*, 1500–1503.

Scuseria, G. E. (1996). Ab initio calculations of fullerenes. *Science, 271*, 942–945.

Seiders, T. J., Elliot, E. L., Grube, G. H., & Siegel, J. S. (1999). Synthesis of corannulene and alkyl derivatives of corannulene. *Journal of the American Chemical Society, 121*, 7804–7813.

Seiders, T. J., Baldridge, K. K., Grube, G. H., & Siegel, J. S. (2001). Structure/energy correlation of bowl depth and inversion barrier in corannulene derivatives: Combined experimental and quantum mechanical analysis. *Journal of the American Chemical Society, 123*, 517–525.

Serra, S., Cavazzoni, C., Chiarotti, G. L., Scandolo, S., & Tosatti, E. (1999). Pressure-induced solid carbonates from molecular CO_2 by computer simulation. *Science, 284*, 788–790.

Shao, N., Gao, Y., Yoo, S., An, W., & Zeng, X. C. (2006). Search for lowest-energy fullerenes: C_{98} to C_{110}. *The Journal of Physical Chemistry. A, 110*, 7672–7676.

Shao, N., Gao, Y., & Zeng, X. C. (2007). Search for lowest-energy fullerenes 2: C_{38} to C_{80} and C_{112} to C_{120}. *The Journal of Physical Chemistry C, 111*, 17671–17677.

Shukla, M. K., & Leszczynski, J. (2009). Fullerene (C_{60}) forms stable complex with nucleic acid base guanine. *Chemical Physics Letters, 469*, 207–209.

Shustova, N. B., Kuvychko, I. V., Bolskar, R. D., Seppelt, K., Strauss, S. H., Popov, A. A., & Boltalina, O. V. (2006). Trifluoromethyl derivatives of insoluble small-HOMO − LUMO-Gap hollow higher fullerenes. NMR and DFT structure elucidation of C_2-(C_{74}-D_{3h})$(CF_3)_{12}$, C_s-(C_{76}-$T_d(2)$)$(CF_3)_{12}$, C_2-(C_{78}-$D_{3h}(5)$)$(CF_3)_{12}$, C_s-(C_{80}-$C_{2v}(5)$)$(CF_3)_{12}$, and C_2-(C_{82}-$C_2(5)$)$(CF_3)_{12}$. *Journal of the American Chemical Society, 128*, 15793–15798.

Shustova, N. B., Newell, B. S., Miller, S. M., Anderson, O. P., Bolskar, R. D., Seppelt, K., Popov, A. A., Boltalina, O. V., & Strauss, S. H. (2007). Discovering and verifying elusive fullerene cage isomers: Structures of C_2-p^{11}-(C_{74}-D_{3h})$(CF_3)_{12}$ and C_2-p^{11}-(C_{78}-$D_{3h}(5)$)$(CF_3)_{12}$. *Angewandte Chemie, International Edition, 46*, 4111–4114.

Simeon, T. M., Yanov, I., & Leszczynski, J. (2005). Ab initio quantum chemical studies of fullerene molecules with substitutes $C_{59}X$ [X = Si, Ge, Sn], $C_{59}X^-$ [X = B, Al, Ga, In], and $C_{59}X$ [X = N, P, As, Sb]. *International Journal of Quantum Chemistry, 105*, 429–436.

Sinha, N., & Yeow, J. T.-W. (2005). Carbon nanotubes for biomedical applications. *IEEE Transactions on Nano Bioscience, 4*, 180–195.

Sinnokrot, M. O., & Sherrill, C. D. (2004). Highly accurate coupled cluster potential energy curves for the benzene dimer: Sandwich, T-shaped, and parallel-displaced configurations. *The Journal of Physical Chemistry. A, 108*, 10200–10207.

Slanina, Z., Zhao, X., Lee, S.-L., & Osawa, E. (1997). C_{90} temperature effects on relative stabilities of the IPR Isomers. *Chemical Physics, 219*, 193–200.

Slanina, Z., Uhlik, F., Yoshida, M., & Osawa, E. (2000a). A computational treatment of 35 IPR isomers of C_{88}. *Fullerene Science and Technology, 8*, 417–432.

Slanina, Z., Zhao, X., Deota, P., & Osawa, E. (2000b). Relative stabilities of C_{92} IPR fullerenes. *Journal of Molecular Modeling, 6*, 312–317.

Smalley, R. E. (1992). Self-assembly of the fullerenes. *Accounts of Chemical Research, 25*, 98–105.

Smith, B. W., Monthioux, M., & Luzzi, D. E. (1998). Encapsulated C_{60} in carbon nanotubes. *Nature, 396*, 323–324.

Smith, B. W., Monthioux, M., & Luzzi, D. E. (1999). Carbon nanotube encapsulated fullerenes: A unique class of hybrid materials. *Chemical Physics Letters, 315*, 31–36.

Sofo, J. O., Chaudhari, A. S., & Barber, G. D. (2007). Graphane: A two-dimensional hydrocarbon. *Physical Review B, 75*, 153401-1–153401-4.

Sotiropoulou, S., & Chaniotakis, N. A. (2003). Carbon nanotube array-based biosensor. *Analytical and Bioanalytical Chemistry, 375*, 103–105.

Stevens, R. M. D., Frederick, N. A., Smith, B. L., Morse, D. E., Stucky, G. D., & Hansma, P. K. (2000). Carbon nanotubes as probes for atomic force microscopy. *Nanotechnology, 11*, 1–5.

Stevens, R. M. D., Nguyen, C. V., & Meyyappan, M. (2004). Carbon nanotube scanning probe for imaging in aqueous environment. *IEEE Transactions on Nano Bioscience, 3*, 56–60.

Stewart, J. J. P. (1989). Optimization of parameters for semiempirical methods I Method. *Journal of Computational Chemistry, 10*, 209–220.

Stoilova, O., Jérôme, C., Detrembleur, C., Mouithys-Mickalad, A., Manolova, N., Rashkova, I., & Jérôme, R. (2007). C_{60}-containing nanostructured polymeric materials with potential biomedical applications. *Polymer, 48*, 1835–1843.

Stone, A. J., & Wales, D. J. (1986). Theoretical studies of icosahedral C_{60} and some related species. *Chemical Physics Letters, 128*, 501–503.

Strano, M. S. (2003). Probing chiral selective reactions using a revised Kataura plot for the interpretation of single-walled carbon nanotube spectroscopy. *Journal of the American Chemical Society, 125*, 16148–16153.

Strano, M. S. (2007). Carbon nanotubes: Sorting out left from right. *Nature Nanotechnology, 2*, 340–341.

Suchanek, W. L., Libera, J. A., Gogotsi, Y., & Yoshimura, M. (2001). Behavior of C_{60} under hydrothermal conditions: Transformation to amorphous carbon and formation of carbon nanotubes. *Journal of Solid State Chemistry, 160*, 184–188.

Suenaga, K., Wakabayashi, H., Koshino, M., Sato, Y., Urita, K., & Iijima, S. (2007). Imaging active topological defects in carbon nanotubes. *Nature Nanotechnology, 2*, 358–360.

Sulman, E., Yanov, I., & Leszczynski, J. (1999). An active site model and the catalytic activity mechanism of the new fullerene-based catalyst - $(\eta^2\text{-}C_{60})Pd(PPh_3)_2$. *Fullerenes, Nanotubes, and Carbon Nanostructures, 7*, 467–484.

Sun, G. (2003). Assigning the major isomers of fullerene C_{88} by theoretical ^{13}C NMR spectra. *Chemical Physics Letters, 367*, 26–33.

Sun, G., & Kertesz, M. (2002). ^{13}C NMR spectra for IPR isomers of fullerene C_{86}. *Chemical Physics, 276*, 107–114.

Suzuki, S., & Kobayashi, Y. (2007). Healing of low-energy irradiation-induced defects in single-walled carbon nanotubes at room temperature. *The Journal of Physical Chemistry C, 111*, 4524–4528.

Sygula, A., & Rabideau, P. W. (1999). Non-pyrolytic syntheses of buckybowls: Corannulene, cyclopentacorannulene, and a semibuckminsterfullerene. *Journal of the American Chemical Society, 121*, 7800–7803.

Tagmatarchis, N., Arcon, D., Prato, M., & Shinohara, H. (2002). Production, isolation and structural characterization of [92]fullerene isomers. *Chemical Communications*, 2992–2993.

Tang, A. C., & Huang, F. Q. (1995). Electronic structures of giant fullerenes with I_h symmetry. *Physical Review B, 51*, 13830–13832.

Tang, A. C., Li, Q. S., Liu, C. W., & Li, J. (1993). Symmetrical clusters of carbon and boron. *Chemical Physics Letters, 201*, 465–469.

Taylor, R. (1992). The third form of carbon: A new era in chemistry. *Interdisciplinary Science Reviews, 17*, 161–170.

Taylor, R., Hare, J. P., Abdul-Sada, A. K., & Kroto, H. W. (1990). Isolation, separation and characterisation of the fullerenes C_{60} and C_{70}: The third form of carbon. *Journal of the Chemical Society, Chemical Communications*, 1423–1425.

Taylor, R., Langley, G. J., Dennis, T. J. S., Kroto, H. W., & Walton, D. R. M. (1992). A mass spectrometric–NMR study of fullerene-78 isomers. *Journal of the Chemical Society, Chemical Communications*, 1043–1046.

Taylor, R., Langley, G. J., Avent, A. G., Dennis, T. J. S., Kroto, H. W., & Walton, D. R. M. (1993). ^{13}C NMR spectroscopy of C_{76}, C_{78}, C_{84} and mixtures of C_{86}–C_{102}; Anomalous chromatographic behaviour of C_{82}, and evidence for $C_{70}H_{12}$. *Journal of the Chemical Society, Perkin Transactions, 2*, 1029–1036.

Terrones, M., Terrones, G., & Terrones, H. (2002). Structure, chirality, and formation of giant icosahedral fullerenes and spherical graphitic onions. *Structural Chemistry, 13*, 373–384.

Thilgen, C., & Diederich, F. (2006). Structural aspects of fullerene chemistry – A journey through fullerene chirality. *Chemical Reviews, 106*, 5049–5135.

Thrash, T. P., Cagle, D. W., Alford, J. M., Wright, K., Ehrhardt, G. J., Mirzadeh, S., & Wilson, L. J. (1999). Toward fullerene-based radiopharmaceuticals: High-yield neutron activation of endohedral ^{165}Ho metallofullerenes. *Chemical Physics Letters, 308*, 329–336.

Troshin, P. A., Avent, A. G., Darwish, A. D., Martsinovich, N., Abdul-Sada, A. K., Street, J. M., & Taylor, R. (2005). Isolation of two seven-membered ring C_{58} fullerene derivatives: $C_{58}F_{17}CF_3$ and $C_{58}F_{18}$. *Science, 309*, 278–281.

Troyanov, S. I., & Tamm, N. B. (2009). Cage connectivities of C_{88} (33) and C_{92} (82) fullerenes captured as trifluoromethyl derivatives, $C_{88}(CF_3)_{18}$ and $C_{92}(CF_3)_{16}$. *Chemical Communications*, 6035–6037.

Valsakumar, M. C., Subramanian, N., Yousuf, M., Sahu, P. C., Hariharan, Y., Bharathi, A., Sastry, V. S., Janaki, J., Rao, G. V. N., Radhakrishnan, T. S., & Sundar, C. S. (1993). Crystal structure and disorder in solid C_{70}. *Physical Review B, 48*, 9080–9085.

Velasco-Santos, C., Martínez-Hernández, A. L., Consultchi, A., Rodríguez, R., & Castaño, V. M. (2003). Naturally produced carbon nanotubes. *Chemical Physics Letters, 373*, 272–276.

Vostrowsky, O., & Hirsch, A. (2004). Molecular peapods as supramolecular carbon allotropes. *Angewandte Chemie, International Edition, 43*, 2326–2329.

Wahl, F., Worth, J., & Prinzbach, H. (1993). The pagodane route to dodecahedranes: An improved approach to the $C_{20}H_{20}$ parent framework; partial and total functionalizations – Does C_{20}-fullerene exist? *Angewandte Chemie International Edition in English, 32*, 1722–1726.

Wanbayor, R., & Ruangpornvisuti, V. (2008). Theoretical study of adsorption of C1–C3 alkoxides on various cap-ended and open-ended armchair (5,5) single-walled carbon nanotubes. *Carbon, 46*, 12–18.

Wang, G.-W., Zhang, X.-H., Zhan, H., Guo, Q.-X., & Wu, Y.-D. (2003). Accurate calculation, prediction, and assignment of ^3He NMR chemical shifts of Helium-3-encapsulated fullerenes and fullerene derivatives. *Journal of Organic Chemistry, 68*, 6732–6738.

Wang, C., Zhou, G., Liu, H., Wu, J., Qiu, Y., Gu, B.-L., & Duan, W. (2006). Chemical functionalization of carbon nanotubes by carboxyl groups on Stone-Wales defects: A density functional theory study. *The Journal of Physical Chemistry. B, 110*, 10266–10271.

Wang, X., Tabakman, S. M., & Dai, H. (2008). Atomic layer deposition of metal oxides on pristine and functionalized grapheme. *Journal of the American Chemical Society, 130*, 8152–8153.

Wang, L., Drahushuk, L. W., Cantley, L., Koenig, S. P., Liu, X., Pellegrino, J., Strano, M. S., & Bunch, J. S. (2015a). Molecular valves for controlling gas phase transport made from discrete ångström-sized pores in graphene. *Nature Nanotechnology, 10*, 785–790.

Wang, Y., Díaz-Tendero, S., Manuel Alcamí, M., & Martín, F. (2015b). Cage connectivity and frontier π orbitals govern the relative stability of charged fullerene isomers. *Nature Chemistry, 7*, 927–934.

WenXing, B., ChangChun, Z., & WanZhao, C. (2004). Simulation of Young's modulus of single-walled carbon nanotubes by molecular dynamics. *Physica B, 352*, 156–163.

Wikipedia – http://en.wikipedia.org/wiki/Carbon.

Woodward, R. B., & Hoffmann, R. (1969). The conservation of orbital symmetry. *Angewandte Chemie (International Edition in English), 8*, 781–853.

Wu, J., & Hagelberg, F. (2008). Computational study on C_{80} enclosing mixed trimetallic nitride clusters of the form $Gd_xM_{3-x}N$ (M = Sc, Sm, Lu). *The Journal of Physical Chemistry C, 112*, 5770–5777.

Wu, Y.-T., & Siegel, J. S. (2006). Aromatic molecular-bowl hydrocarbons: Synthetic derivatives, their structures, and physical properties. *Chemical Reviews, 106*, 4843–4867.

Wu, X., & Zeng, X. C. (2009). Periodic graphene nanobuds. *Nano Letters, 9*, 250–256.

Xia, J., Chen, F., Li, J., & Tao, N. (2009). Measurement of the quantum capacitance of grapheme. *Nature Nanotechnology, 4*, 505–509.

Xie, S.-Y., Gao, F., Lu, X., Huang, R.-B., Wang, C.-R., Zhang, X., Liu, M.-L., Deng, S.-L., & Zheng, L.-S. (2004). Capturing the labile fullerene[50] as $C_{50}Cl_{10}$. *Science, 304*, 699.

Xue, Y., Ding, Y., Niu, J., Xia, Z., Roy, A., Chen, H., Qu, J., Wang, Z. L., & Dai, L. (2015). Rationally designed graphene-nanotube 3D architectures with a seamless nodal junction for efficient energy conversion and storage. *Science Advances, 1*, 1400198.

Yakobson, B. I., Brabec, C. J., & Bernholc, J. (1996). Nanomechanics of carbon tubes: Instabilities beyond linear response. *Physical Review Letters, 76*, 2511–2514.

Yamada, M., Nakahodo, T., Wakahara, T., Tsuchiya, T., Maeda, Y., Akasaka, T., Kako, M., Yoza, K., Horn, E., Mizorogi, N., Kobayashi, K., & Nagase, S. (2005). Positional control of encapsulated atoms inside a fullerene cage by exohedral addition. *Journal of the American Chemical Society, 127*, 14570–14571.

Yamada, M., Akasaka, T., & Nagase, S. (2010). Endohedral metal atoms in pristine and functionalized fullerene cages. *Accounts of Chemical Research, 43*, 92–102.

Yang, S. H., Shin, W. H., Lee, J. W., Kim, S. Y., Woo, S. I., & Kang, J. K. (2006a). Interaction of a transition metal atom with intrinsic defects in single-walled carbon nanotubes. *The Journal of Physical Chemistry B, 110*, 13941–13946.

Yang, S. H., Shin, W. H., & Kang, J. K. (2006b). Ni adsorption on Stone-Wales defect sites in single-wall carbon nanotubes. *Journal of Chemical Physics, 125*, 084705-1–084705-5.

Yang, F. H., Lachawiec, A. J., Jr., & Yang, R. T. (2006c). Adsorption of spillover hydrogen atoms on single-wall carbon nanotubes. *The Journal of Physical Chemistry. B, 110*, 6236–6244.

Yanov, I., Leszczynski, J., Sulman, E., Matveeva, V., & Semagina, N. (2004). Modeling of the molecular structure and catalytic activity of the new fullerene-based catalyst $(\eta^2\text{-}C_{60})Pd(PPh_3)_2$: An application in the reaction of selective hydrogenation of acetylenic alcohols. *International Journal of Quantum Chemistry, 100*, 810–817.

Yu, D., Goh, K., Wang, H., Wei, L., Jiang, W., Zhang, Q., Dai, L., & Chen, Y. (2014). Scalable synthesis of hierarchically structured carbon nanotube–graphene fibres for capacitive energy storage. *Nature Nanotechnology, 9*, 555–562.

Yuan, H., & He, Z. (2015). Graphene-modified electrodes for enhancing the performance of microbial fuel cells. *Nanoscale, 2015*, 7022–7029.

Yumura, T., Nozaki, D., Bandow, S., Yoshizawa, K., & Iijima, S. (2005a). End-cap effects on vibrational structures of finite-length carbon nanotubes. *Journal of the American Chemical Society, 127*, 11769–11776.

Yumura, T., Sato, Y., Suenaga, K., & Iijima, S. (2005b). Which do endohedral Ti_2C_{80} metallofullerenes prefer energetically: $Ti_2@C_{80}$ or $Ti_2C_2@C_{78}$? A theoretical study. *The Journal of Physical Chemistry B, 109*, 20251–20255.

Yumura, T., Kertesz, M., & Iijima, S. (2007). Local modifications of single-wall carbon nanotubes induced by bond formation with encapsulated fullerenes. *The Journal of Physical Chemistry. B, 111*, 1099–1109.

Zhang, J., & Zuo, J. M. (2009). Structure and diameter-dependent bond lengths of a multi-walled carbon nanotube revealed by electron diffraction. *Carbon, 47*, 3515–3528.

Zhang, B. L., Wang, C. Z., Ho, K. M., Xu, C. H., & Chan, C. T. (1993). The geometry of large fullerene cages: C_{72} to C_{102}. *Journal of Chemical Physics, 98*, 3095–3102.

Zhang, G., Qi, P., Wang, X., Lu, Y., Mann, D., Li, X., & Dai, H. (2006). Hydrogenation and hydrocarbonation and etching of single-walled carbon nanotubes. *Journal of the American Chemical Society, 128*, 6026–6027.

Zhang, H., Cao, G., Wang, Z., Yang, Y., Shi, Z., & Gu, Z. (2008). Influence of ethylene and hydrogen flow rates on the wall number, Crystallinity, and length of millimeter-long carbon nanotube array. *The Journal of Physical Chemistry C, 112*, 12706–12709.

Zhao, K., & Pitzer, R. M. (1996). Electronic structure of C_{28}, $Pa@C_{28}$, and $U@C_{28}$. *Journal of Physical Chemistry, 100*, 4798–4802.

Zhao, Y., & Truhlar, D. G. (2007). Size-selective supramolecular chemistry in a hydrocarbon nanoring. *Journal of the American Chemical Society, 129*, 8440–8442.

Zhao, Y., & Truhlar, D. G. (2008). Computational characterization and modeling of buckyball tweezers: Density functional study of concave–convex interactions. *Physical Chemistry Chemical Physics, 10*, 2813–2818.

Zhao, X., Slanina, Z., & Goto, H. (2004a). Theoretical studies on the relative stabilities of C_{96} IPR fullerenes. *The Journal of Physical Chemistry. A, 108*, 4479–4484.

Zhao, X., Goto, H., & Slanina, Z. (2004b). C_{100} IPR fullerenes: Temperature-dependent relative stabilities based on the Gibbs function. *Chemical Physics, 306*, 93–104.

Zhou, Z., Steigerwald, M., Hybertsen, M., Brus, L., & Friesner, R. A. (2004). Electronic structure of tubular aromatic molecules derived from the metallic (5,5) armchair single wall carbon nanotube. *Journal of the American Chemical Society, 126*, 3597–3607.

Zhou, L., Gao, C., Zhu, D. D., Xu, W., Chen, F. F., Palkar, A., Echegoyen, L., & Kong, E. S.-W. (2009). Facile functionalization of multilayer fullerenes (carbon nanoonions) by nitrene chemistry and grafting from strategy. *Chemistry - European Journal, 15*, 1389–1396.

Zhu, Z. H., Hatori, H., Wang, S. B., & Lu, G. Q. (2005). Insights into hydrogen atom adsorption on and the electrochemical properties of nitrogen-substituted carbon materials. *The Journal of Physical Chemistry. B, 109*, 16744–16749.

Zhu, Y., Li, L., Zhang, C., Casillas, G., Sun, Z., Yan, Z., Ruan, G., Peng, Z., Raji, A.-R., Kittrell, C., Hauge, R. H., & Tour, J. M. (2012). A seamless three-dimensional carbon nanotube graphene hybrid material. *Nature Communications, 3*, 1225.

Zope, R. R., Baruah, T., Pederson, M. R., & Dunlap, B. I. (2008). Static dielectric response of icosahedral fullerenes from C_{60} to C_{2160} characterized by an all-electron density functional theory. *Physical Review B, 77*, 115452-1–115452-5.